 DNA 4608F

DEVELOPMENT OF THE BRINELL SANDWICH PASSIVE SOIL STRESS GAGE

U.S. Army Engineer Waterways Experiment Station
Weapons Effects Laboratory
P.O. Box 631
Vicksburg, Mississippi 39180

31 December 1977

Final Report for Periods February 1973—September 1973 and July 1975—December 1977

MIPR No. 78-544

THIS WORK SPONSORED BY THE DEFENSE NUCLEAR AGENCY
UNDER SUBTASKS J24CAXYX98423 AND L11CAXSX35248.

Prepared for
Director
DEFENSE NUCLEAR AGENCY
Washington, D. C. 20305

DISCLAIMER NOTICE

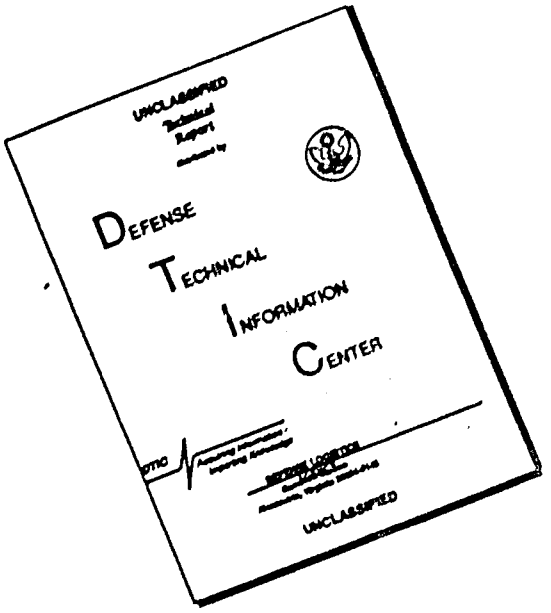

THIS DOCUMENT IS BEST QUALITY AVAILABLE. THE COPY FURNISHED TO DTIC CONTAINED A SIGNIFICANT NUMBER OF PAGES WHICH DO NOT REPRODUCE LEGIBLY.

Destroy this report when it is no longer needed. Do not return to sender.

PLEASE NOTIFY THE DEFENSE NUCLEAR AGENCY, ATTN: TISI, WASHINGTON, D.C. 20305, IF YOUR ADDRESS IS INCORRECT, IF YOU WISH TO BE DELETED FROM THE DISTRIBUTION LIST, OR IF THE ADDRESSEE IS NO LONGER EMPLOYED BY YOUR ORGANIZATION.

(18) DNA, SBIE / UNCLASSIFIED (19) 4608F, AD-E300 356

SECURITY CLASSIFICATION OF THIS PAGE (When Data Entered)

REPORT DOCUMENTATION PAGE

READ INSTRUCTIONS BEFORE COMPLETING FORM

1. REPORT NUMBER: DNA 4608F
2. GOVT ACCESSION NO.
3. RECIPIENT'S CATALOG NUMBER

4. TITLE (and Subtitle): (6) DEVELOPMENT OF THE BRINELL SANDWICH PASSIVE SOIL STRESS GAGE.

5. TYPE OF REPORT & PERIOD COVERED: (9) Final Report. Feb [redacted]—Sep 73, Jul 75-Dec 77

6. PERFORMING ORG. REPORT NUMBER

7. AUTHOR(S): (14) Andrew Peckna

8. CONTRACT OR GRANT NUMBER(s): (15) MIPR [redacted] 78-544 new

9. PERFORMING ORGANIZATION NAME AND ADDRESS
U. S. Army Engineer Waterways Experiment Station
Weapons Effects Laboratory
P. O. Box 631, Vicksburg, Mississippi 39180

10. PROGRAM ELEMENT, PROJECT, TASK AREA & WORK UNIT NUMBERS
Subtasks J24CAXYX984-23 and L11CAXSX352-48

11. CONTROLLING OFFICE NAME AND ADDRESS: (11)
Director
Defense Nuclear Agency
Washington, D.C. 20305

12. REPORT DATE: 31 Dec [redacted] 1977
13. NUMBER OF PAGES: 122

14. MONITORING AGENCY NAME & ADDRESS (if different from Controlling Office): (12) 121 p.

15. SECURITY CLASS (of this report): UNCLASSIFIED
15a. DECLASSIFICATION/DOWNGRADING SCHEDULE

16. DISTRIBUTION STATEMENT (of this Report): (16) J24CAXY, L11CAXS
Approved for public release; distribution unlimited.

17. DISTRIBUTION STATEMENT (of the abstract entered in Block 20, if different from Report): (17) X984, X352

18. SUPPLEMENTARY NOTES
This work sponsored by the Defense Nuclear Agency under Subtasks J24CAXYX98423 and L11CAXSX35248.

19. KEY WORDS (Continue on reverse side if necessary and identify by block number)

Brinell	Peak Stress
Compression	Soil
Gage	Strain Rate
Passive	Stress

steel

20. ABSTRACT (Continue on reverse side if necessary and identify by block number)
The interior of the Brinell Sandwich soil stress gage consists of a layer of small hardened ~~steel~~ balls between softer materials. Indentations in the softer materials (their diameters are measured by a microscope) indicate the maximum compressive force that has been exerted at the location of each ball. A flat, disk-shaped gage body package seals off the space around the balls from external pressure and provides protection against shear in the plane of the sandwich. These gages combine high axial stiffness with good resolution → over

DD FORM 1 JAN 73 1473 EDITION OF 1 NOV 65 IS OBSOLETE

UNCLASSIFIED
SECURITY CLASSIFICATION OF THIS PAGE (When Data Entered)

5. TYPE OF REPORT & PERIOD COVERED (Continued)

Jul 75—Dec 77

20. ABSTRACT (Continued)

over a range of more than a factor of 100. Sensing ranges of two versions tested are 4 MPa to 470 MPa, and 0.67 MPa to 100 MPa. Laboratory investigations have shown that with pulses ranging from static to approximate half-sines with rise times of 0.1 millisecond, gage performance is not influenced by rate effects.

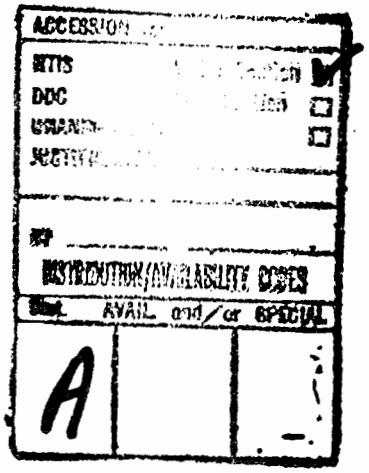

PREFACE

This project was sponsored by the Defense Nuclear Agency (DNA) under Subtask J24CAXYX984, "Stemming and Containment Diagnostics," Work Unit 23, "Passive Peak Stress Measurements," and under Subtask L11CAXSX352, "Development of Field Instrumentation," Work Unit 48, "Development of Passive Gage." The work was accomplished by the U. S. Army Engineer Waterways Experiment Station (WES) during the periods February 1973 through September 1973, and July 1975 through December 1977. Mr. C. McFarland and Mr. T. E. Kennedy of the DNA were technical monitors.

This project was under the general supervision of Mr. W. J. Flathau, Chief, Weapons Effects Laboratory (WEL), WES. It was initiated under the supervision of Mr. L. F. Ingram, Chief, Phenomenology and Effects Division (PE), WEL, and most of the work was performed under the supervision of Mr. J. T. Ballard, Chief, Structures Division (SD), WEL.

Conception and design were by Dr. A. Peekna, the principal investigator, who also prepared most of this report. The static and dynamic tests in hydraulic fluid and the laboratory tests in sand were performed at the Soil Dynamics Division of the Soils and Pavements Laboratory, WES. Mr. B. F. Wright helped conceive the method of obtaining short pulses in the dynamic fluid chamber. The static and dynamic tests with a single ball were performed by Mr. G. P. Bonner, who also wrote the corresponding chapter (Chapter 7) of this report. Chapter 7 is essentially a thesis submitted in partial fulfillment of the requirements for the degree of Master of Science in Engineering Mechanics at Mississippi State University; Dr. A. Peekna was the on-site advisor. The impressions were measured at the Engineering Sciences Division, Concrete Laboratory, WES, by Mr. G. S. Wong. Appendix B, the assembly procedure, was written by Mr. J. B. Lamb.

Directors of WES during the project were BG E. D. Peixotto and COL G. H. Hilt; COL J. L. Cannon was Commander and Director during the conclusion of the project and the preparation of this report. Technical Director was Mr. F. R. Brown.

CONVERSION FACTORS, U. S. CUSTOMARY TO METRIC (SI)
UNITS OF MEASUREMENT

U. S. customary units of measurement used in this report can be converted to metric (SI) units as follows:

Multiply	By	To Obtain
inches	2.54	centimetres
feet	0.3048	metres
pounds (mass)	453.59237	grams
pounds (force)	4.448222	newtons
pounds (mass) per cubic inch	27.68	grams per cubic cm
pounds (force) per square inch	.006894757	megapascals
g (acceleration of gravity)	9.81	metres per sec^2
microns	10^{-6}	metres

CONTENTS

FIGURES

DEVELOPMENT OF THE BRINELL SANDWICH PASSIVE SOIL STRESS GAGE

CHAPTER 1

INTRODUCTION

1.1 BACKGROUND

Passive stress gages can provide cost-effective measurements of peak stress in soil or on a soil-structure interface. Generally, a soil stress gage will not indicate exactly the same stress that would occur if the gage were not present in the medium. For example, when the gage is placed in the free field or on a structure made of stiff material such that it sticks out into the external medium, the gage will tend to overregister if its deforming portion is stiffer than the medium, and to underregister if it is less stiff than the medium. Overregistration is preferable to underregistration; the overregistration factor of a flat, disk-shaped gage is not very sensitive to variations in media properties, whereas underregistration in a strong and stiff medium can be severe. A flush-mounted gage in a stiff structure will always tend to underregister; however, provided the ratio of gage deflection to diameter is small and the external medium is not very stiff, the underregistration of a flush-mounted gage will not be excessive. For a thorough review of the interaction between soils and pressure cells, the reader is referred to a recent report by M. J. Hvorslev (Reference 1).

A soil stress gage of maximum versatility should have a flat disk shape and be as stiff as possible. Since pretest predictions of peak stress resulting from nuclear and high-explosive detonations are often very inaccurate, the widest possible sensing range is clearly advantageous. For maximum usefulness when dealing with pulses of different rise times and durations, the gage should be free of rate effects over as broad a range of pulse shapes as possible.

Some previous passive gages of various types are described in References 2-15. Four of these (References 7, 11, 13, and 14) operate by the ball-indentation principle, which is also used in the Brinell Sandwich passive soil stress gage.

1.2 PURPOSE

The objective was to design and test a passive peak-reading stress gage suitable for use in soil and weak rock. The gage should be capable of producing peak stress data competitive in quality with the results obtainable from active gages, but at a small fraction of the cost.

1.3 SCOPE

The general description and application procedures are outlined in Chapter 2; details such as drawings, assembly procedures, etc. are included in the Appendices. The key to a partial bibliography of mechanical properties of metals at high rates of strain is included in Chapter 3; emphasis is on the less strain rate sensitive metals. Experimental and analytical documentation of gage performance is given in Chapters 4-7. Performance characteristics are summarized in Chapter 8; the reader may wish to proceed directly from Chapter 2 to Chapter 8 in a first reading. Some of the material reported herein has been published previously (Reference 16).

CHAPTER 2

DESCRIPTION AND OPERATION

2.1 DESCRIPTION

The basic Brinell Sandwich consists of a layer of small hardened steel balls between softer materials. The balls may be closely packed or separated from each other by a spacer. A cross section is shown in Figure 2.1. The gage body package serves to seal off the space around the balls from external pressure, and to provide protection against shear in the plane of the sandwich.

When the gage is loaded, the balls indent the softer insert plates. The diameters of indentations in an appropriate sampling pattern are measured with a microscope and compared with indentation diameters produced by loads of known magnitude under laboratory conditions. A photomicrograph of an impression is shown in Figure 2.2.

Two versions of the Brinell Sandwich soil stress gage have been used to date. In the high-ranged gage, the balls are closely packed, forming a plane hexagonal array except at the edge. Measured mean density in the hexagonal array (at the gage center) was 20.305 balls per square centimetre (131.00 per square inch). In the lower-ranged version, the balls are separated by a 1.27-millimetre- (0.050-inch-) thick spacer into an array with 3.875 balls per square centimetre (25 per square inch); this is a square array except at the edge, but the ball density there is very nearly the same as at the center.

The materials used for the inserts are either 7075-T6 aluminum for both inserts or, more often, 7075-T6 and 6061-T6; the choice depends on desired range and stiffness. The choice of these alloys was based on a search of published literature on strain rate sensitivity (the dependence of plastic flow stress on strain rate).

The choice of material for the gage body is considerably less critical. The density of aluminum is much closer to media densities than that of steel, hence use of aluminum minimizes acceleration sensitivity. The alloy 7075-T651 is used because of its high strength

and stress-relieved temper. Because stress gages are often placed in grout designed to simulate the native backfill material, be it soil or a weak rock such as tuff, the gage body parts are normally plated with electroless nickel. Otherwise, the typically alkaline grouts react with the aluminum and produce hydrogen gas, which forms a matrix of bubbles next to the gage surfaces while the grout sets. Such a bubble matrix is to be avoided since its presence may significantly change the stress exerted on the gage; soft coatings should be avoided for the same reason. Electroless nickel is a hard and very uniform coating that appears to provide adequate protection. The effect of electroless nickel plating on the integrity of Portland cement slurry cast around aluminum is demonstrated in Figure 2.3; similar results were obtained with HARM (CC) (CS II 9.00) grout.

2.2 APPLICATION PROCEDURES

Detailed drawings and specifications for the gage parts are given in Appendix A. The instructions for assembly are given in Appendix B.

Calibration of each new sheet of material for the 7075-T6 and 6061-T6 aluminum inserts avoids the effects of slight variations in mechanical properties between different batches of the same alloy. This is done statically by means of a single ball in series with a load cell. In order to take full advantage of the sizeable useful range of this gage, the use of load cells of two different rated load ranges is recommended. Equivalent peak pressures are obtained by multiplying each value of the peak load by the ball density (number per unit area) in the gage. The impression diameters are measured with a binocular microscope calibrated with a stage micrometer; nominal magnifications of 160X, 80X, and 56X provide an adequate range. The binocular feature, together with appropriate lighting arrangements, is a significant help in improving impression edge definition. As specified in the ASTM standard for Brinell hardness testing (Reference 17), each impression so obtained is measured in mutually perpendicular directions. The calibration procedure is discussed in greater detail in Appendix C. The resulting curves of peak pressure versus indentation diameter,

usually plotted on log-log paper, are used in reducing the data from recovered gages.

Considerable care must be taken in the placement of soil stress gages of any type. Investigations of several procedures for placing disk-shaped gages in sand and clay are reported in References 18 and 19. If grout or concrete is cast on the flat underside of a gage positioned to measure vertical stress, it is recommended that the gage be tilted slightly in order to avoid the possibility of trapping air bubbles on the downward face. Any free-field positioning fixtures may attach to the gage only at its edge and should be such as to disturb the state of stress in the vicinity of the sensing faces as little as possible. In making measurements on a structure interface, good contact with the structure material must be assured. Hard epoxy has proved satisfactory for fastening gages to metal backings and to concrete structures that have already been cast. The possibility of air-voids in the epoxy may be minimized by not attempting to spread it evenly, but by placing a large blob in the center and forcing the epoxy outwards as the gage is pressed onto the surface.

Care must be taken to prevent secondary loading of the gage due to impacts during recovery. If the gage is embedded in grout, the direction of cutting should be toward the gage edge, never toward a sensing face. It is better not to clean the exterior of recovered gages in the field, but to bring them back to the laboratory together with any pieces of grout, epoxy, and/or concrete that may be attached.

Because of the large number of indenters and relatively flexible gage body faces, this gage indicates a stress distribution instead of merely the total load on the array. This feature not only minimizes the influence of friction between the gage parts at the edge, influence of lateral stresses, etc., but can also be used to diagnose problems due to imperfect placement and recovery. During data reduction, each indented insert is carefully examined for anomalies in the distribution of impression sizes. Normally, the impression sizes are nearly constant in a central region and diminish near the edge. In the event that an anomaly such as a local low or high region is found, it is worthwhile

to carefully examine the gage body parts for corroborating evidence, such as a void in the epoxy or grout sticking to the gage, or evidence of a hit on the gage or on the grout sticking to the gage. Once the problem is identified, it becomes possible to obtain valid upper and/or lower limits on the peak stress.

Occasionally the distribution of impression sizes may indicate a linear stress gradient from one side of the gage to the other, i.e., the distribution of indicated stress in the central region is still flat but tilted. Such gradients are somewhat ambiguous with the effects of shear. However, provided that the sampling pattern of impressions is not offset from center, the effect of shear on the peak stress indicated by the gage is minimal. This is discussed more fully in Chapter 5.

Normally five impressions in a centered sampling pattern are measured on one insert, and just the central impression on the other. Averaging over five impressions diminishes the effect of local variations in hardness of the insert material; the ASTM standard on Brinell hardness testing (Reference 17) specifies a minimum of five impressions in calibrating standardized hardness test blocks whose test face is less than 100 square centimetres. The single impression measured on the other insert serves only as a quality-control check. Because large impressions in the alloy 6061-T6 appear to involve a barely detectable strain rate effect, the peak stress is usually obtained from impressions in the 7075-T6 insert. Since impression edge definition becomes more difficult with impressions smaller than 0.3 millimetre diameter, impressions in the softer 6061-T6 are used for better resolution near the lower end of the sensing range.

If the gage is used in an environment involving a combination of shear stress and multiple peaks in the normal stress, the result is usually not just one clean set of impressions; more often one or more other sets of secondary impressions are superposed on the impression edges. These secondary impressions are usually crescent-shaped. Nevertheless, it has been possible to measure the diameter of the primary impression in at least one direction in almost all cases.

Unmeasurable superpositions of impressions, from which only upper limits can be obtained, have been rare. Sometimes the impressions are slightly out of round, indicating that the ball had rolled slightly; such are measured along the minor axis. The attendant increased difficulty of impression measurement increases the error band on the indicated peak stress to a typical value of ten percent over most of the sensing range.

The gage body parts (other than the inserts) are often reusable. However, before any are reused, they should be inspected in a machine shop to check if any deformation has not brought the flatness of the inner surfaces outside the specifications; the detailed drawings are in Appendix A.

The influence of the presence of the gage in the medium is often expressed in terms of the registration ratio, defined as the stress indicated by the gage divided by what the stress would be if the gage were not present. This may be measured by preparing a soil or grout specimen containing the gage in the actual field placement configuration, and subjecting it to a known stress input in the laboratory. The specimen must be sufficiently large so that boundary effects do not significantly influence gage-medium interaction. This is discussed more fully in Chapter 6. Because of the nonlinearity of most soils and grouts, the registration ratio is usually not a constant but depends on the stress, as well as on the particular variety of soil or batch of grout used.

The gage characteristics are summarized in Chapter 8; the reader may wish to proceed from here directly to Chapter 8 in a first reading.

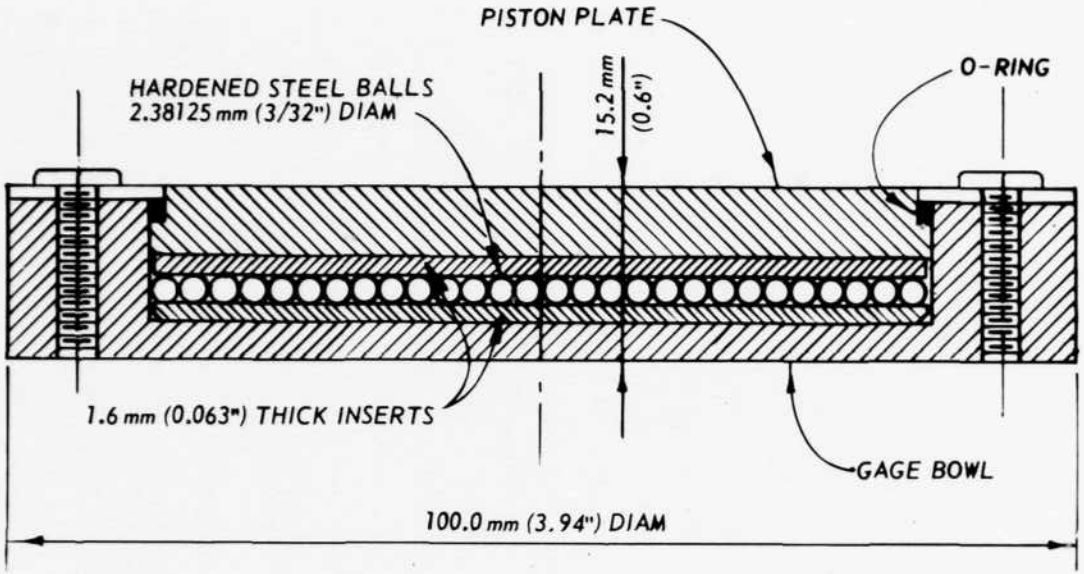

Figure 2.1. Brinell Sandwich soil stress gage. The hardened steel balls may be closely packed or separated by a spacer, depending on desired range and stiffness.

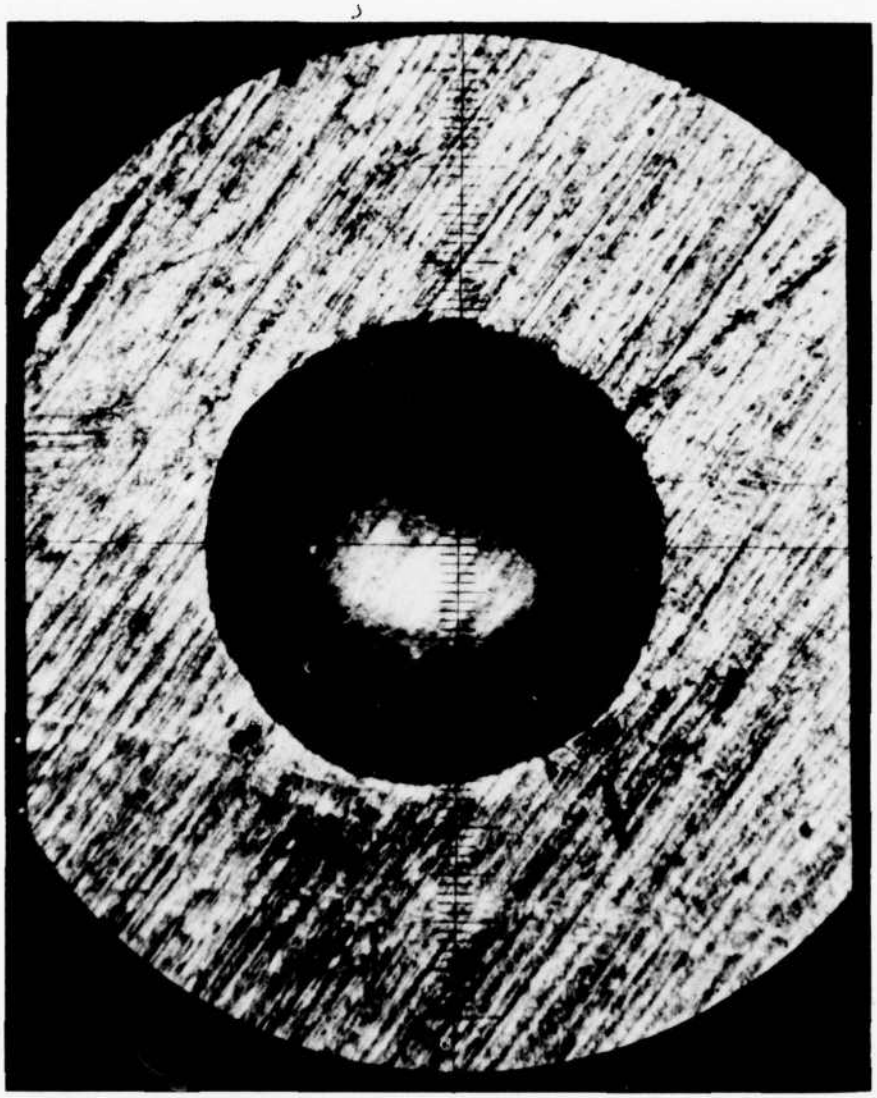

Figure 2.2. Photomicrograph of an impression. Each scale division is approximately 16 microns.

a. Cement slurry cast around bare 7075-T651 aluminum.

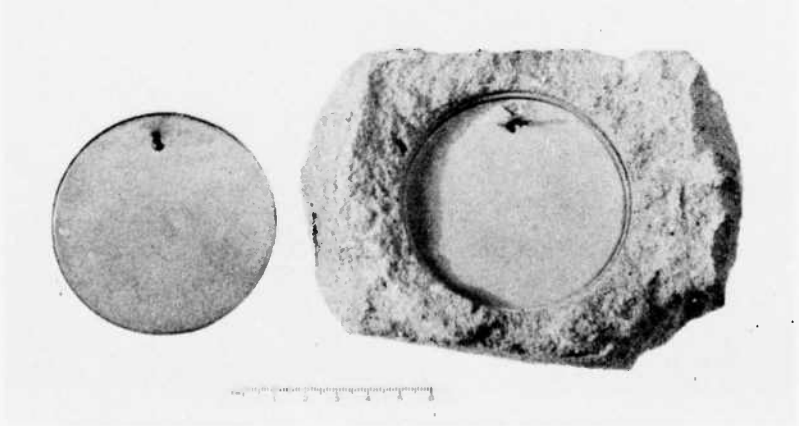

b. Same batch of cement slurry cast around 7075-T651 aluminum plated with electroless nickel.

Figure 2.3. Effect of proper anticorrosive coating on the integrity of Portland cement slurry around aluminum.

CHAPTER 3

STRAIN RATE SENSITIVITY AND THE CHOICE OF INSERT MATERIALS

The choice of insert materials is critical. A partial search of published experimental data on strain rate sensitivity (the dependence of plastic flow stress on strain rate) was conducted, with emphasis on the less strain rate sensitive metals. Tables 3.1, 3.2, and 3.3 provide the key to the resulting partial bibliography of mechanical properties of metals at high rates of strain (References 20-61). In any of the uniaxial configurations, data at plastic strain rates up to at least 100 sec^{-1} were required for inclusion in the listing; this strain rate corresponds to a strain of ten percent produced in one millisecond. Two reviews (References 20 and 23) are also included.

As is evident from Tables 3.1, 3.2, and 3.3, not much data on the ball-indentation configuration were found. The most common configuration used in high-rate testing is uniaxial stress compression, because it lends itself so readily to the Hopkinson bar technique. Strain rate sensitivity is generally less for metals having a face-centered cubic crystal structure, such as aluminum and copper, than for metals with a body-centered cubic structure, such as iron and most steels. The aluminum alloys 7075-T6 and 6061-T6 have the lowest strain rate sensitivity in uniaxial stress compression of any materials on which published data were found in this search. The strain rate sensitivity in uniaxial stress compression is negligible up to strain rates close to 1000 sec^{-1} for both 7075-T6 (References 29 and 44) and 6061-T6 (References 29, 34, 35, and 44). However, tension data on 6061-T6 indicate a noticeable rate effect (References 41, 42, and 43); the ultimate tensile strength increases by a factor of 1.2 upon going from a strain rate of 10 sec^{-1} to 100 sec^{-1} and the stress-strain curve shifts upward by roughly the same amount throughout the plastic region (References 41 and 42). It was decided to use the alloys 7075-T6 and 6061-T6 for the insert materials, and to conduct experimental investigations of the influence of the pulse rise time and duration on ball indentations in these alloys. These are reported in Chapters 4 and 7.

Table 3.1. Key to a partial bibliography on the mechanical properties of aluminum alloys at high rates of strain. Numbers under the various stress configuration headings denote references at the end of the text.

Aluminum Alloy	Uniaxial Stress Tension	Uniaxial Stress Compression	Shear	Flexure	Uniaxial Strain Compression	Ball Indentation
Single crystals of aluminum			20, 21			
Nearly pure aluminum	22	20, 23, 24, 25, 26, 27, 28, 29	20, 21			
Al - 2 at. % Cu alloy			21			
1045-0		30				
1060-0		23, 29, 31			32	
1100-0	20, 33, 34	20, 23, 29, 33, 34, 35	20, 33, 36, 37, 38			
1100-F		23				39, 40
1119-0		23				
2024-0		23, 29				
2024-T4	41					39
5454-0		23				
5454-H34		23				
6061-0		23, 29				40
6061-T6	41, 42, 43	23, 29, 34, 35, 44		47	45, 46	
6061-T651		23				
6351-T51		23				
7075-0		23, 29				
7075-T6		23, 29, 44		47		

Table 3.2. Key to a partial bibliography on the mechanical properties of miscellaneous nonferrous metals at high rates of strain. Numbers under the various stress configuration headings denote references at the end of the text.

Metal or Alloy	Uniaxial Stress Tension	Uniaxial Stress Compression	Shear	Ball Indentation
Annealed copper	22	20, 23, 24, 25, 26, 30, 48, 49	20, 50, 51	
Annealed brass		26, 30	20	
Commercially pure lead		20, 24, 25, 48	37	39, 52
Lead-tin eutectic			51	
Zinc, single crystals			20	
Annealed 99.99% zinc		26		
Annealed 99.98% magnesium		26		
Mg alloy similar to AZ61A			53	
6Al-4V titanium	41	44		
5Al-2.5Sn titanium	41			
C120-AV, A110-AT, A55 titaniums	43			
Tantalum	41			
Tungsten	41			
Uranium - 10% Mo	41			

Table 3.3. Key to a partial bibliography on the mechanical properties of iron and steels at high rates of strain. Numbers under the various stress configuration headings denote references at the end of the text.

Alloy	Uniaxial Stress Tension	Uniaxial Stress Compression	Shear	Flexure	Ball Indentation
Annealed iron	22	23, 25, 54			
1010 steel				47	
Annealed C1018 steel					40
Cold-rolled SAE 1018	43				
Mild steel	20, 55		20		
EN2A mild steel			56		
Reinforcing bars of grades 60 and 75 A615 billet steel	57				
A free-machining steel			58		
1.5% Cr Mo steel			59		
Tool steel					39
YST 50, YST 80 steels				47	
Vascomax-300 steel	41				
V-mod. 4330 steel	41				
302, 310 stainless steels				47	
304 stainless steel	60	61			
304L, 347 stainless steels	60				

CHAPTER 4

STATIC AND DYNAMIC TESTS IN HYDRAULIC FLUID

Static and dynamic tests were performed in a dynamic fluid chamber. A representative of the group of dynamic pulses obtained by normal operation of the fluid chamber is shown in Figure 4.1a. However, it was found that by operating the fluid chamber with a volume of nitrogen immediately above the fluid and by minimizing chamber volume, considerably shorter pulses could be obtained, especially with the higher peak pressures. One of the fastest pulses from this group is displayed in Figure 4.1b. The rise time was defined as in Figure 4.1 because the beginning shoulder of the pulse is both poorly defined and unimportant in checking for possible strain rate effects.

The results are plotted in Figures 4.2 and 4.3, and the parts of these plots involving the higher peak pressures and correspondingly large impressions (which are the most sensitive indicators of possible strain rate effects) are expanded in Figures 4.4 and 4.5. Each point represents the mean impression diameter at the gage center, based on a sample pattern of seven impressions for the high-ranged gage, and five impressions for the lower-ranged gage. In the absence of detectable rate effects, all three sets of points should lie along the same line (within random point scatter) irrespective of pulse rise time and duration. This is indeed true for the alloy 7075-T6. However, large impressions in the alloy 6061-T6 appear to involve a barely detectable rate effect, as indicated in Figure 4.5. Of course, this is easily avoided by always installing at least one 7075-T6 insert in the gage, and not utilizing large impressions in 6061-T6 as readout. Small impressions in 6061-T6 may be used for better resolution near the lower end of the sensing range. Static and dynamic tests with a single ball, involving pulses shorter by a factor of ten, are reported in Chapter 7.

Tests in hydraulic fluid between peak pressures of 100 MPa and 400 MPa were also attempted. Due to problems with the reference transducer, the resulting data could not be considered calibration quality. The threshold at which the inserts bottom on the spacer in

the lower-ranged gage was found to be between approximately 130 MPa and 180 MPa. The fluid pressure threshold for permanent deformation of the gage body parts was found to be approximately 200 MPa, but the gages could always be easily disassembled. Absence of any O-ring failures was encouraging.

Some tests on the high-ranged gage, with balls closely packed, were performed with a uniaxial static testing machine. The gage bodies used in these tests had been machined for extra radial clearance. The load was distributed over the entire active face of the gage. The equivalent pressure was computed by dividing the total load by the total number of balls, then multiplying by the ball density in a close packed hexagonal array. Root-mean-square impression diameters were computed from a sample pattern covering the insert face. The results are included in Figure 4.2.

The amount of random point scatter in Figures 4.2 and 4.3 provides a measure of resolution. From the data of Figures 4.2 and 4.3, the error band on the indicated stress over most of the sensing range is ± 4 percent of reading, with approximately 95 percent confidence level.

High pressures close the radial clearance just inside of the O-ring. This elastic deformation may be theoretically predicted (Reference 62), and was also indicated by contact marks when the peak fluid pressure was above 50 MPa ($\approx$7300 psi). However, the effect of edge friction is mitigated by the large number of indenters and relatively flexible gage body faces.

When the peak pressures are converted to load per ball, the data in Figures 4.2 and 4.3 collapse onto a common set of curves together with the appropriately scaled data taken with a single 2.5 mm ball (Chapter 7). This indicates that under conditions of isotropic pressure, the effect of edge friction upon impressions at the center is negligible for the two gage versions tested. It also implies the absence of detectable effects of neighboring indentations when the balls are closely packed, at least up to the maximum impression diameter in the tests with the uniaxial static testing machine. This was 1.25 mm (a little more than half the ball diameter) in 6061-T6 (Figure 4.2);

the behavior of the two alloys may safely be assumed sufficiently similar so that impressions in 7075-T6 should likewise remain unaffected by their neighbors at least up to this limit. Since it would take approximately 470 MPa to produce 1.25 mm impressions in 7075-T6, it can be concluded that calibrations of 7075-T6 with a single ball should be adequate at least over a sensing range extending up to 470 MPa.

Some tests were done with the lower-ranged gage in which the edge of the spacer was trimmed so as to allow a ring of balls around it. This diminished the depth of the impressions at the edge by approximately a factor of two, thus serving as a simulation of significantly higher edge friction. In such tests at peak pressures of approximately 15 MPa and 77 MPa, the indicated stress at the center increased by 6 percent and 4 percent of reading, respectively. When the gage is mounted on a stiff structure, the gage bowl bottom is not free to flex, so that all differential movement must be accommodated by flexure of the piston plate. In order to simulate this condition with high edge friction, the above tests were repeated with a gage bowl having an extra thick (2.54 cm) bottom. This time the effect of the ring of balls around the edge increased the indicated stress at the center by 10 percent and 3 percent of reading, at peak pressures of approximately 20 MPa and 79 MPa, respectively. These results are compared with theoretical predictions in Chapter 5. With a normal spacer, without a ring of balls around the edge, the effect of stiffening the gage bowl bottom on the impressions at the center was undetectable; at a peak pressure of approximately 76 MPa the indicated stress decreased by less than 1 percent of reading, which is well within the point-scatter error band of ± 4 percent of reading.

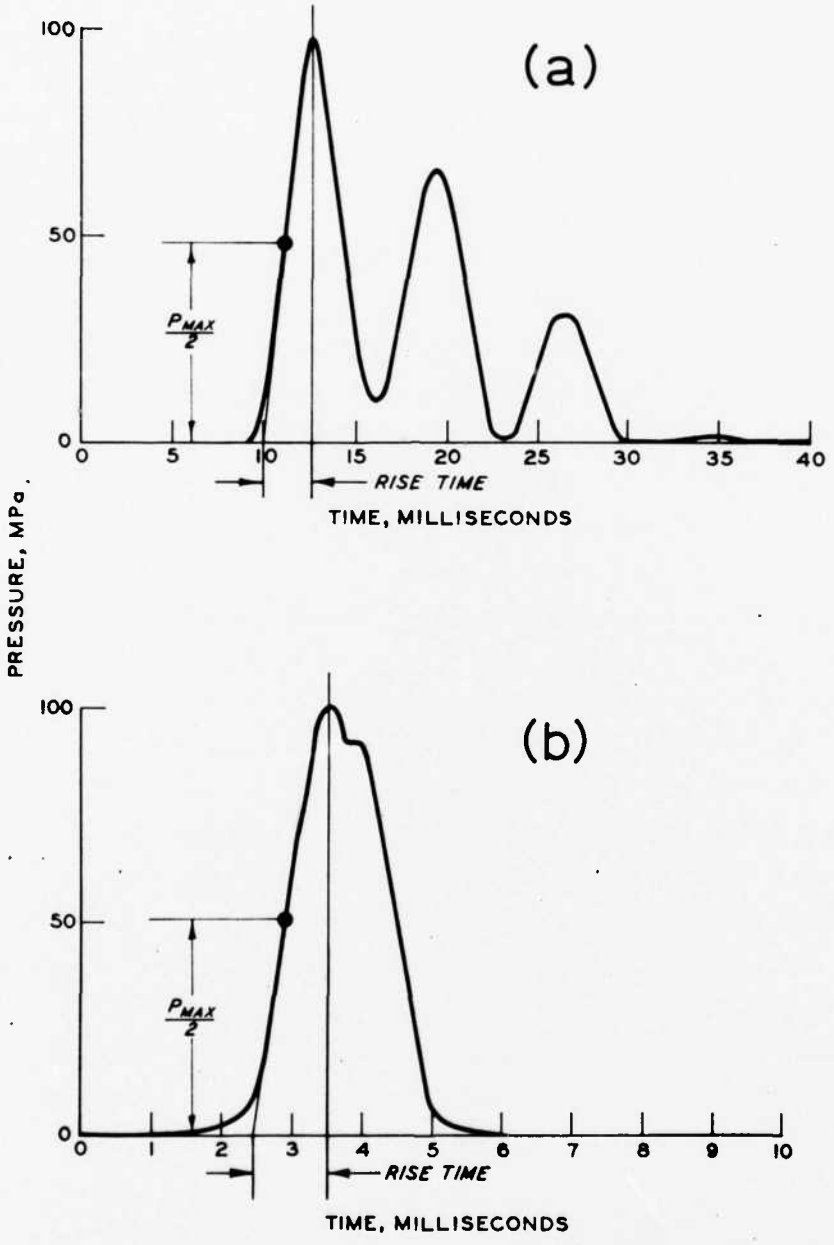

Figure 4.1. Representative pulses from tests in a dynamic fluid chamber. (a) Representative of the dynamic pulses obtained by normal operation of the fluid chamber, (b) One of the fastest pulses, rise time 1.0 millisecond, obtained by operating the chamber with a volume of nitrogen over the fluid.

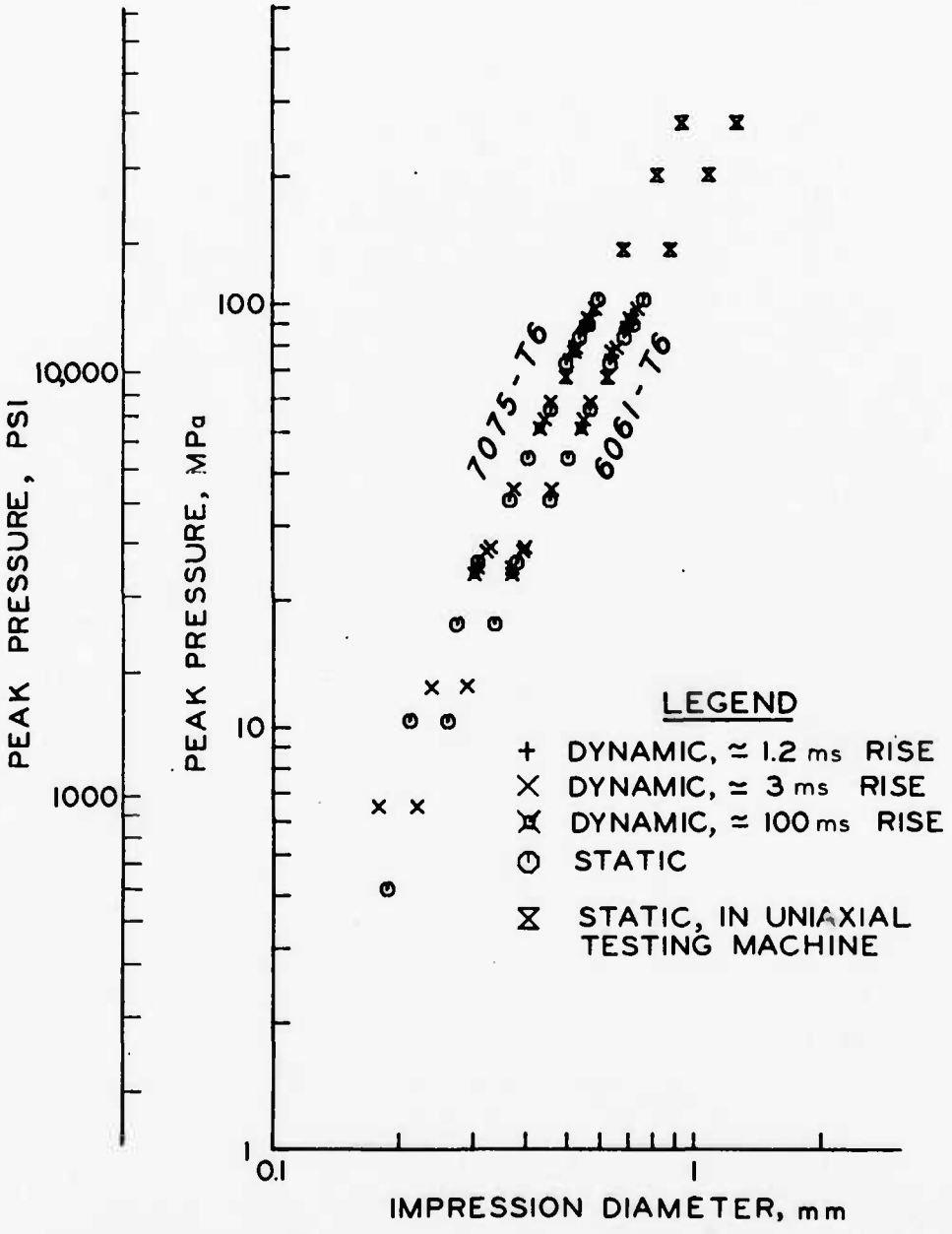

Figure 4.2. Tests in hydraulic fluid for the high-ranged Brinell Sandwich soil stress gage, with the steel balls closely packed.

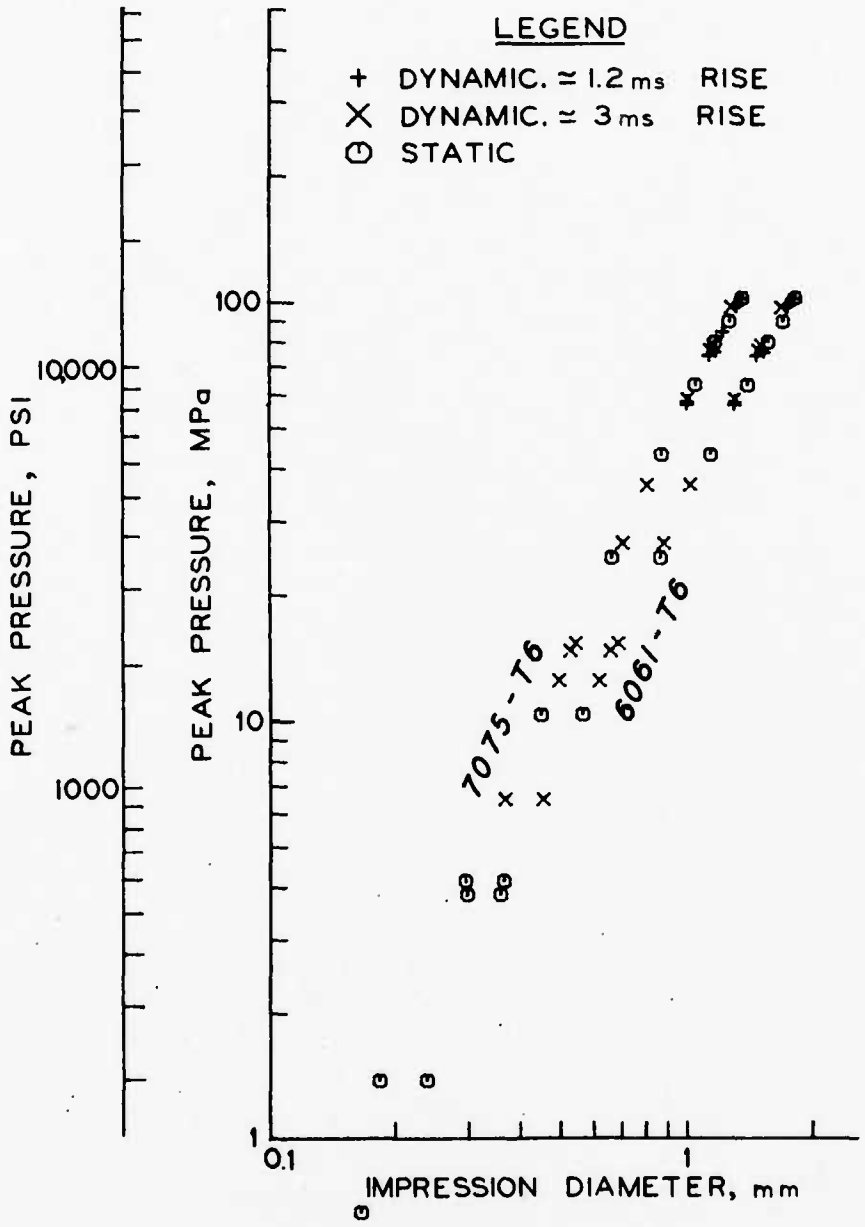

Figure 4.3. Tests in hydraulic fluid for the lower-ranged Brinell Sandwich soil stress gage, with 3.875 balls per sq cm (25 per sq in.), separated by a spacer.

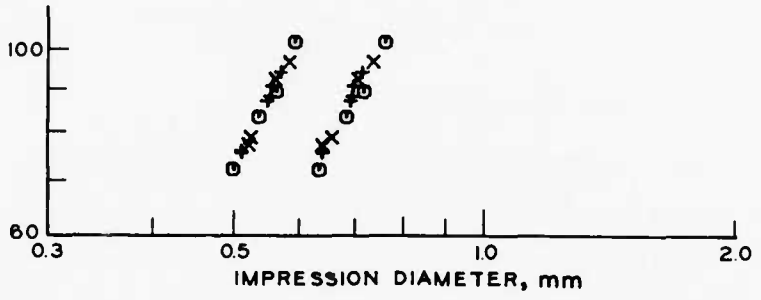

Figure 4.4. Part of Figure 4.2 expanded for clearer display of comparisons between different pulse rise times and durations.

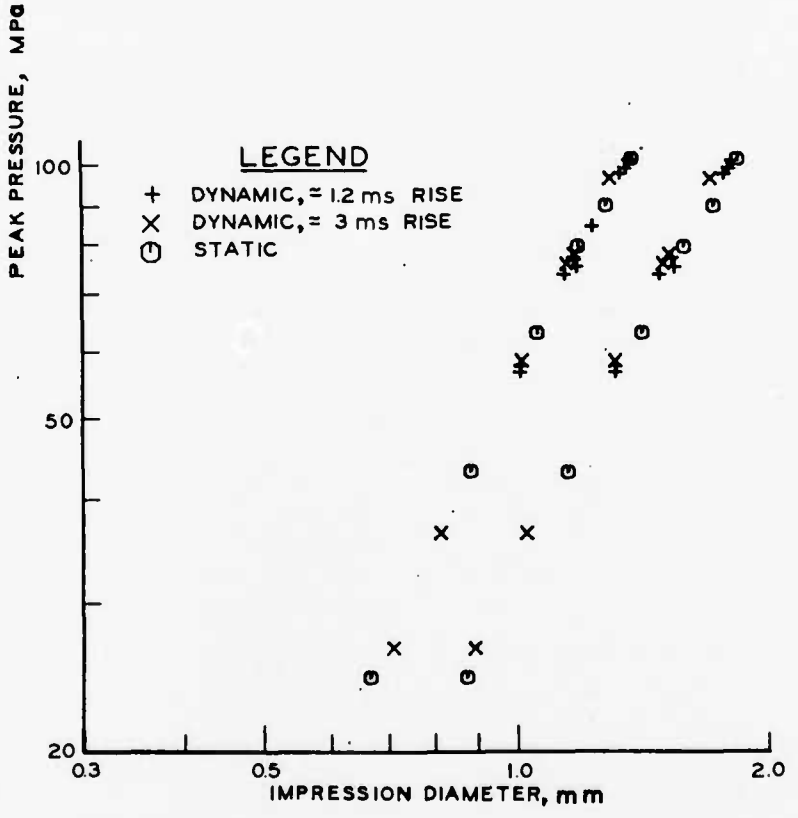

Figure 4.5. Part of Figure 4.3 expanded for clearer display of comparisons between different pulse rise times and durations.

CHAPTER 5

CALCULATED CHARACTERISTICS

5.1 GAGE STIFFNESS; STRESS VERSUS STRAIN

Theoretical treatments of indentation by a hard sphere may be found in several published works; only a few are mentioned here. Numerical solutions of indentation into a rigid-plastic material by frictionless and rough spheres are given in References 63 and 64, respectively. A finite element solution of the elasto-plastic indentation of a layered medium by a frictionless rigid sphere is presented in Reference 65. The semiempirical approach taken in Reference 66 is based on a statistical analysis of published data.

In the initial design calculations, Brinell's original observation that the ratio of force to the surface area of the indentation is nearly constant (Reference 64) was assumed to hold exactly; together with handbook values of Brinell hardness (Reference 67), this was used to estimate the relations between pressure and indentation diameters, as well as gage stiffness. Such predictions of indicated stress were within a factor of 1.3 of the actual fluid chamber data in Figures 4.2 and 4.3.

The calculated stress-strain relations for initial loading displayed in Figure 5.1 are actually semiempirical in that the strain due to plastic impression formation was computed by converting measured impression diameters (the data in Figures 4.2 and 4.3) to indentation depth. Since piling up of the aluminum at the impression edges was neglected, the actual stiffness is expected to be somewhat greater. Elastic deflection at the indentations was approximated by the elastic deflection at the center of a circular area the same size as the indentation subjected to uniform pressure (Reference 62). Elastic strain in the gage body parts was also included. The offset at zero stress in Figure 5.1 corresponds to the maximum discrepancy permitted between the measured thickness of the assembled gage at the center and the sum of the measured thicknesses of the parts.

Some experimental confirmation of these stress-strain curves has been obtained in the dynamic tests with a single ball (Chapter 7), in which the pulse rise time predictions based on Figure 5.1b are in very good agreement with the actual results.

Comparison of Figures 5.1a and 5.1b shows that the gage stiffness can be increased somewhat by using it with both inserts made of 7075-T6. The stiffness could be increased somewhat further by having one of the inserts made of a very hard material such as hardened steel and using the impressions in only the 7075-T6 as readout. However, because of the desirability of a more extended sensing range as well as improved data reduction quality control, the gage has almost always been used with one insert of 7075-T6, and the other of 6061-T6 aluminum.

The stiffness may also be increased by decreasing the ball size. However, it was found that gage assembly became significantly more difficult with 1.5875-mm (1/16-inch) balls than with the 2.38125-mm (3/32-inch) balls normally used.

5.2 INERTIA EFFECTS

With very short rise times, gage performance will depend on frequency response as well as possible strain rate effects. If the stress versus strain behavior of the high-ranged gage, with balls closely packed, were to be conservatively characterized by a modulus of 7500 MPa (≈1100000 psi), and the lower-ranged gage by a modulus of 1400 MPa (≈200000 psi), then their response times to a step function in external stress applied to both gage faces simultaneously would be 15 microseconds and 35 microseconds, respectively. These correspond to half-periods of equivalent elastic systems, which would have natural frequencies of 33 kHz and 14 kHz, respectively.

The acceleration sensitivity at low frequencies is easily obtained by computing the mass mismatch on one side of the ball array relative to the soil around it. In soil of 1.7 gm/cc density, the predicted acceleration sensitivity is approximately 0.1 kPa per g of acceleration (≈0.015 psi/g).

5.3 EFFECTS OF EXTREME LATERAL STRESSES

When making measurements on a structure interface, it must be kept in mind that the lateral stresses in the structure often greatly exceed the normal stresses being measured. At the center of a square plate or two-way slab, the lateral stresses would be axisymmetric, while at a location undergoing flexure in one direction the lateral stresses would be largely uniaxial. High lateral stresses close the radial clearance just inside of the O-ring and affect the functioning of the gage in two ways: (1) axial (frictional) forces diminish axial movement at the edge, and (2) because the area of contact is not aligned with the flexural neutral plane of the piston plate (as may be seen in Figure 2.1), lateral forces exert moments on the piston plate edge. It is easy to see that the axisymmetric situation is the worst case.

Since the stress versus strain behavior of the gage is predicted to be very nearly linear (Figure 5.1), the functioning of a gage mounted on a structure, with the gage bowl bottom not flexing, was analyzed in terms of a circular plate on a linear foundation. Solutions of this problem with various axisymmetric loads and edge conditions are given by Markus (Reference 68). Because Reference 68 is in German, the pertinent equations are also given in Appendix D. For the purpose of this analysis, the stress-strain relations of Figure 5.1 were conservatively characterized by a modulus of 7500 MPa for the high-ranged gage, and by 1400 MPa for the lower-ranged version; the corresponding foundation moduli were obtained by dividing these numbers by the gage thickness.

A conservative upper limit on the effect of frictional forces at the edge can be obtained by treating the piston plate as simply supported around its edge, i.e., allowing no axial movement there whatsoever. This extreme condition would be difficult to attain in practice because structural response sufficient for closing the radial clearance and exerting enough force to prevent sliding would have to precede the normal stress on the gage. The effect of preventing all axial movement at the edge of a gage mounted on a structure and loaded with uniform normal stress q on its outer face is predicted to increase the

indicated stress at the center by 0.18q in both gage versions, high-ranged and low-ranged.

The upper limit on the moment that radial forces can exert on the piston plate edge is attained when plastic yielding is reached over the entire possible contact area just inside of the O-ring (Figure 2.1). The magnitude of external radial stress on the gage edge would have to exceed 200 MPa (≈30,000 psi) in order for this condition to be reached. This maximum edge moment was computed from the ultimate strength of the material and the undeformed dimensions of the gage. The effect of this maximum moment on the simply supported edge of the piston plate in a gage mounted on a structure is predicted to decrease the indicated stress at the center by 1.3 MPa (≈190 psi) in the high-ranged gage and by 11.8 MPa (≈1700 psi) in the lower-ranged version. Treating the piston plate edge as simply supported is justified because the axial forces at the edge arising from the application of the maximum edge moment are in themselves insufficient to overcome friction.

In a hypothetical on-structure application with both extremes of (1) no axial movement at the edge, and (2) maximum edge moment, the predicted increases in indicated stress are 0.18q minus 1.3 MPa in the high-ranged gage, and 0.18q minus 11.8 MPa in the lower-ranged version. The two effects need not occur with proportional severity; for example, there is usually some axial movement at least at the beginning of the pulse even if the maximum edge moment were to be attained near the peak. However, they always partly cancel each other.

The upper limit on the increase in indicated stress, 0.18q, can be equivalently expressed as 15 percent of reading. In the high-ranged gage, the upper limit on the decrease in indicated stress (1.3 MPa) could exceed 15 percent of reading only at readings below 8.7 MPa (≈1300 psi); the sensing range is from 4 MPa to 470 MPa. It is very unlikely that such extreme combinations of low normal stresses and high radial stresses would ever occur; recall that the external radial stress on the gage edge would have to exceed 200 MPa (≈30,000 psi) for the maximum edge moment to be reached. For all practical purposes, 15 percent of reading is a conservative upper limit on the effect of

high lateral stresses on the high-ranged gage, with balls closely packed.

However, the effect of the maximum edge moment on the lower-ranged version is of sufficient magnitude (11.8 MPa, or 1700 psi) to warrant not recommending it in applications where extreme lateral stresses are expected to more or less coincide with the main peak in normal stress.

Tests in the fluid chamber (Chapter 4) with a low-ranged gage having an extra thick bottom and a special spacer allowing a ring of balls around the edge provide some experimental confirmation. In these tests, the stress indicated by the impressions at the edge was approximately 45 percent of the fluid pressure p. The situation may be analyzed as a superposition of 0.45p acting on a gage with a normal spacer and without restrictions on movement at the edge, plus 0.55p acting with axial movement at the edge being prevented. In the absence of edge moments exerted by lateral forces, the predicted increase in indicated stress is (0.18)(0.55p), or 10 percent of the fluid pressure p. Actual increases were 11 percent of the fluid pressure (10 percent of reading) in a test at 20 MPa, and 3 percent of the fluid pressure in a test at 79 MPa. The discrepancy between this prediction and the test result at 79 MPa is outside the error band of ± 4 percent of reading. However, because of the large rotation of the piston plate edge in the test at 79 MPa, the inward corner of the piston plate was brought hard against the inner edge of the gage bowl, thus setting up a resisting moment. This was indicated by clearly visible contact marks. An edge moment of 0.2 times the maximum moment would suffice to bring the discrepancy within the ± 4 percent error band.

5.4 EFFECTS OF SHEAR

The strength of the gage assembly in shear is limited by tangential stresses in the gage bowl edge (which result from moments) and also by bearing stresses on the piston plate edge. The amount of shear that can be resisted by the ball array clearly depends on the size of the impressions. At low values of normal stress, when almost none of the shear is resisted by the ball array, the maximum shear stress that can

be applied to the gage faces before significant yielding takes place is estimated to be approximately 25 MPa (≈3600 psi).

The ambiguity of indicated stress gradients with the effects of shear has been mentioned in Chapter 2. Referring to the cross section of the gage shown in Figure 2.1, if the gage is mounted on a stiff structure, with the gage bowl bottom not flexing, it is easy to see that shear stress applied to the outer face creates moments that tend to make the piston plate tilt slightly, thereby causing a stress gradient at the ball array even though there may be none at the outer face itself. If the piston plate is assumed to be rigid and all the shear force is assumed to be resisted at its lower surface inside the gage, then the indicated stress gradient in MPa/cm is predicted to be 0.2 times the external shear stress in MPa. However, the assumption of a rigid piston plate is not realistic, and when the problem is analyzed in terms of a flexible plate on a linear foundation, it is seen that the distribution of both the externally applied shear and the resisting forces become important. Under some sets of conditions, predicted stress gradients in the central region are higher.

The possible effects of shear on the stress indicated at the center of the gage are of greater interest. Since some sliding or shear of the soil or grout backfill along the surface of a structure is often expected, the effects of shear are of interest especially in on-structure applications. The response of a gage mounted on a stiff structure to shear applied to its outer face was treated in terms of a rectangular plate on a linear foundation, with the same cross section as the piston plate in the direction of shear, and infinitely long in the other direction. This approximation reduces the problem to one of two dimensions, making it possible to use the theory of beams on linear foundations (References 62 and 69).

The forces arising from shear may be divided into three categories: (1) external applied shear, (2) shear resisted by the ball array, and (3) reaction forces at the downstream edge, including axial (frictional) forces. The effect of shear on bending and tilting behavior is the same as that of a distributed moment whose magnitude is half the plate

thickness times the shear stress. The distributed moment due to uniform or merely symmetrically applied external shear cannot by itself alter the indicated stress at the center. However, since the magnitude of shear that can be resisted by the ball array depends on the size of the impressions, some asymmetry is to be expected in the shear resisted by the ball array. The relative importance of the shear resisted by the ball array is highest at high normal stresses. Upper limits on the ratio of the shear that can be resisted by the ball array to the normal stress are easily obtained from geometrical considerations. A computation assuming the center of force on the impression to be eccentric by half the impression radius may safely be considered conservative when the peaks in shear and normal stress are coincident. Conservative upper limits on the effect of shear resisted by the ball array were computed by assuming this resistance to be uniformly distributed over the downstream half of the piston plate. Deflections at the downstream edge were used in computing the possible range of axial (frictional) forces. Worst-case combinations of possible conditions were assumed.

It turns out that at least over the gage sensing ranges considered here, the worst combinations of conditions exist at low stresses, where almost none of the reaction to shear is supported by the ball array and where plastic yielding does not prevent the horizontal reaction at the downstream edge from being located at the inner corner. When the applied shear stress is equal in magnitude to the normal stress, the predicted upper limits on the error in normal stress at the center are 10 percent of reading for the high-ranged gage, and 22 percent of reading for the lower-ranged version.

These upper limits do not include effects on the impressions due to the balls rolling slightly. As has been mentioned in Chapter 2, impressions that are slightly out of round are measured along the minor axis. Although significant differences between stresses indicated by impressions that were slightly out of round and stresses from other recovered gages believed to have been subjected to roughly the same normal stress have not been noticed, a laboratory investigation, perhaps statically with a single ball, would give a more definite indication.

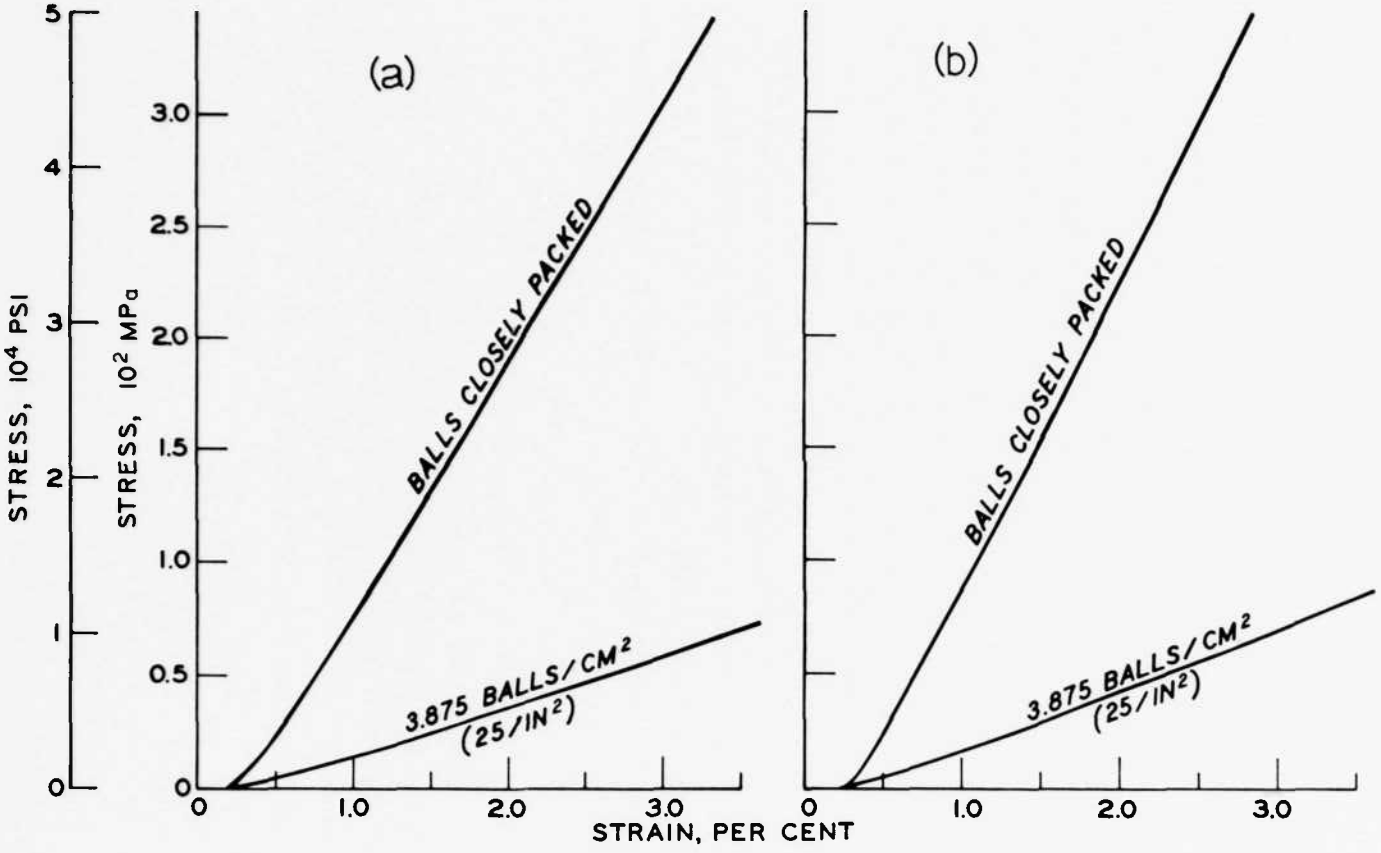

Figure 5.1. External compressive stress versus calculated axial strain at the gage center. (a) One insert 7075-T6, other insert 6061-T6. (b) Both inserts 7075-T6.

CHAPTER 6

LABORATORY TESTS IN SAND

The test fixture was the same dynamic fluid chamber that was used for the tests in hydraulic fluid. The specimen volume, 13.34 cm diameter and 6.35 cm high, contained Reid-Bedford sand, with a gage embedded in the middle. Properties of Reid-Bedford sand are described in Reference 70. The sand was sprinkled in place, with a nominal density of 1.65 gm/cc (103 pounds per cubic foot). A rubber membrane separated the specimen volume from the hydraulic fluid above it. The results are plotted in Figure 6.1. Both the high-ranged and lower-ranged gage consistently overregistered; in view of the high gage stiffness (Figure 5.1), this is not surprising. The overregistration is greatest at the lowest test pressure (Figure 6.1b).

However, the specimen volume was not sufficiently large to eliminate the influence of boundary effects. If the specimen volume were larger, these gages would still overregister but different registration ratios would most likely be obtained.

Estimates of minimum specimen size may be obtained from McNulty's experimental investigation of arching in sand with a circular trap door (Reference 71). For measuring registration ratios in an on-structure configuration, a minimum specimen volume 38 cm (15 inches) in diameter and 15 cm (6 inches) high is desirable. The diameter may be somewhat smaller in a device without wall friction, such as a triaxial test device; a 30-cm-diameter specimen without wall friction would be roughly equivalent to a 38-cm-diameter 15-cm-deep rigid chamber. For measuring registration ratios with soil or grout on both sides of the gage, a specimen size with height and diameter of 30 cm (12 inches) in a triaxial test device is expected to be an acceptable minimum.

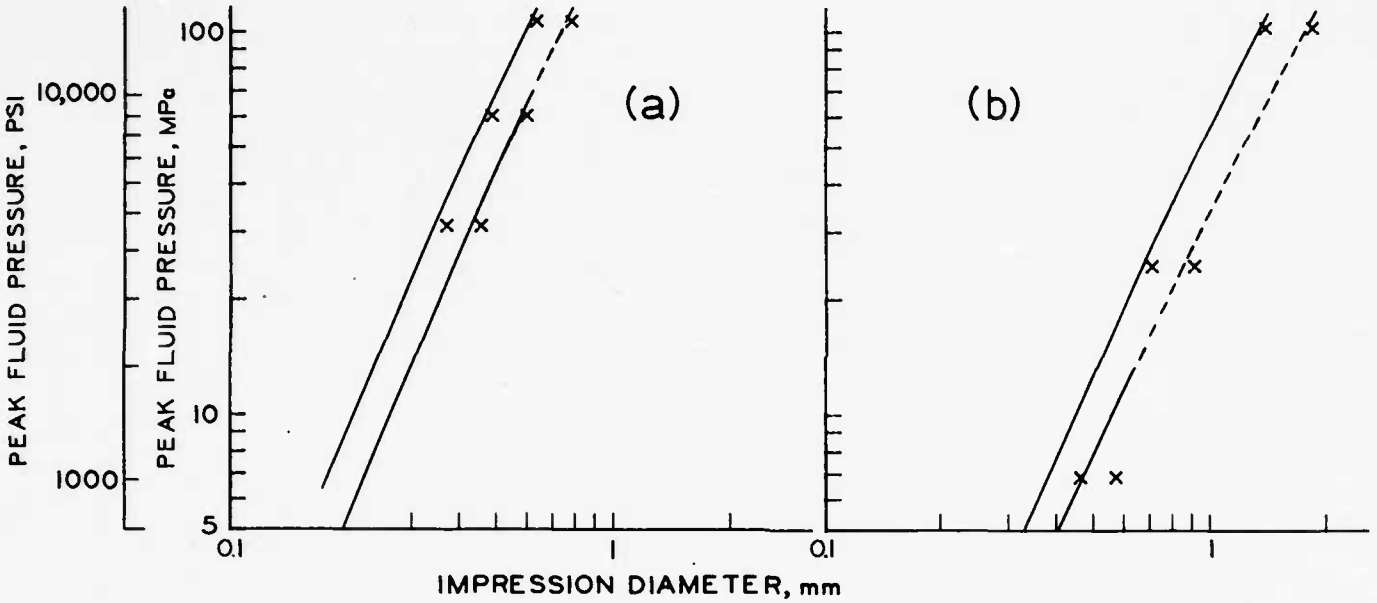

Figure 6.1. Dynamic tests of the Brinell Sandwich soil stress gage in Reid-Bedford sand. (a) High-ranged gage, with balls closely packed, (b) lower-ranged gage, 3.875 balls per sq cm (25 per sq in.), separated by a spacer. The lines are from calibrations in hydraulic fluid (Figures 4.2 and 4.3).

CHAPTER 7

STATIC AND DYNAMIC TESTS WITH A SINGLE BALL

7.1 PURPOSE

The objective of this part of the investigation was to devise a method of subjecting the aluminum alloys 7075-T6 and 6061-T6 to dynamic ball indentations with half sine pulses of known magnitude and rise times of 0.1 and 0.2 msec, and to investigate possible dependence of the relationship between peak load and indentation diameter on input rise time and duration.

7.2 EXPERIMENTAL SYSTEM

7.2.1 Apparatus. The apparatus selected for use in this study had to be economical and easily assembled due to time and budget constraints. Due to its simplicity, a pendulum was designed for the loading device.

One possible choice for the loading device, the split Hopkinson's pressure bar, was rejected for the following reasons:

a. The inherent problems associated with a large mismatch between specimen size and bar diameter as noted by Yeung Wye Kong, Parsons, and Cole (Reference 72).

b. Anticipated problems with multiple impacts.

c. Necessity of converting stress and strain values to the quantities of interest, i.e., load and indentation diameters.

d. Lack of available space.

e. Costs.

7.2.2 General Description. The pendulum consisted of either a 45- or a 113-gram steel bob supported by four 3-metre lengths of nylon cord. The bobs were machined to hold a Rockwell test machine ball holder. The indenter was a 2.5-mm-diameter hardened steel ball manufactured for Rockwell and Brinell hardness testing and was secured to the Rockwell fixture by a threaded sleeve, shown in Figures 7.1 and 7.2.

The load sensing element consisted of four strain gages symmetrically epoxied to the Rockwell ball holder shank and wired as a 4-arm

Wheatstone bridge with two gages sensing in the axial and two in the circumferential directions, as shown in Figure 7.3.

The signal conditioning instrumentation consisted of a WES-designed DC amplifier and a ±15-volt DC power supply. The recording medium was a Tektronix Model 551 oscilloscope equipped with a Polaroid camera.

A reaction mass was machined from a 11.4-cm-diameter, 1.3-metre-long steel bar and fitted with clamps to hold the aluminum test specimens and a photocell with light source, as shown in Figures 7-9. The purpose of the photocell and light source was to provide a trigger for the oscilloscope.

7.2.3 Specifications. The specifications of various parts of the system are as follows:

7.2.3.1 Load Sensor.

a. Strain gages: Micro Measurements Model EA-06-050AH-120

b. Epoxy: M-Bond AE10/15

c. Material: High-strength steel

d. Sensitivity: 0.56 μV/V/N

e. Weight: Body and wires = 5.08 gram
Ball = 0.07 gram
Retainer = 0.38 gram
Total = 5.53 gram

f. Static calibration: The load sensor was statically calibrated against a Baldwin-Lima-Hamilton secondary standard load cell of 4448-N (1000-lb) capacity. The loads were applied by a hydraulic jack with the load sensor and standard load cell supported in a rigid frame. The load sensor and standard load cell were read out on two Doric Model DS100T2 digital voltmeters. The static calibration curve is presented in Figure 7.7. After the loading cycle was completed, one arm of the Wheatstone bridge was shunted with precision resistors to produce electrical output equivalent to several load levels. These resistors are later shunted across the same bridge arm to establish load range on the oscilloscope before the impact tests.

7.2.3.2 Signal Conditioner.

a. Schematic diagram: Shown in Figure 7.8

b. Frequency response: Flat ±5 percent DC to 50 kHz, as shown in Figure 7.9

7.2.3.3 Oscilloscope.

a. Model: Tektronix 551

b. Measured frequency response: Flat DC to 5 MHz on DC input mode

7.2.3.4 Reaction Mass. It was desired to make the length of the reaction mass such that the time required for the return of the stress wave generated by the impact should be in excess of the duration of contact between the ball and specimen, that is, $t > 0.2$ msec. Assuming the stress wave velocity of steel is

$$c = 5000 \text{ m/sec}$$

and with

$$t = 2\,L/c$$

where L is the length of the bar, we have, for $t > 0.2$ msec,

$$L > 0.5 \text{ metre}$$

An 11.4-cm-diameter steel bar was available with $L = 1.3$ m. This bar was considered conservatively adequate for use as the reaction mass. Reflections from the supports were minimized by supporting the bar on ribbed rubber iso-pads. The edge on the impact face of the bar was beveled at 45 degrees to promote dispersion of radial stress waves. The steel bar was harder (200 Brinell as determined by a portable hardness tester) than the 7075-T6 and 6061-T6 aluminum alloys being investigated (Reference 67).

7.3 FEASIBILITY STUDY

7.3.1 Scaling. In order to relate the deformation properties of the passive stress gage to those of a single ball indentation, several transformations are required. An outline of these transformations follows.

Because the stress-strain curves for the gage in Figure 5.1 are very nearly linear, the curve for a gage with balls closely packed and

both inserts 7075-T6 (Figure 5.1b) was approximated by a modulus of 13100 MPa, for pressures in the 350-MPa range. Subtracting out strains in the aluminum gage body raises this to 16200 MPa. Given

modulus E = 16200 MPa

gage thickness T = 15.2 mm = 0.0152 m

ball density D = 20.305 balls/cm^2 = 203050 balls/m^2

the single-ball 7075-T6 indentation spring constant k during loading is given as

$$k = 2\left(\frac{E}{T}\right)\frac{1}{D} = 10.5 \text{ MN/m} \qquad (7.1)$$

The factor 2 in the equation is required due to the impressions in the two aluminum inserts in the gage.

The balls used in the passive stress gage have diameters of 2.38125 mm (3/32 in.). The balls used with the pendulum load sensor have diameters of 2.5 mm as required by the Rockwell fixture's dimensions. The 2.5-mm-diameter balls are not available in the United States and must be ordered from Europe. The 2.38125-cm-diameter balls are used in the actual gage because of the large number required, their availability and low cost as compared with the 2.5-mm-diameter balls.

To preserve geometric similarity in comparing indentations caused by balls of 2.38125-mm and 2.5-mm diameter, relative dimensions must be scaled. This scaling is accomplished for forces (F) as the square of the diameter ratio and for displacements (Δ) as the ratio of diameters (Reference 73). This is given in equation form as

$$F_{2.5 \text{ mm}} = F_{2.38 \text{ mm}}\left(\frac{2.5 \text{ mm}}{2.38 \text{ mm}}\right)^2$$

$$\Delta_{2.5 \text{ mm}} = \Delta_{2.38 \text{ mm}}\left(\frac{2.5 \text{ mm}}{2.38 \text{ mm}}\right)$$

$$k_{2.5} = \frac{F_{2.38}\left(\frac{2.5}{2.38}\right)^2}{\Delta 2.38\left(\frac{2.5}{2.38}\right)}$$

$$k_{2.5} = 1.05\, k_{2.38} = 11.0 \text{ MN/m} \qquad (7.2)$$

This spring constant is that of a single 2.5-mm-diameter ball indenting a single 7075-T6 aluminum specimen.

The spring constant for the shank of the load sensor (where the strain gages are located) was calculated as 125.6 MN/m. The resulting spring constant of the ball-indentation and shank in series is given by

$$k_{loading} = \frac{1}{\frac{1}{k_{ball\text{-}indent.}} + \frac{1}{k_{shank}}} \approx 10.1 \text{ MN/m} \qquad (7.3)$$

7.3.2 Prediction of Rise Time and Fall Time. For this purpose, the load sensor, bob, and reaction mass can be represented by a model consisting of a rigid reference plane (the reaction mass), a spring with force constant k (indentation, ball, and shank in series), and a mass M (that of the load sensor and bob). The natural frequency f of an undamped single degree of freedom system is given by

$$f = \frac{1}{2\pi}\sqrt{\frac{k}{M}} \qquad (7.4)$$

The natural period is $1/f$ and the rise time is

$$t_{rise} = \frac{1}{4f} .$$

For $K = 10.1$ MN/m (from equation 7.3), the rise time is given by

$$t_{rise} = \frac{1}{\frac{2}{\pi}\sqrt{\frac{10{,}100{,}000}{M}}} \qquad (7.5)$$

where M must be in kilograms. The spring constant for a single 2.5-mm ball and 7075-T6 indentation during unloading is similarly obtained from the stress-strain curve in Figure 5.1b after having subtracted out the plastic strain. The result is

$$k_{unloading} = 39.5 \text{ MN/m}$$

The fall time for the system is given by

$$t_{fall} = \frac{1}{\frac{2}{\pi}\sqrt{\frac{39{,}500{,}000}{M}}} \qquad (7.6)$$

Comparing equations 7.5 and 7.6, it is seen that

$$\frac{t_{fall}}{t_{rise}} = \sqrt{\frac{10,100,000}{39,500,000}} \qquad (7.7)$$

and

$$t_{fall} = 0.506\ t_{rise} \ .$$

Table 7.1 was constructed by means of equations 7.5 and 7.6 for bobs weighing 45 grams and 113 grams and several desired peak force levels.

7.3.3 Mechanical Aspects of the Accuracy of the Force Measurement. Referring to Figure 7.10, a fundamental question arises concerning the relationship between the force at the ball-specimen interface and the measured force at the location of the strain gages.

The behavior of the system during the loading portion of the pulse may be analyzed as a free vibration problem. Considering the reaction mass as fixed, the motion of the load sensor and bob system can be represented as a superposition of its normal modes. Zero damping is assumed as the worst case. Letting y_i represent the displacements from equilibrium position of various points i within the system, and $\dot{y}_i$ the corresponding velocities, the following initial conditions are established:

$$\text{at time } (t) = 0$$
$$\text{all } y_i = 0$$

and

$$\text{all } \dot{y}_i = V_o$$

where V_o is the velocity before impact. These initial conditions arise from the fact that the load sensor and bob system is not vibrating and is moving with velocity V_o before making contact with the specimen. These initial conditions determine the amplitudes of the various normal modes of the system.

For any given normal mode, the ratio of the force at the ball-specimen interface to the force at the center line of the strain gages is the same as in the steady-state response of a single degree of freedom composed of the spring constant during loading k and the lumped mass m between the gage center line and the indentation (Figure 7.10). From equation 7.3

$$k \approx 10.1 \text{ MN/metre}$$

With the mass of this portion of the system (0.82 gram), equation 7.4 gives

$$f_n = \frac{1}{2\pi}\sqrt{\frac{10,100,000}{0.00082}} \approx 18 \text{ kHz}$$

where f_n is the natural frequency of this single degree of freedom system. An expression for the steady-state response of such an undamped system is given by Dove (Reference 74) and others as

$$\frac{-kX_j}{F_j} = \frac{1}{1 - \left(\frac{f_j}{f_n}\right)^2} \tag{7.8}$$

where X_j is the displacement of the lumped mass between the gage center line and the indentation, for mode j, F_j is the corresponding force due to mode j at the strain gage location, and f_j is the frequency of mode j. Equation 7.8 predicts very high values for the ratio $-kX_j/F_j$ when $f_j/f_n \approx 1$. Therefore, a mode of the total system (the bob and load sensor) around 18 kHz may go undetected by the strain gages and yet produce a significant force amplitude at the indentation. This condition may be interpreted as the existence of a stress node at the center line of the strain gages in any 18-kHz longitudinal normal mode of the system.

Since an elastic bar, in this case the pendulum bob, has an infinite number of normal modes, a complete analysis is much easier for models consisting exclusively of lumped masses. Such a simplified model of the load sensor and bob system was formulated by dividing the mass of the bob into two lumped masses concentrated at the ends; details are in Appendix E. Different values were assigned for the spring constant of the bob. In one case, two 22.5-gram masses were assumed to be concentrated at the ends of a spring with a force constant of 140 MN/in. This combination was chosen to produce an 18-kHz normal mode. (A 45-gram steel bob of 5-cm length would have a spring constant of about 490 MN/m.) This combination provided a conservative prediction of less than 1 percent for the force amplitude ratio at the

indentation of second to first normal mode. This prediction assumes no hard secondary impacts such as those due to any looseness between bob and load sensor. Although this model does not accurately represent the experimental system, it does indicate that the effects of normal modes higher than the first are expected to be small.

By means of equations 7.8 and 7.4, the ratio of the force at the ball-specimen interface to the force at the strain gage location for the lowest mode can also be calculated as a function of the ratio of the mass m to the left of the gage center line (Figure 7.10), to the total mass M of the load sensor and bob system. This is given in equation form as

$$\frac{-kX_1}{F_1} = \frac{1}{1 - \left(\frac{f_1}{f_r}\right)^2} = \frac{1}{1 - \left[\frac{\sqrt{\frac{k}{M}}}{\sqrt{\frac{k}{m}}}\right]^2}$$

Since the k's are very nearly the same, this can be reduced to

$$\frac{-kX_1}{F_1} = \frac{1}{1 - \frac{m}{M}} \quad .$$

Note that the same result is obtained if the load sensor and bob are assumed to be rigid. That is, referring to Figure 7.10, the ratio of total mass to the mass right of the strain gage center line is

$$\frac{M}{M - m} = \frac{1}{1 - \frac{m}{M}} \quad .$$

Using 0.82 gram (calculated from load sensor dimensions, Figure 7.2, and the density of steel) for m, this ratio becomes

$$\frac{-kX_1}{F_1} = 1.018$$

for the 45-gram bob and

$$\frac{-kX_1}{F_1} = 1.007$$

for the 113-gram bob. All dynamic data were corrected by these respective ratios.

The bobs (shown in Figure 7.11) were made as short as possible without sacrificing stability during the swing. The lengths of both the 45- and 113-gram bobs were 4.6 cm. The frequency of the first normal mode of a free bar of this length would be given by

$$\frac{c}{2L} \approx 50 \text{ kHz}$$

where c is the sonic velocity in steel and L is the length of the bar. This frequency would very nearly equal the frequency of the second normal mode of the system with the ball in contact.

The effects of this mode should also be examined. Referring again to equation 7.8, for $f_j = 50$ kHz and $f_n = 18$ kHz

$$\frac{-kX_2}{F_2} = -0.15 \quad .$$

This means that if the 50-kHz mode were superimposed on the data at 1 percent the amplitude of the fundamental frequency, the difference between the peak as seen by the strain gages, and the peak at the indentation would be at most 1.15 percent.

In summary, the difference between the actual force at the indentation and the force read by the strain gages due to longitudinal modes is expected to be less than 2 percent.

Some transverse modes are predicted for the load sensor and bob systems. These may be calculated by approximating the systems as free beams with 5-cm lengths and constant cross sections (Reference 62) as follows:

45-gm bob (1.37-cm-diam)

$$f_{\text{transverse}} = 23 \text{ kHz}$$

113-gm bob (2.03-cm-diam)

$$f_{\text{transverse}} = 34 \text{ kHz} \quad .$$

Due to possible lack of alignment of the load sensor and bob axis with the direction of motion, some excitation of transverse modes is

possible. However, their effect on the longitudinal forces is expected to be insignificant. When approximated as a cantilever beam with 0.40 cm (0.158 inch) diameter and 1.11 cm (0.44 inch) length, the load sensor is also predicted to exhibit a 23-kHz mode (Reference 62); this is expected to enhance the sensitivity of the load sensor to a 23 kHz transverse mode while the ball is not in contact.

7.4 PROCEDURE

The aluminum alloy specimens were cut to fit the clamps attached to the reaction mass. The 7075-T6 and 6061-T6 specimens were cut from the same respective sheets of material as the inserts used in the tests in hydraulic fluid (Chapter 4). The axial tension bolt fastening the load sensor to the bob was tightened to a torque of 2.26 N-m (20 in.-lbs), providing an estimated preload of 3100 N (700 lbs). A specimen was clamped to the reaction mass, the pendulum cords were adjusted so that the bob and load sensor position was centered on the sample and interrupted the light beam. The oscilloscope vertical amplifier gain was adjusted for the expected load range. This adjustment was accomplished by shunting resistors across a sensor bridge arm to simulate loads of approximately 50 and 100 percent expected load range. The scope beam was swept at 1 cm/sec as the resistors were sequentially shunted. With the camera lens open, this produced calibration "steps" that were later used to scale the data photographs.

Next, the scope trigger level was adjusted so that as the bob was pulled away from the specimen and gently returned, the light beam was interrupted and the resulting signal from the photocell triggered the scope. This was the most difficult step in the procedure. Performed correctly, this adjustment permits the load-time wave form to be captured on film. The trigger level required readjustment for different release heights of the bob and different scope sweep speeds.

Once correct trigger level adjustment was attained, the camera lens was opened and the bob raised to a given height and released. The operator could observe the scope screen through a viewing port and see that the load-time wave form was presented within the lens range before

advancing the film. The bob was caught by the operator after rebounding from the specimen and gently returned to the rest position. Light oil (3-in-1) was applied to the ball before each impact, as well as in the static tests. This was done because the balls as used in the gage are coated with light oil (Appendix B).

The successful prints were numbered to correlate with their respective indentations and labeled with their load sensitivity and sweep speed, then coated with a preservative. The peak loads were scaled and recorded. After a number of load-time photographs were made, the specimens with numbered indentations were moved to another area where the indentations were measured through a 56X-80X-160X binocular microscope. As in Brinell hardness testing (Reference 17), the indentation diameters were measured in mutually perpendicular directions. These lengths were averaged and multiplied by the magnification factor to give the diamter of the indentation in mm. Any asymmetric buildup of material at the edge of the indentation or elongation of the indentation was noted; either of these conditions was interpreted as an indication of an oblique impact and the corresponding data were discarded.

7.5 RESULTS AND CONCLUSIONS

7.5.1 Results. Dynamic data were taken on 7075-T6 and 6061-T6 specimens using both the 45- and 113-gram bobs. Use of both bobs produced two different inputs with distinct rise times. Some representative pulses are shown in Figures 7.12 and 7.13. Peak loads and corresponding indentation diameters are listed in Tables 7.2 through 7.6.

Modes around 50 kHz (believed longitudinal) and 20 kHz (believed transverse), if detected at all, were of very low amplitude. Measured conservatively, the maximum amplitude of the 50-kHz mode at the peak was less than 1 percent of peak load in the worst case. With the 45-gram bob, a mode around 20 kHz was sometimes detected. This mode, believed to be transverse, was detected only after loading and the maximum amplitude was less than 1/2 percent of peak load. In addition

to predictions, the transverse nature of the 20 kHz mode was also suggested by comparison of output waveforms resulting from impacting the bob longitudinally and transversely with a hammer. The detection of a transverse mode on the output of a load sensor designed for longitudinal measurements is not surprising when it is recalled that the load sensor was predicted to resonate transversely at around 20 kHz.

In order to enhance the detection of higher modes, an Endevco 2264A-20K-R accelerometer was epoxied to the rear of the 45-gram bob. The presence of a 50-kHz mode is readily apparent in Figure 7.14 on the accelerometer output although not clearly discernible on the load sensor output. The 20-kHz mode, while not observed on the accelerometer trace during loading, was seen after loading in a few cases, with a very low amplitude. The location of the seismic mass of the accelerometer was eccentric with respect to the axis of the bob; this made possible the detection of a transverse mode by the accelerometer. The accelerometer data were also used as a rough check on the strain gage load measurement. The amplitudes of the two outputs are compared in Table 7.7.

The small bump at the start of the pulse and the rounding of the corner at the end were more noticeable with lower peak loads; this is demonstrated by comparing Figures 7.13 and 7.14 with Figure 7.12. These are believed to be due to flexural behavior of the aluminum specimen resulting from a small gap between it and the reaction mass at the beginning and end of the pulse. It was not considered practical or necessary to clamp the specimens in such a way as to totally avoid it; indentations in a thin specimen tend to create slight outward convexity. When the ball was impacted directly against the steel reaction mass, these effects were not observed (Figure 7.15).

Figure 7.16, a plot of peak load versus indentation diameter for the 7075-T6 and 6061-T6 alloys, is the main end product of this experiment. Each point from static tests is the average of eight nearly identical loads and indentations, while each dynamic point represents a single impact. Examination of Figure 7.15 indicates no detectable difference between the dynamic and static data for the 7075-T6 alloy

and only a barely detectable difference for the 6061-T6. These findings are very similar to data taken with the dynamic fluid chamber as a loading device (Chapter 4). Similarity is also noted between these data and results with 7075-T6 (References 29 and 44) and 6061-T6 (References 29, 34, 35, and 44) in uniaxial stress compression. These results are also consistent with certain findings of Mok (Reference 40). However, these data do not resemble the findings on rate effects of 6061-T6 alloy in uniaxial stress tension (References 41, 42, and 43).

Uncertainties in this experiment are of either mechanical or electrical origin. The mechanical uncertainties, as stated previously, are believed to be less than 2 percent of peak indicated load. When undetected oblique impact effects are included, the mechanical uncertainties are conservatively estimated at 5 percent. Electrical uncertainties are estimated at 5 percent. This figure is conservative, considering the quality of the equipment and strain gage work in this experiment, but is realistic based on experience in performing similar measurements. Since these two sources of uncertainty are independent, the upper limit on the uncertainties in this experiment is estimated as $\sqrt{(5\%)^2 + (5\%)^2}$, or 7% of the peak load, or, equivalently, peak stress indicated by the Brinell gage.

7.5.2 Conclusions. The objectives of this experiment were met in that the devised apparatus did subject the aluminum alloys 7075-T6 and 6061-T6 to load pulses with 0.1- to 0.2-msec rise times. The results of this experiment indicate that measurements with the Brinell passive stress gage are not influenced by strain rate effects with rise times and durations down to 0.1 and 0.2 msec. The upper limit on experimental uncertainties is conservatively estimated at 7 percent.

When converted to pressure and indentation diameter produced by the 2.38125-mm balls in the actual Brinell gage, these data are in excellent agreement with data obtained in the fluid chamber (Chapter 4). This indicates that static single-ball calibrations are sufficient for all static or dynamic applications to rise times of 0.1 msec and durations to 0.2 msec.

The experiment also proved the validity of the predicted rise and fall times of the load pulses and consequently of the calculated stress-strain curves (Chapter 5) on which these predictions were based.

Table 7.1. Predicted rise times, fall times, and drop heights with 7075-T6.

	Weight (grams)	Rise Time (msec)	Fall Time (msec)	Drop Height (m) for Loads of 1900 N	4000 N
Bob + Sensor, Nominal	45	0.105	0.053	0.39	1.79
Bob + Sensor, Actual	47.8	0.108	0.055	0.37	1.69
Bob + Sensor + Accelerometer Actual	53.8	0.115	0.058	0.33	1.50
Bob + Sensor, Nominal	113	0.166	0.084	0.15	0.71
Bob + Sensor, Nominal	118	0.170	0.086	0.15	0.69

Table 7.2. Static 6061-T6 and 7075-T6 alloys.

Test Number		Mean Load (N)	Indentation Mean Diameter (mm)
7075-T6	1	2676	1.3250
	2	2232	1.2053
	3	1789	1.0821
	4	1341	0.9429
	5	905	0.7783
	6	4040	1.6158
	7	3382	1.4859
6061-T6	1	229	0.5287
	2	451	0.7247
	3	907	1.0292
	4	1810	1.4432

NOTE: Each test is the average of eight nearly identical loads and indentations.

Table 7.3. 7075-T6 alloy - 45-gram bob.

Load (N)	Indentation Diameter (mm)
1299	0.9251
1286	0.9222
1410	0.9599
1379	0.9454
1392	0.9483
1303	0.9106
1837	1.0672
1873	1.0904
1779	1.0672
1873	1.1020
2135	1.1716
2193	1.2006
1997	1.1310
2024	1.1542
2144	1.1861
2162	1.1832
2624	1.3137
2513	1.2760
2544	1.2818
2527	1.2702
2664	1.3282
3020	1.4065
2954	1.3978
2976	1.3891
2691	1.3456
3238	1.4529
3470	1.5283
2633	1.3253
3327	1.4819
3194	1.4645
3532	1.5428
3688	1.5805
3759	1.5515
3750	1.5428
3799	1.5834
4191	1.6356
3674	1.5312
3737	1.5689

Table 7.4. 7075-T6 alloy - 113-gram bob.

Load (N)	Indentation Diameter (mm)
3238	1.476
1842	1.096
2251	1.212
1721	1.067
1561	1.000
1397	0.954
1455	0.974
1183	0.882
1241	0.905
1183	0.887
1094	0.858

Table 7.5. 6061-T6 alloy - 45-gram bob.

Load (N)	Indentation Diameter (mm)
525	0.789
1036	1.061
1192	1.134
1326	1.209
1704	1.372
1855	1.441
1788	1.398
2144	1.537
2086	1.534
2237	1.572
2220	1.560
1343	1.218
1330	1.212
1134	1.122
770	0.919
663	0.870
712	0.887
730	0.896
836	0.974
836	0.957
249	0.537
249	0.548
280	0.568
289	0.589
325	0.600
440	0.705
374	0.648
525	0.786
489	0.745

Table 7.6. 6061-T6 alloy - 113-gram bob.

Load (N)	Indentation Diameter (mm)
836	0.963
1161	1.154
1348	1.206
1290	1.218
1277	1.192
1223	1.163
1570	1.322
1793	1.430

Table 7.7. Simultaneous accelerometer and load sensor loads.

Acceleration (g)	F_{acc} (N)	$F_{L.S.}$ (N)	Diff. (%)
1815	956	956	0
1980	1045	1054	-1
2475	1303	1294	+1
2046	1081	1005	+7
2871	1517	1535	-1
2013	1063	1059	0
2607	1379	1357	+2
1703	899	956	-6
2132	1125	1099	+3
2871	1512	1535	-1
2325	1228	1134	+8
2859	1508	1370	+9
3950	2086	1766	+15
2686	1419	1312	+8
3950	2086	1859	+11

NOTE: F_{acc} = Peak force calculated from the peak acceleration and the total mass (53.8 grams).

$F_{L.S.}$ = Peak load as read from load sensor output.

$$\text{Difference (\%)} = \frac{F_{acc} - F_{L.S.}}{F_{acc}} \times 100.$$

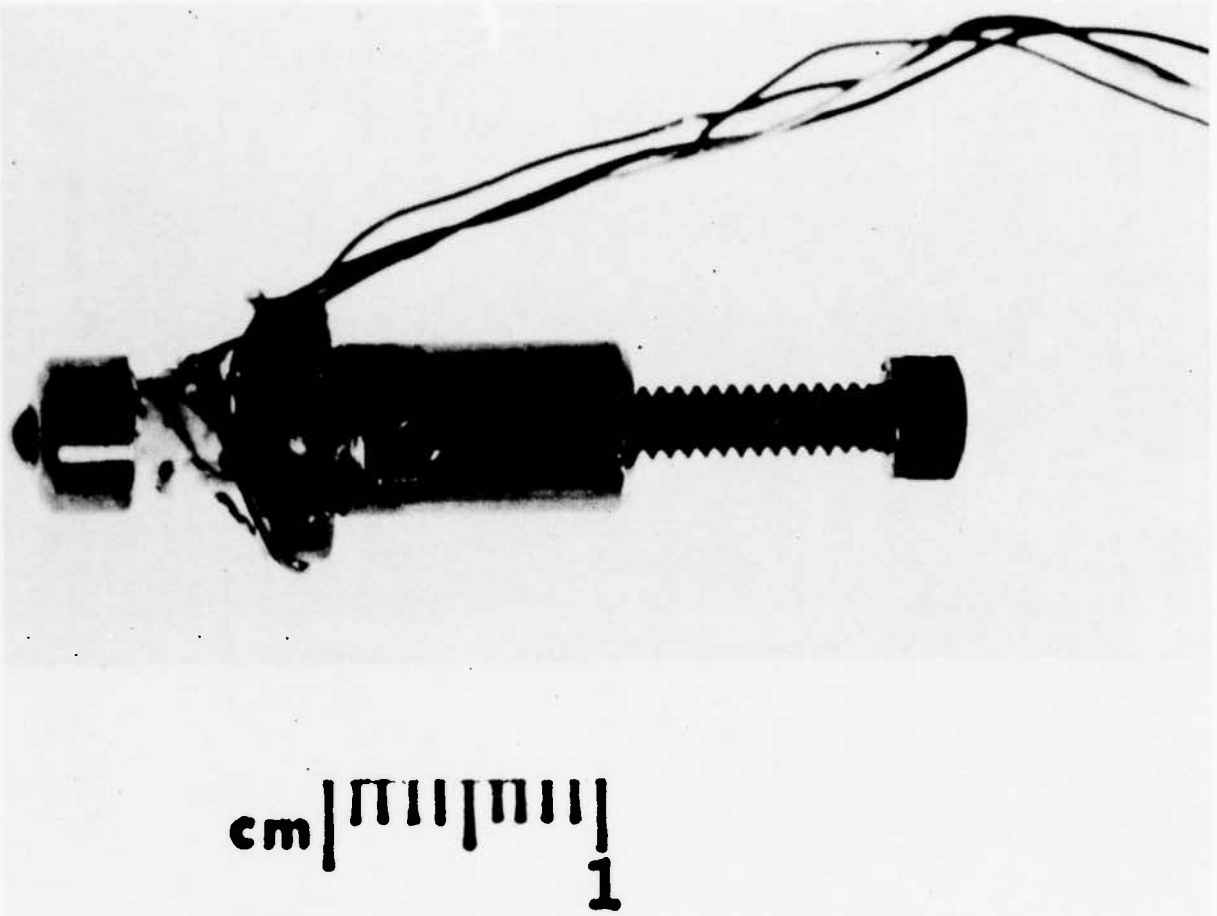

Figure 7.1. Load sensor, with axial tension bolt.

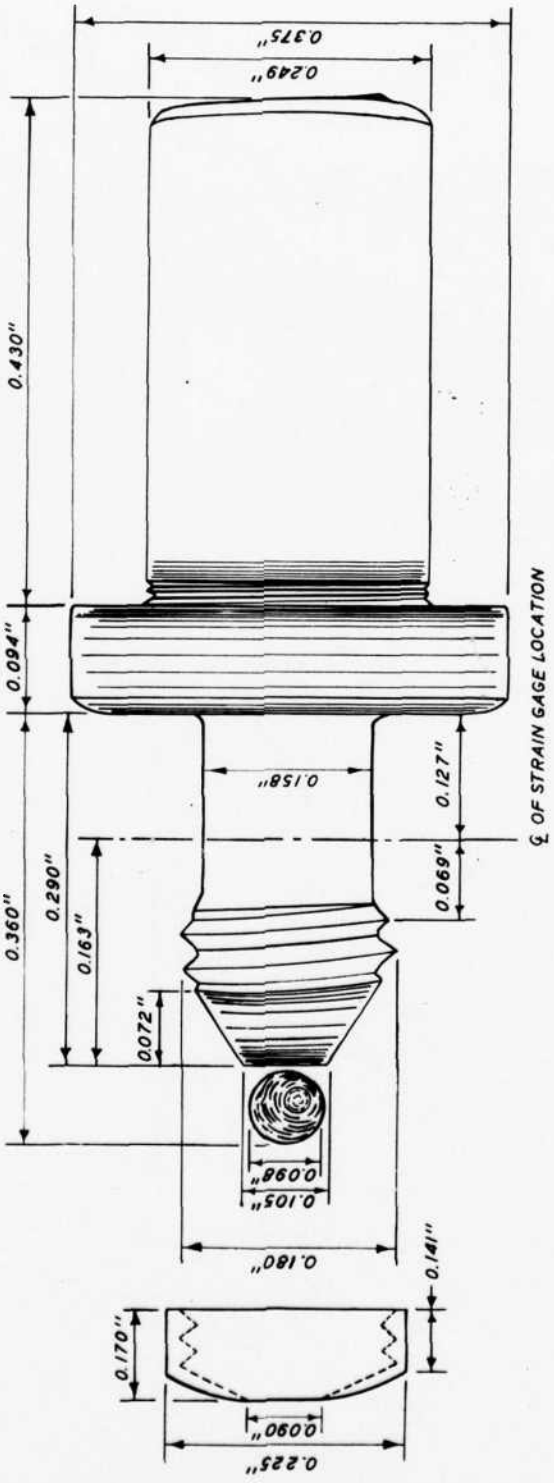

Figure 7.2. Sleeve, ball, and load sensor. Dimensions are in inches.

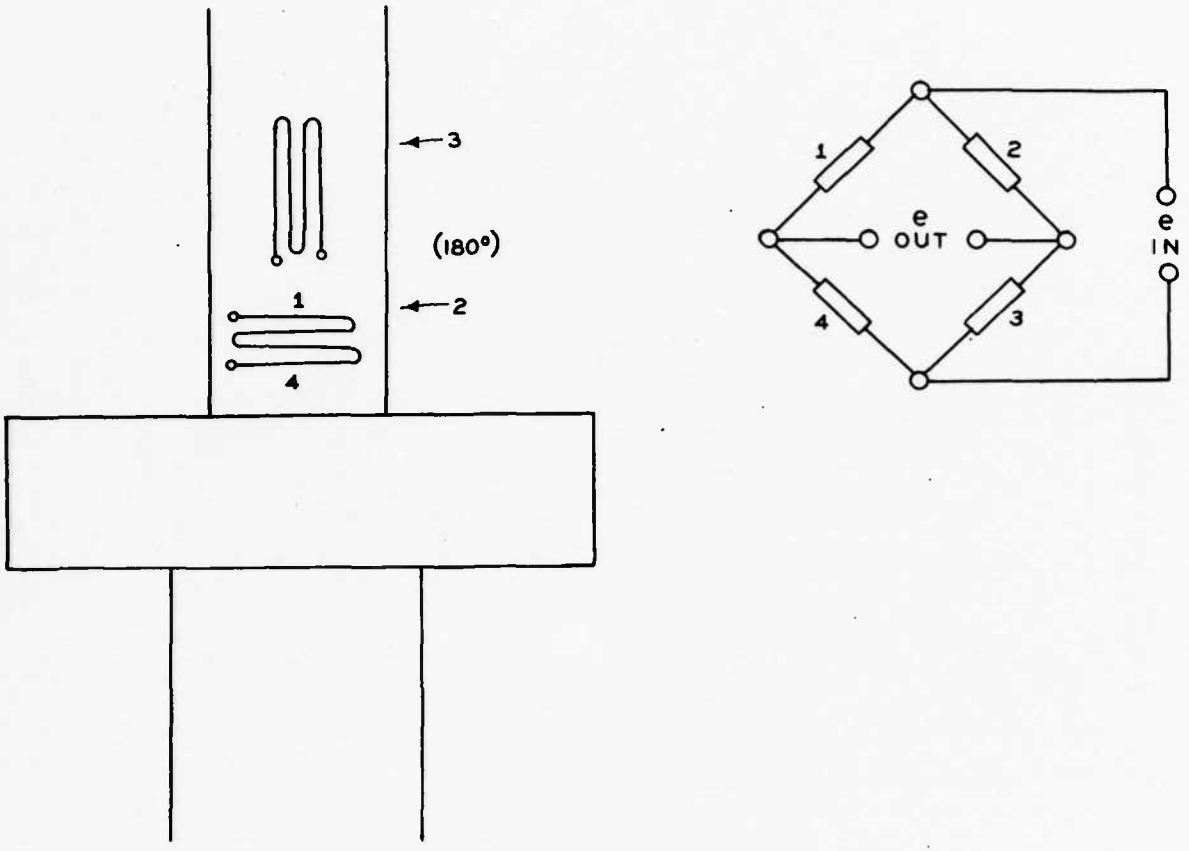

Figure 7.3. Schematic of strain gage locations and circuit.

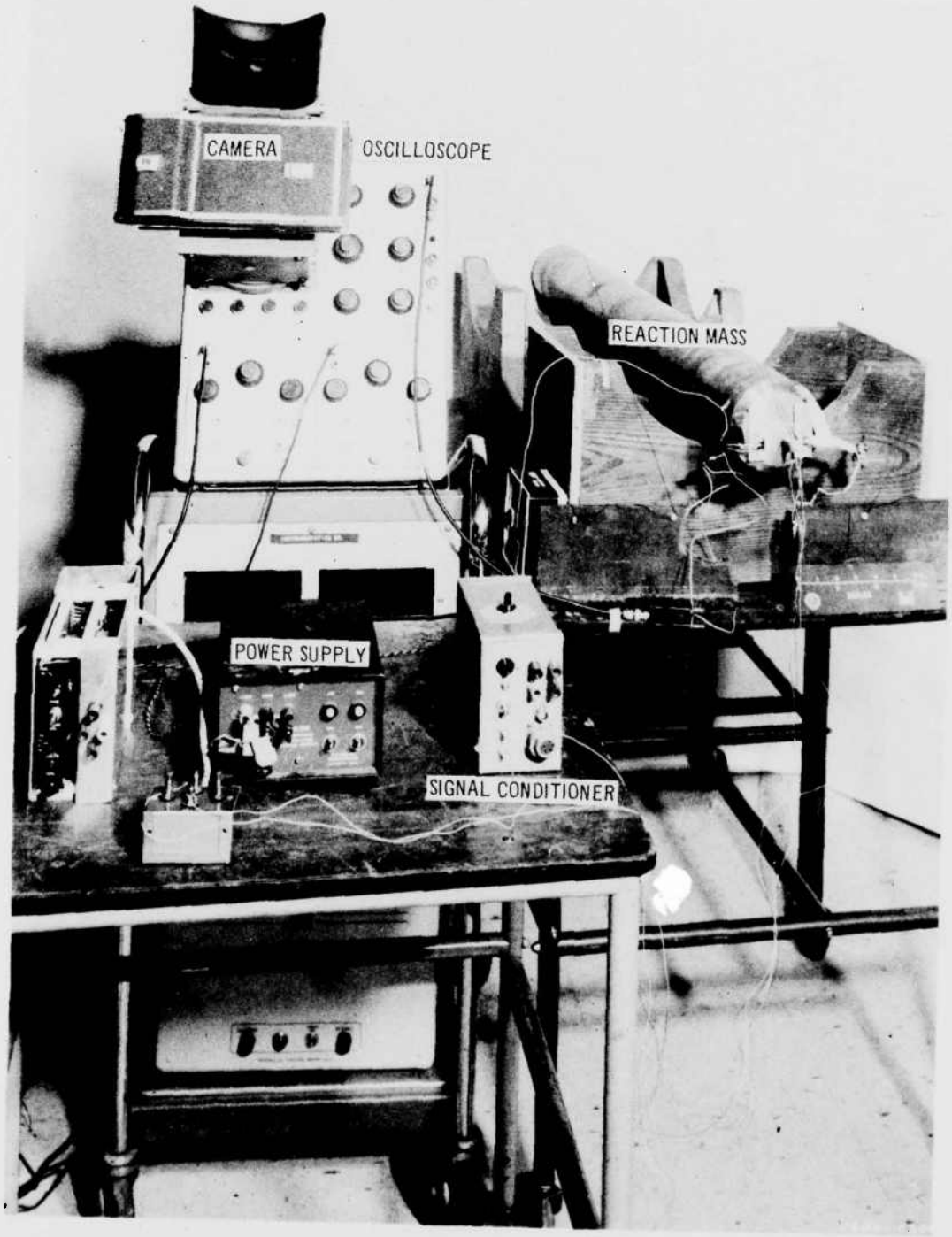

Figure 7.4. Experimental apparatus.

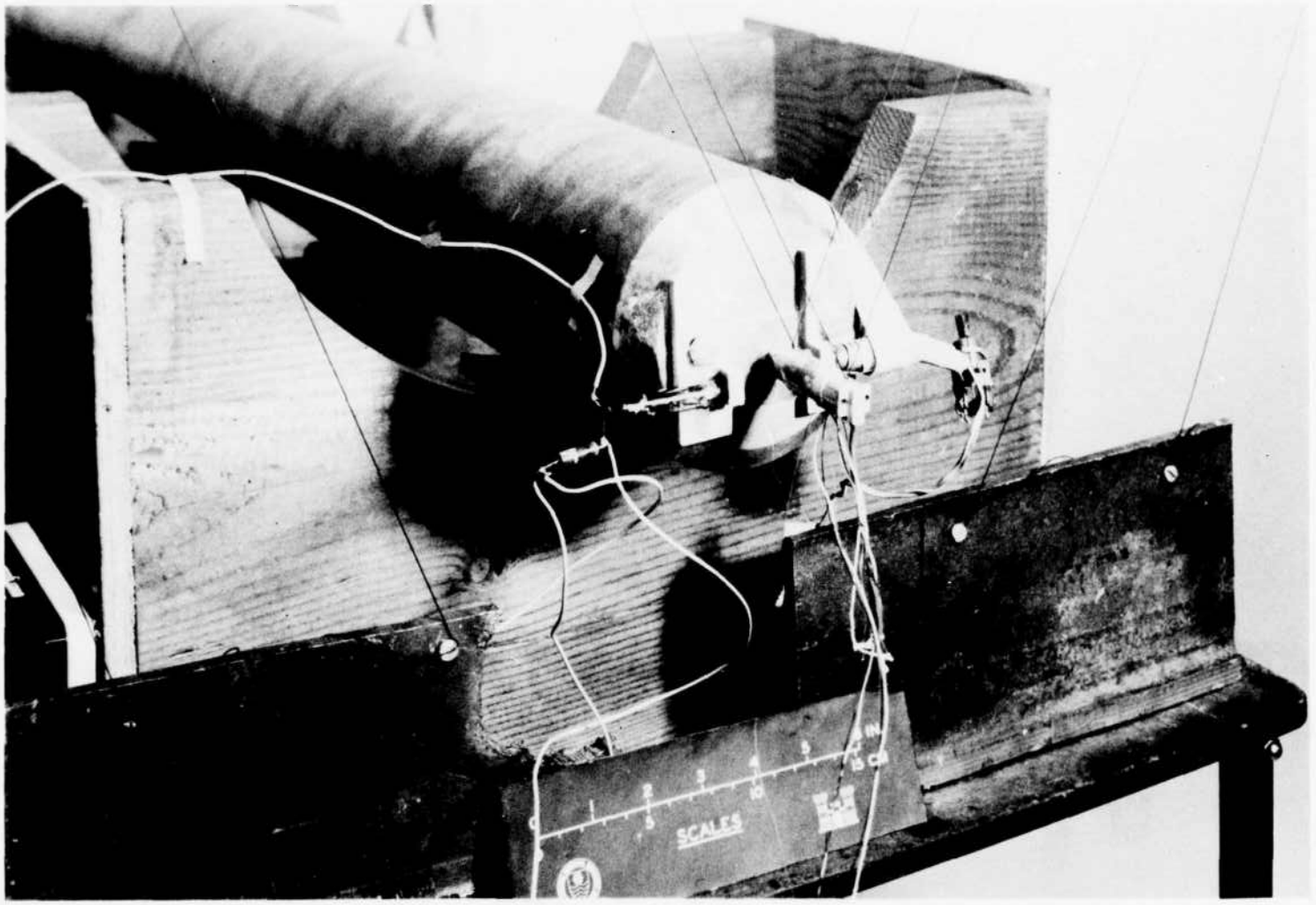

Figure 7.5. Close-up of experimental apparatus.

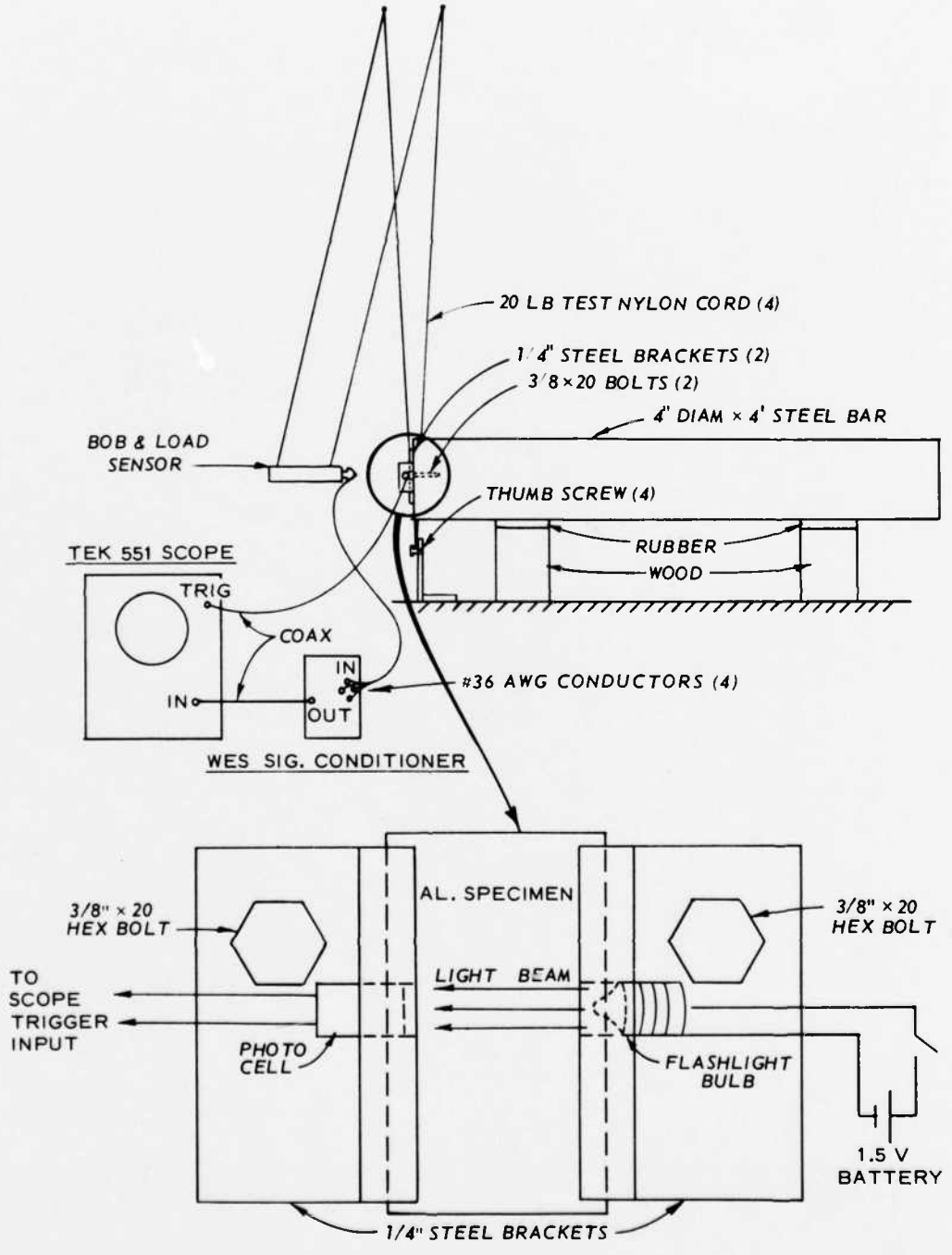

Figure 7.6. Schematic of experimental apparatus.

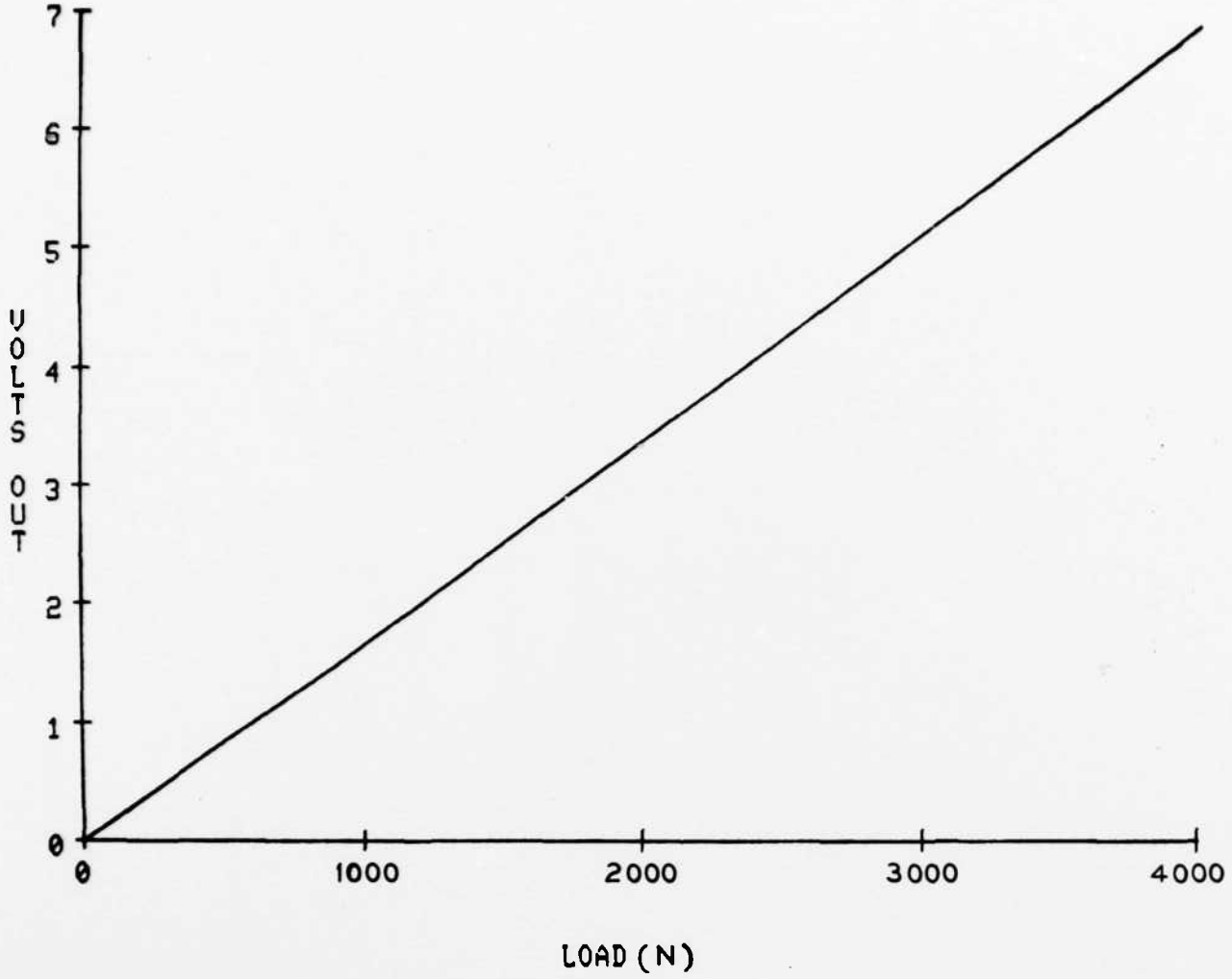

Figure 7.7. Load sensor static calibration plot.

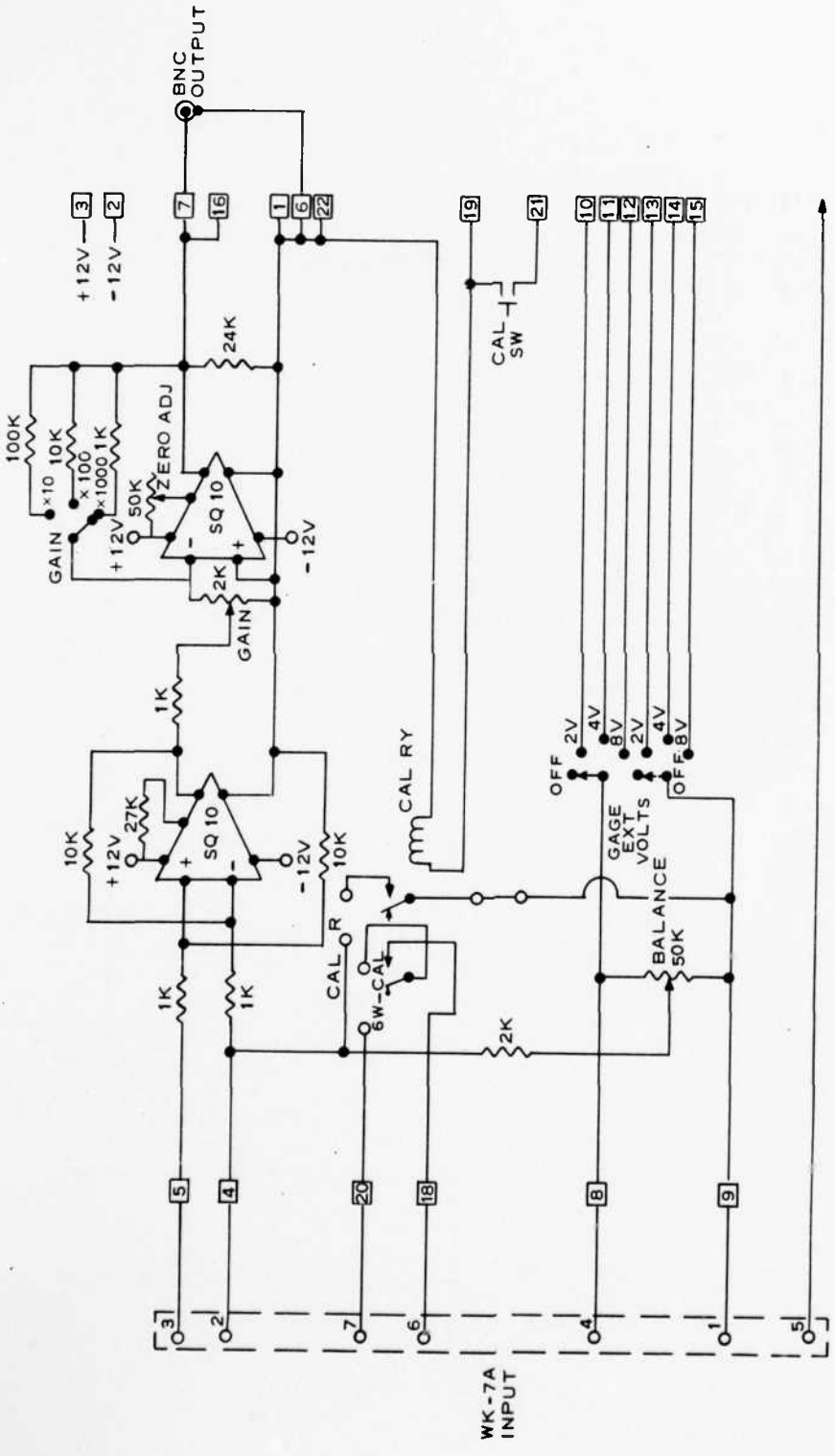

Figure 7.8. Amplifier and signal conditioning module schematic.

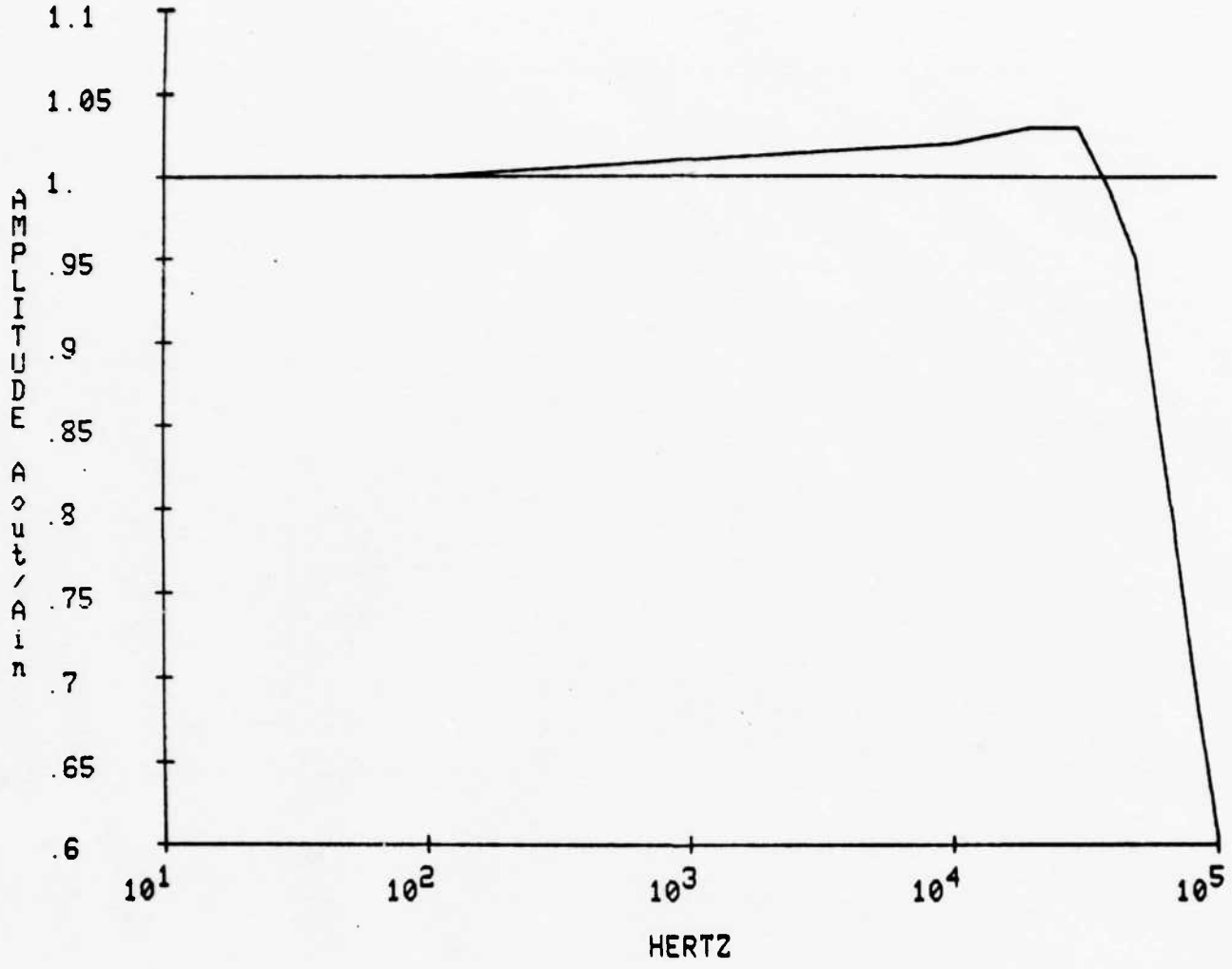

Figure 7.9. Frequency response plot of signal conditioner-amplifier.

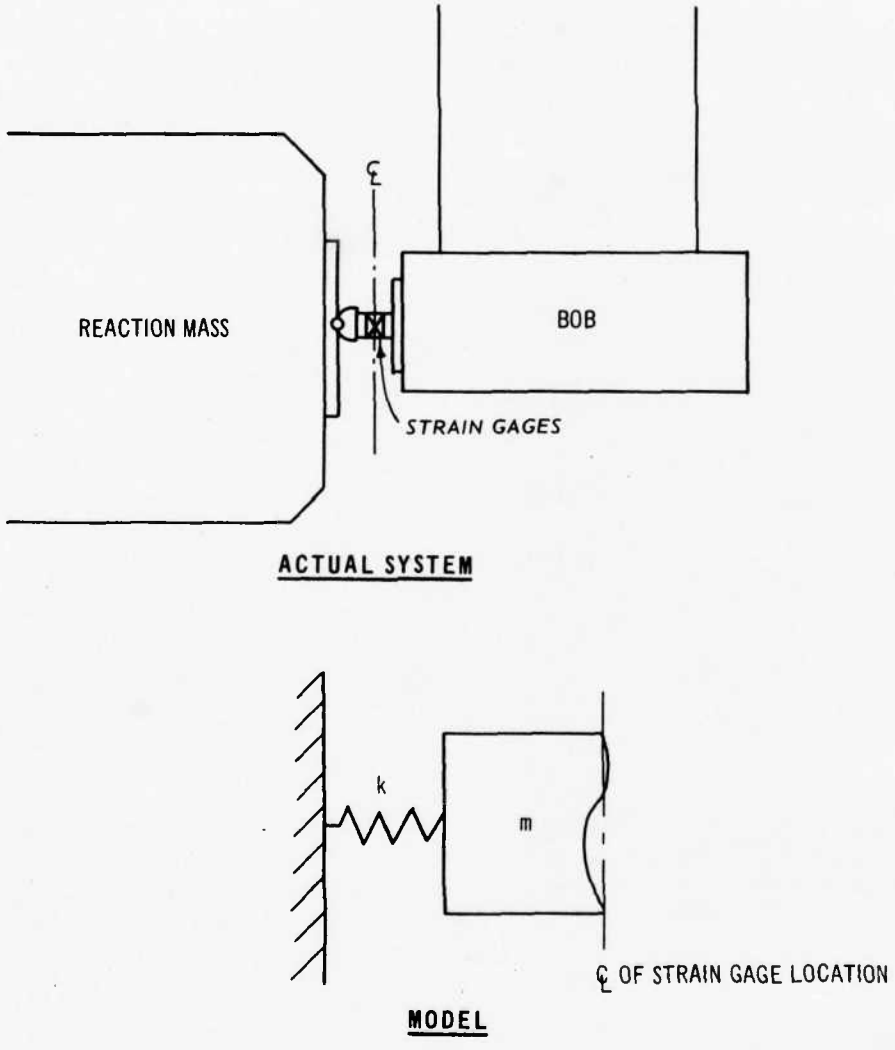

Figure 7.10. Reaction mass, sensor, bob, and model of the part of the system between the strain gage center line and the indentation.

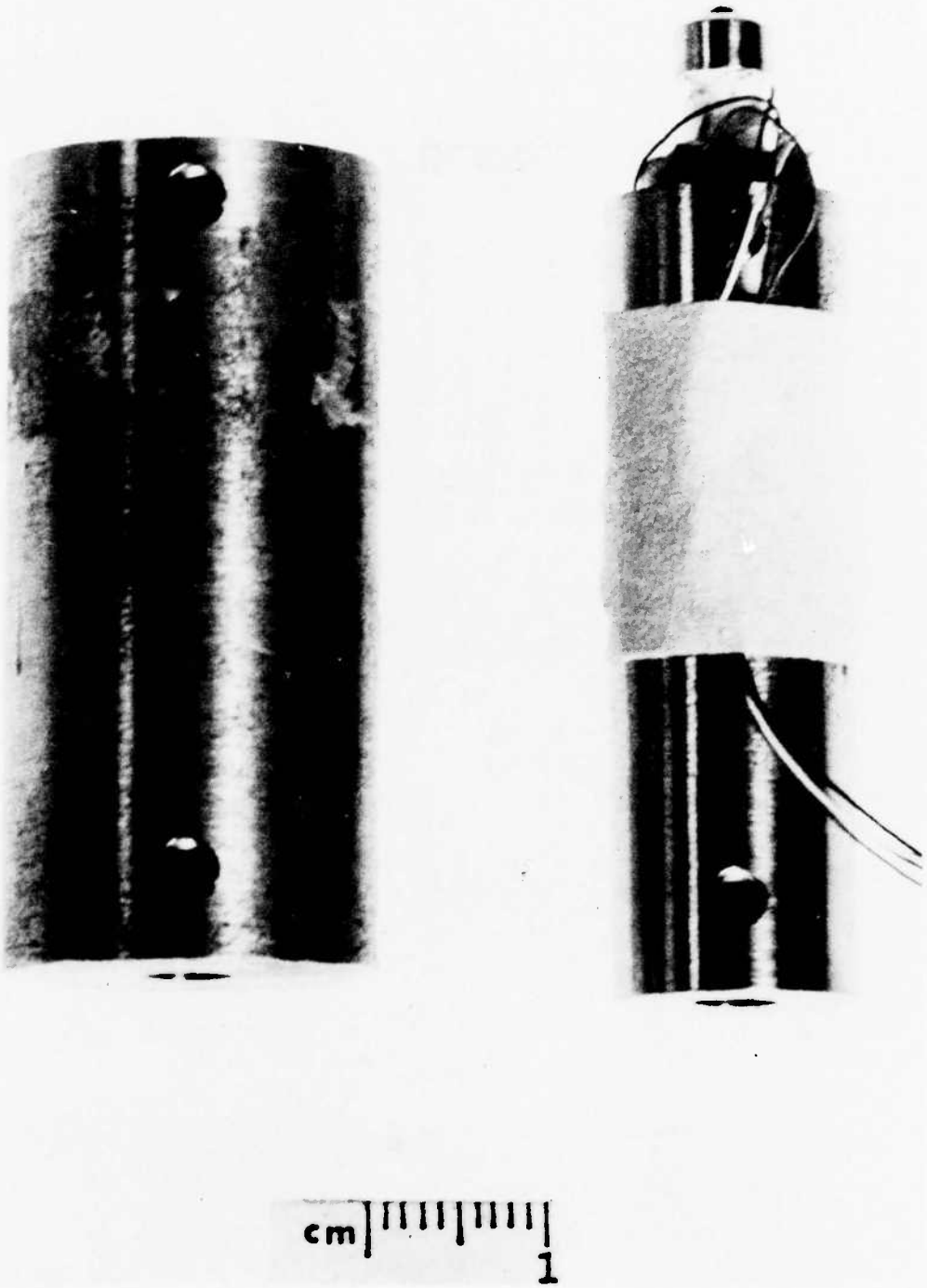

Figure 7.11. Load sensor mounted in 45-gram bob and 113-gram bob.

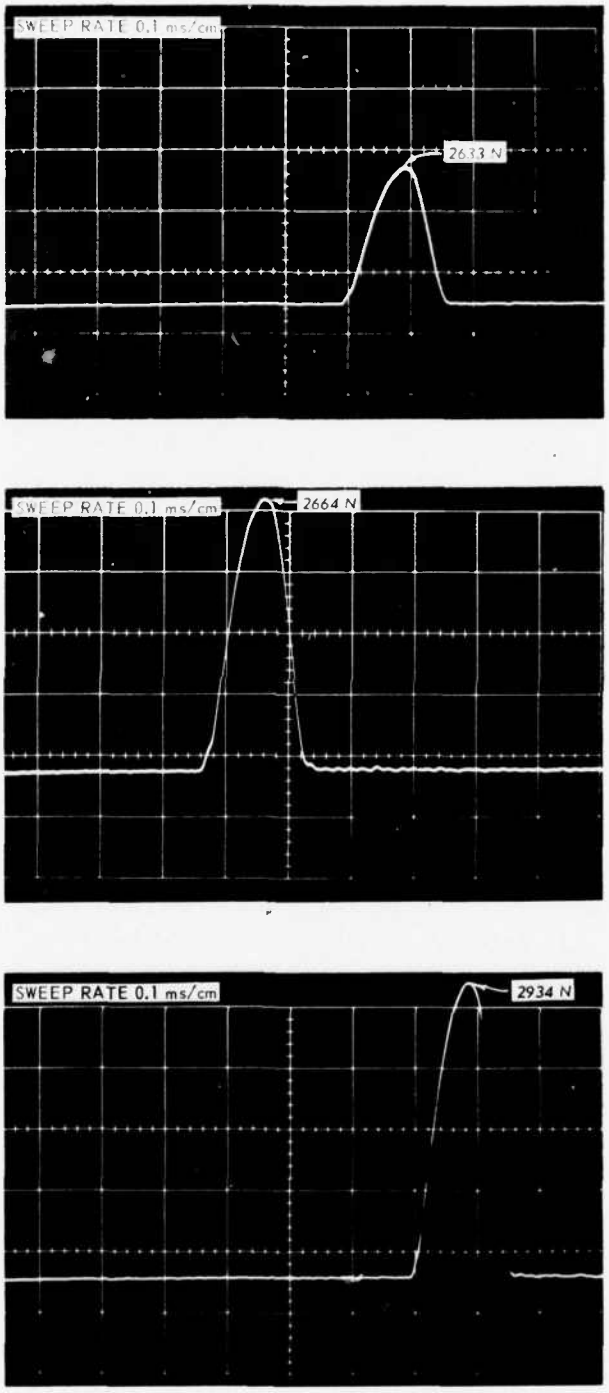

Figure 7.12. 7075-T6, 45-gram bob load-time records.

Figure 7.13. 6061-T6, 113-gram bob load-time records.

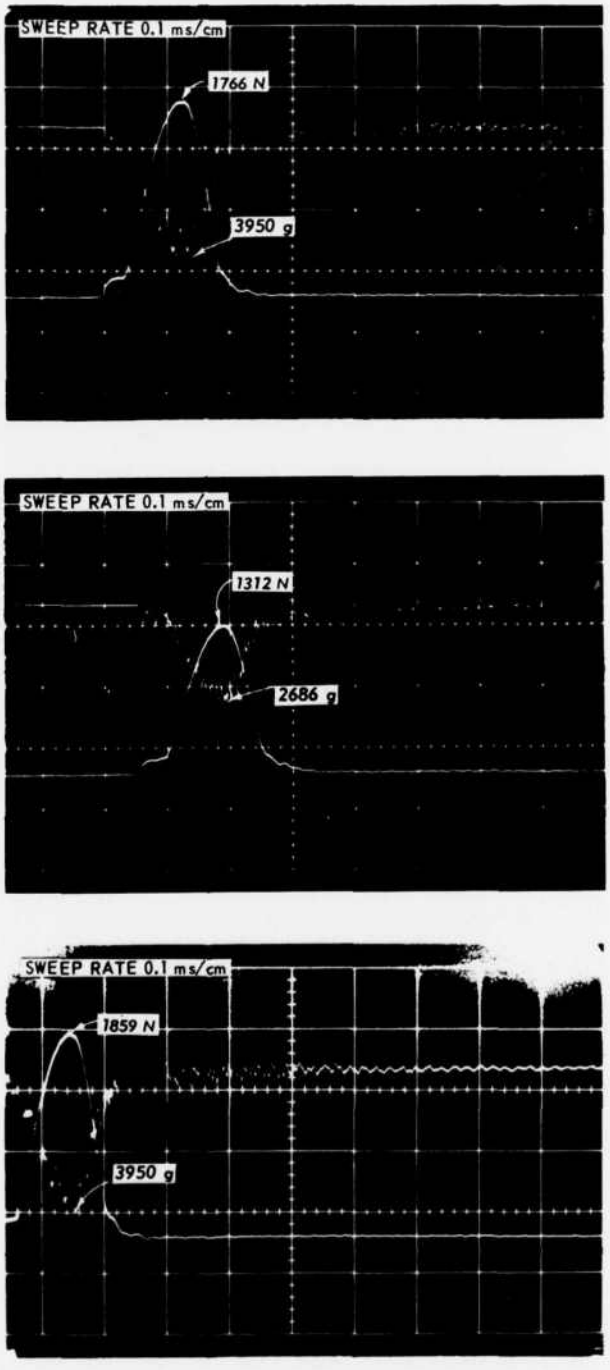

Figure 7.14. 7075-T6 with 45-gram bob and Endevco 2264A-20K-R accelerometer.

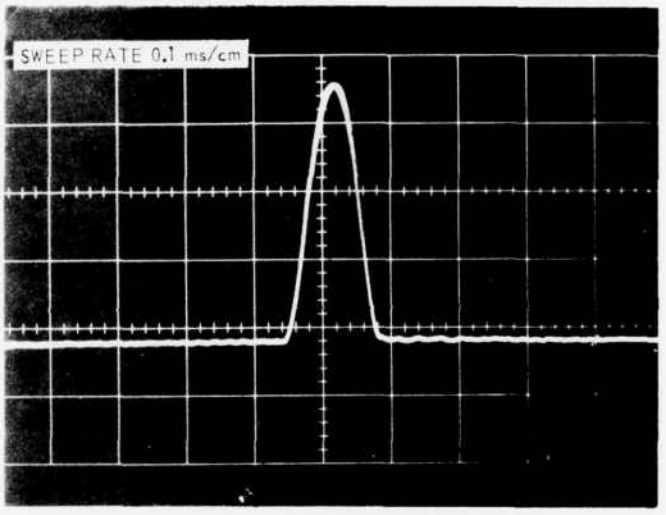

Figure 7.15. 45-gram bob, with the ball impacting the steel reaction mass. Peak load is approximately 2000 N.

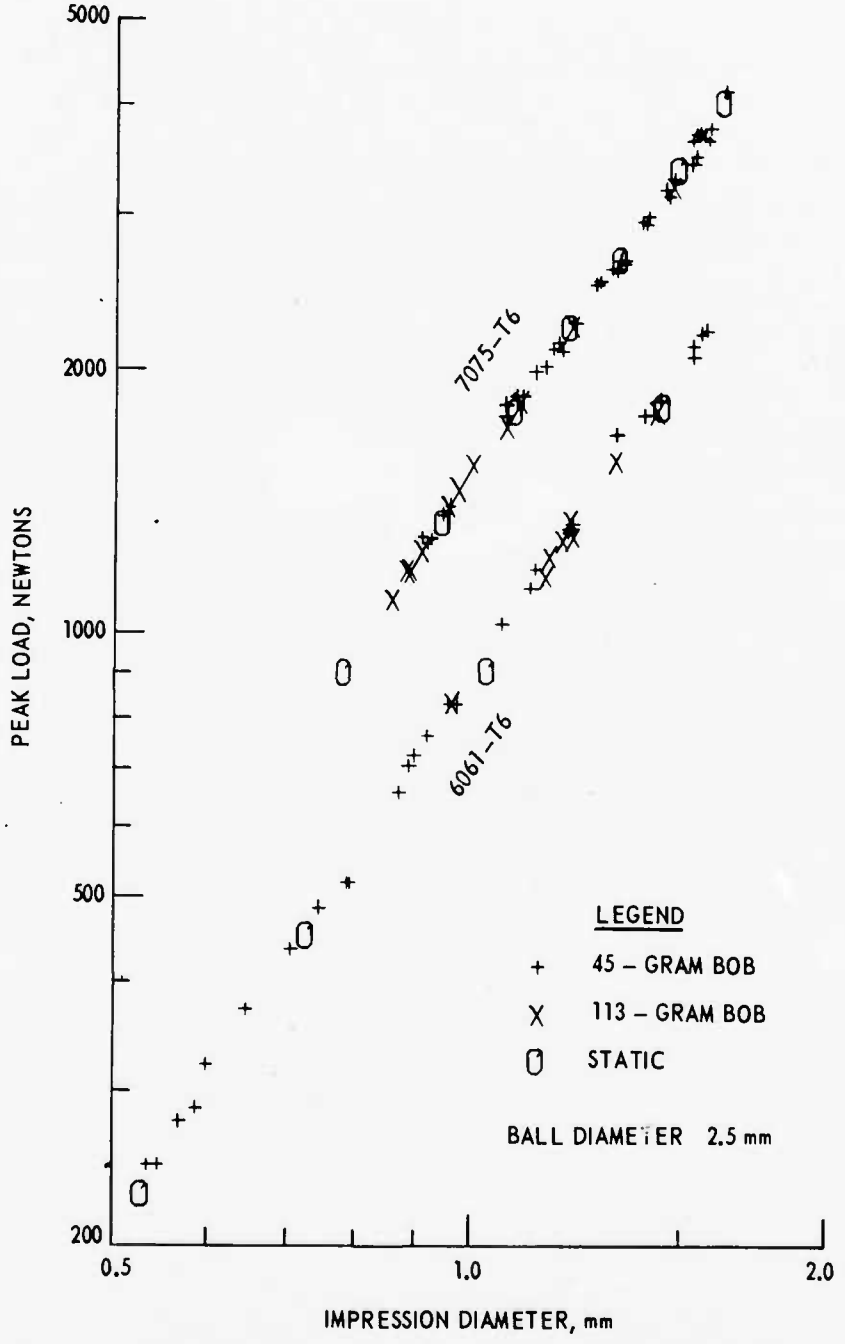

Figure 7.16. Peak load versus impression diameter from static and dynamic tests with a single 2.5-mm ball. Each point from static tests is based on eight nearly identical loads and indentations.

CHAPTER 8

SUMMARY OF PERFORMANCE CHARACTERISTICS

The performance characteristics of the two versions of the Brinell Sandwich soil stress gage are summarized in Table 8.1. The combination of high stiffness, flat geometry, absence of rate effects over a wide range of pulses, and good resolution over a sensing range of more than a factor of 100 makes it possible to obtain peak stress data competitive in quality with data from active gages in both free-field and on-structure applications in a wide variety of earth media.

The tabulated upper limits on the effect of shear do not include effects on the impressions due to the balls rolling slightly. Although significant differences between stresses indicated by impressions that were slightly out of round and stresses from other recovered gages believed to have been subjected to roughly the same normal stress have not been noticed, a laboratory investigation, perhaps statically with a single ball, would give a more definite indication.

The unique possibility of diagnosing the effects of imperfect placement and recovery (by means of examining the distribution of impression sizes) is another important feature.

Table 8.1. Summary of characteristics of Brinell Sandwich soil stress gages, with one insert of 7075-T6, the other of 6061-T6 aluminum.

Feature	Balls Closely Packed, 20.305/cm^2	3.875 Balls Per cm^2	Determination Method
Range lower limit	4 MPa (≈600 psi)	0.67 MPa (≈100 psi)	Experiment
Range upper limit	≥470 MPa	≥100 MPa <180 MPa	Experiment
Stiffness modulus at center	≈7500 MPa (≈1100000 psi)	≈1400 MPa (≈200000 psi)	Calculation
Response time to a step function	≈15 μs	≈35 μs	Calculation
Strain rate effects	No influence on measurements with pulses ranging from static to half-sine with 0.1 ms rise		Experiment
Error band over most of range, ≈95% conf. level*	±4% of reading ±10% of reading with shear plus multiple peaks in normal stress		Experiment
Acceleration sensitivity	≈0.1 kPa/g (≈0.015 psi/g) in soil of 1.7 gm/cc density		Calculation
Upper limit on effects of extreme lateral stresses**	15% of reading	Not rec'd. with extreme lateral str. (see Ch. 5)	Calculation
Upper limit on effects of shear when shear stress = normal stress**	10% of reading	22% of reading	Calculation

*This is a measure of resolution and does not include uncertainties due to ignorance of the registration ratio in the medium, etc.

**These are for on-structure applications. The upper limits on the effect of shear do not include effects on the impressions due to the ball rolling slightly.

RFFERENCES

1. M. J. Hvorslev; "The Changeable Interaction Between Soils and Pressure Cells; Tests and Reviews at the Waterways Experiment Station;" Technical Report No. S-76-7, June 1976; U. S. Army Engineer Waterways Experiment Station, CE, Vicksburg, Miss.

2. W. J. Astleford, G. R. Somerville, C. F. Schuetze, and R. H. Hemion; "A Feasibility Study of Impact Surface Pressure Gauging with Dye-Filled Microcapsules;" Report No. DOT HS-800 965, November 1973; Southwest Research Institute, San Antonio, Tex. (Available through the National Technical Information Service, Springfield, VA.)

3. H. L. Boardman; "Apparatus and Methods for Recording Acceleration;" U. S. Patent No. 3,782,204, January 1974; U. S. Patent and Trademark Office, Washington, D. C.

4. P. Brondsted and T. Wanheim; "Indentation Pressure Transducer;" Experimental Mechanics; Vol 17, No. 6, June 1977, p 239.

5. V. F. DeVost; "Shock Spectra Measurements Using Multiple Mechanical Gages;" Report No. NOLTR 67-151, September 1967; U. S. Naval Ordnance Laboratory, White Oak, MD.

6. V. F. DeVost; "WOX-5A Accelerometer (Artillery Projectile Copper-Ball Accelerometer);" Report No. NOLTR 68-85, May 1968; U. S. Naval Ordnance Laboratory, White Oak, MD.

7. J. H. Edwards; "Weight Measuring and Calibrating Device;" U. S. Patent No. 2,370,784, March 1945; U. S. Patent and Trademark Office, Washington, D. C.

8. A. L. Florence; "Time-Sequencing Passive Impulse Gage;" Technical Report No. AFWL-TR-69-113, July 1970; Air Force Weapons Laboratory, Kirtland Air Force Base, NM.

9. W. M. Hurst; "Deformable Gages;" U. S. Patent No. 3,525,250, August 1970; U. S. Patent and Trademark Office, Washington, D. C.

10. R. W. Manweiler, C. V. Chester, and C. H. Kearney; "Measurement of Shock Overpressure in Air by a Yielding Foil Membrane Blast Gauge;" Report No. ORNL-4868, September 1973; Oak Ridge National Laboratory, Oak Ridge, TN.

11. F. H. McRitchie; "Pressure Measuring Device;" U. S. Patent No. 3,178,935, April 1965; U. S. Patent and Trademark Office, Washington, D. C.

12. J. C. Muirhead, W. A. Jones, W. M. McMurtry, and F. L. McCallum; "Some Self-Recording Pressure Indicators;" Suffield Technical Note No. 118, April 1963; Suffield Experimental Station, Ralston, Alberta.

13. G. I. Pokrovsky and I. S. Fyorokov; Centrifugal Model Testing in the Construction Industry; Vol 2, 1969; Niedra, Moscow. (Translated from Russian by the Building Research Establishment Library Translation Service, Garston Watford, England, 1975, pp 163-164.)

14. F. A. Raum, K. P. Stanyukvich, and Shekhter; Physics of an Explosion; (translated from Russian), pp 779-780.

15. J. R. Vigliante; "Engineering Laboratories Report on Dynamic Calibration of Spherical Copper Crushers;" Report No. DPS-1045, November 1963; Aberdeen Proving Ground, MD.

16. A. Peekna; "Development of the Brinell Sandwich Passive Transducer;" Army Science Conference Proceedings, 22-25 June 1976; Vol 3, p 43.

17. American Society for Testing and Materials, Standard E 10-73; "Standard Method of Test for Brinell Hardness of Metallic Materials;" 1976 Annual Book of ASTM Standards; Part 10, ASTM, Philadelphia, PA.

18. P. F. Hadala; "The Effect of Placement Method on the Response of Soil Stress Gages;" Technical Report No. 3-803, November 1967; U. S. Army Engineer Waterways Experiment Station, CE, Vicksburg, Miss.

19. J. K. Ingram; "Development of a Free-Field Soil Stress Gage for Static and Dynamic Measurements;" Technical Report No. 1-814, February 1968; U. S. Army Engineer Waterways Experiment Station, CE, Vicksburg, Miss.

20. J. D. Campbell; Dynamic Plasticity of Metals; Springer-Verlag; New York, 1972.

21. M. P. Victoria, C. K. H. Dharan, F. E. Hauser, and J. E. Dorn; "Dislocation Damping at High Strain Rates in Aluminum and Aluminum-Copper Alloy;" Journal of Applied Physics; Vol 41, February 1970, p 674.

22. K. Kishida and K. Senda; "New Experimental Method for Determining Dynamic Stress-Strain Relation of Metals;" Experimental Mechanics; Vol 8, No. 12, December 1968, p 567.

23. U. S. Lindholm; "Review of Dynamic Testing Techniques and Material Behaviour;" Mechanical Properties at High Rates of Strain, Proceedings of the Conference on Mechanical Properties of Materials at High Rates of Strain held in Oxford, 2-4 April 1974; The Institute of Physics, London and Bristol, England, 1974, p 3.

24. U. S. Lindholm; "Some Experiments with the Split Hopkinson Pressure Bar;" Journal of the Mechanics and Physics of Solids; Vol 12, 1964, p 317.

25. U. S. Lindholm; "Dynamic Deformation of Metals;" Behavior of Materials Under Dynamic Loading; ASME, NY.

26. E. D. H. Davies and S. C. Hunter; "The Dynamic Compression Testing of Solids by the Method of the Split Hopkinson Pressure Bar;" Journal of the Mechanics and Physics of Solids; Vol 11, 1963, p 155.

27. C. K. H. Dharan and F. E. Hauser; "Determination of Stress-Strain Characteristics at Very High Rates;" Experimental Mechanics; Vol 10, September 1970, p 370.

28. F. E. Hauser, J. A. Simmons, and J. E. Dorn; "Strain Rate Effects in Plastic Wave Propagation;" Response of Metals to High Velocity Deformation; Interscience, NY, 1961, p 93.

29. D. L. Holt, S. G. Babcock, S. J. Green, and C. J. Maiden; "The Strain-Rate Dependence of the Flow Stress in Some Aluminum Alloys;" Transactions of the ASM, Vol 60, 1967, p 152.

30. G. L. Wulf; "Dynamic Stress-Strain Measurements at Large Strains;" Mechanical Properties at High Rates of Strain, Proceedings of the Conference on Mechanical Properties of Materials at High Rates of Strain held in Oxford, 2-4 April 1974; The Institute of Physics, London and Bristol, England, 1974, p 48.

31. A. H. Jones, C. J. Maiden, S. J. Green, and H. Chin; "Prediction of Elastic-Plastic Wave Profiles in Aluminum 1060-0 Under Uniaxial Strain Loading;" Mechanical Behavior of Materials Under Dynamic Loads; Springer-Verlag, NY, 1968, p 254.

32. C. H. Karnes; "The Plate Impact Configuration for Determining Mechanical Properties of Materials at High Strain Rates;" Mechanical Behavior of Materials Under Dynamic Loads; Springer-Verlag, NY, 1968, p 270.

33. U. S. Lindholm; "Some Experiments in Plasticity Under Combined Stress;" Mechanical Behavior of Materials Under Dynamic Loads; Springer-Verlag, NY, 1968, p 77.

34. U. S. Lindholm and L. M. Yeakley; "High Strain-Rate Testing: Tension and Compression;" Experimental Mechanics; Vol 8, January 1968, p 1.

35. K. D. Robertson, S. C. Chou, and J. H. Rainey; "Design and Operating Characteristics of a Split Hopkinson Pressure Bar Apparatus;" AMMRC TR 71-49, November 1971; Army Materials and Mechanics Research Center, Watertown, MA.

36. J. Duffy, J. D. Campbell, and R. H. Hawley; "On the Use of a Torsional Split Hopkinson Bar to Study Rate Effects in 1100-0 Aluminum;" Journal of Applied Mechanics, Transactions of the ASME; March 1971, p 83.

37. J. Duffy; "Some Experimental Results in Dynamic Plasticity;" Mechanical Properties at High Rates of Strain, Proceedings of the Conference on Mechanical Properties of Materials at High Rates of Strain held in Oxford, 2-4 April 1974; The Institute of Physics, London and Bristol, England, 1974, p 72.

38. R. A. Frantz, Jr. and J. Duffy; "The Dynamic Stress-Strain Behavior in Torsion of 1100-0 Aluminum Subjected to a Sharp Increase in Strain Rate;" Journal of Applied Mechanics, Transactions of the ASME; December 1972, p 939.

39. W. Goldsmith and P. T. Lyman; "The Penetration of Hard-Steel Spheres into Plane Metal Surfaces;" Journal of Applied Mechanics; Vol 27, December 1960, p 717.

40. Chi-Hung Mok; "The Dependence of Yield Stress on Strain Rate as Determined From Ball-Indentation Tests;" Experimental Mechanics; Vol 6, February 1966, p 87.

41. K. G. Hoge; "The Effect of Strain Rate on Mechanical Properties of Some Widely Used Engineering Metals;" UCRL-14599, Metals, Ceramics, and Materials, UC-25 TID-4500 (46th Ed.), December 1965; University of California Lawrence Radiation Laboratory, Livermore, CA.

42. K. G. Hoge; "Influence of Strain Rate on Mechanical Properties of 6061-T6 Aluminum Under Uniaxial and Biaxial States of Stress;" Experimental Mechanics; Vol 6, April 1966, p 204.

43. A. L. Austin and R. F. Steidel; "The Tensile Properties of Some Engineering Materials at High Rates of Strain;" ASTM Proceedings; Vol 59, 1959, p 1292.

44. C. J. Maiden and S. J. Green; "Compressive Strain-Rate Tests on Six Selected Materials at Strain Rates From 10^{-3} to 10^{4} in/in/sec;" Journal of Applied Mechanics, September 1966, p 496.

45. L. M. Barker, C. D. Lundergan, and W. Herrmann; "Dynamic Response of Aluminum;" Journal of Applied Physics; Vol 35, April 1964, p 1203.

46. B. M. Butcher and C. H. Karnes; "Strain-Rate Effects in Metals;" Journal of Applied Physics; Vol 37, January 1966, p 402.

47. R. G. Davies and C. L. Magee; "The Effect of Strain Rate Upon the Bending Behavior of Materials;" Journal of Engineering Materials and Technology, Transactions of the ASME; Series H, Vol 99, No. 1, January 1977, p 47.

48. H. Kolsky; "An Investigation of the Mechanical Properties of Materials at Very High Rates of Loading;" Proc. Roy. Phys. Soc.; Vol B62, 1949, p 676.

49. H. Watson, Jr. and E. A. Ripperger; "Dynamic Stress-Strain Characteristics of Metals at Elevated Temperatures;" Experimental Mechanics; July 1969, p 289.

50. W. E. Baker and C. H. Yew; "Strain Rate Effects in the Propagation of Torsional Plastic Waves;" Journal of Applied Mechanics, Transactions of the ASME; December 1966, p 917.

51. S. Clyens and J. D. Campbell; "The Behavior of Copper and Lead-Tin Eutectic in Torsion at High Strain Rates;" Mechanical Properties at High Rates of Strain, Proceedings of the Conference on Mechanical Properties of Materials at High Rates of Strain held in Oxford, 2-4 April 1974; The Institute of Physics, London and Bristol, England, 1974, p 62.

52. C. H. Yew and W. Goldsmith; "Stress Distributions in Soft Metals Due to Static and Dynamic Loading by a Steel Sphere;" Journal of Applied Mechanics; December 1964, p 635.

53. A. M. Eleiche and J. D. Campbell; "Strain-Rate Effects During Reverse Torsional Shear;" Experimental Mechanics; August 1976, p 281.

54. J. E. Hockett and E. G. Zukas; "The Response of Iron to Dynamic Compression;" Mechanical Properties at High Rates of Strain, Proceedings of the Conference on Mechanical Properties of Materials at High Rates of Strain held in Oxford, 2-4 April 1974; The Institute of Physics, London and Bristol, England, 1974, p 53.

55. M. J. Manjoine; "Influence of Rate of Strain and Temperature on Yield Stresses of Mild Steel;" Journal of Applied Mechanics, Transactions of the ASME; December 1944, p A-211.

56. J. L. Lewis and J. D. Campbell; "The Development and Use of a Torsional Hopkinson-Bar Apparatus;" Experimental Mechanics; November 1972, p 520.

57. W. J. Flathau; "Dynamic Tests of Large Reinforcing Bar Splices;" Technical Report No. N-71-2, April 1971; U. S. Army Engineer Waterways Experiment Station, CE, Vicksburg, Miss.

58. M. G. Stevenson; "Stress-Strain Data for Predictions in Machining;" Mechanical Properties at High Rates of Strain, Proceedings of the Conference on Mechanical Properties of Materials at High Rates of Strain held in Oxford, 2-4 April 1974; The Institute of Physics, London and Bristol, England, 1974, p 393.

59. G. H. Daneshi and J. Harding; "The High Speed Punching of a Quenched and Tempered 1-1/2 Percent Cr Mo Steel;" Mechanical Properties at High Rates of Strain, Proceedings of the Conference on Mechanical Properties of Materials at High Rates of Strain held in Oxford, 2-4 April 1974; The Institute of Physics, London and Bristol, England, 1974, p 404.

60. C. Albertini and M. Montagnani; "Testing Techniques Based on the Split Hopkinson Bar;" Mechanical Properties at High Rates of Strain, Proceedings of the Conference on Mechanical Properties of Materials at High Rates of Strain held in Oxford, 2-4 April 1974; The Institute of Physics, London and Bristol, England, 1974, p 22.

61. F. E. Hauser; "Techniques for Measuring Stress-Strain Relations at High Strain Rates;" Experimental Mechanics; Vol 6, August 1966, p 395.

62. R. J. Roark and W. C. Young; Formulas for Stress and Strain; 5th ed, McGraw-Hill, New York, 1975.

63. D. D. Ivlev and R. I. Nepershin; "Impression of a Smooth Spherical Indenter into a Rigid-Plastic Half-Plane;" Mechanics of Solids; Vol 8, No. 4, 1973, pp 144-149. (Translation of Mekhanika Tvergodo Tela, Vol 8, No. 4, 1973, pp 159-166 by Allerton Press, Inc., New York.)

64. O. Richmond, H. L. Morrison, and M. L. Devenpeck; "Sphere Indentation With Application to the Brinell Hardness Test;" International Journal of Mechanical Sciences; Vol 16, No. 1, January 1974, p 75.

65. F. E. Kennedy and F. F. Ling; "Elasto-Plastic Indentation of a Layered Medium;" Journal of Engineering Materials and Technology, Transactions of the ASME; Series H, Vol 96, No. 2, April 1974, p 97.

66. H. A. Francis; "Phenomenological Analysis of Plastic Spherical Indentation;" Journal of Engineering Materials and Technology, Transactions of the ASME; Series H, Vol 98, No. 3, July 1976, p 272.

67. "Materials Selector 76;" Materials Engineering; Vol 82, No. 4, September 1975.

68. G. Markus; Theorie und Berechnung rotationssymmetrischer Bauwerke; Werner-Verlag, Duesseldorf, 1967. (Translation of Koerszimmetrikus Szerkezetek Elmelete es Szamitasa; Mueszaki Koenyvkiado; Budapest, 1964.)

69. S. Timoshenko; Strength of Materials Part II, Advanced Theory and Problems; 3rd ed, Van Nostrand Reinhold, New York, 1958.

70. T. E. Kennedy, G. E. Albritton, and R. E. Walker; "Initial Evaluation of Free-Field Response of the Large Blast Load Generator;" Technical Report No. 1-723, 1966, Appendix A; U. S. Army Engineer Waterways Experiment Station, CE, Vicksburg, Miss.

71. J. W. McNulty; "An Experimental Study of Arching in Sand;" Technical Report No. 1-674, May 1965; U. S. Army Engineer Waterways Experiment Station, CE, Vicksburg, MS.

72. Y. C. T. Yeung Wye Kong, B. Parsons, and B. N. Cole; "The Dispersive Behavior of a Hopkinson Pressure Bar in Material Property Tests;" Mechanical Properties at High Rates of Strain, Proceedings of the Conference on Mechanical Properties of Materials at High Rates of Strain held in Oxford, 2-4 April 1974; The Institute of Physics, London and Bristol, England, 1974, p 33.

73. L. S. Marks; Mechanical Engineer's Handbook; 6th ed., McGraw-Hill, New York, 1958.

74. R. C. Dove and Paul M. Adams; Experimental Stress Analysis and Motion Measurement; Charles E. Merrill Books, Inc., Columbus, Ohio, 1964.

75. H. Goldstein; Classical Mechanics; Addison-Wesley, Reading, Mass., 1959.

APPENDIX A

DRAWINGS AND SPECIFICATIONS FOR THE GAGE PARTS

A.1 GAGE BODY PARTS

Detailed drawings for the gage body parts, gage bowl, piston plate, and retainer ring are given in Figures A.1, A.2, and A.3, respectively. The inside surfaces of the gage bowl and piston plate are specified flat-to-convex with a close tolerance (Figures A.1 and A.2) in order to provide for snug assembly in the prime sensing area at the gage center. A flatness inspection facility of the sort illustrated in Figure A.4 is required. Some experimenting on the first piece is necessary to attain the required flatness. A lathe that will cut a concave surface on a normal face cut can be made to cut a convex surface by running it in reverse, with the cutting tool working on the far side of the lathe center line. Altering the feed direction can also change the convexity or concavity of the resulting surface. Making a very thin final cut on a piece cooled to room temperature (one that had been rough-cut previously) and keeping a stream of cutting fluid on the surface minimizes effects due to heating.

The gage body parts (Figures A.1, A.2, and A.3) are normally plated with electroless nickel; bare aluminum surfaces are satisfactory only if they will never be exposed to wet grout or concrete mix. Rather than attempt to mask the interior surfaces of the gage bowl and piston plate, it has been proven convenient to plate the entire piece. The uniformity of electroless nickel is such that maintenance of the flatness tolerances on the inner surfaces presents no special problems. As noted in Figures A.1, A.2, and A.3, all dimensions on these drawings apply to the finished pieces, and appropriate allowances must be made for the net buildup in the plating process while machining these parts. Electroless nickel plating with a net buildup of approximately 0.0005 inch per surface has given adequate protection.

A.2 SPACER (FOR LOWER-RANGED VERSION ONLY)

The drawing of the spacer for 3.875 balls per square centimetre (25 per square inch) is given in Figure A.5.

A.3 INSERTS

The specifications for the inserts are outlined as follows.

A.3.1 Material. 0.063-inch-thick 7075-T6 aluminum flat sheet and 0.063-inch-thick 6061-T6 aluminum flat (not coiled) sheet. The material must be "bare" 7075-T6 and 6061-T6; "Alclad" sheets must be avoided. All the inserts for a given project should be made from the same respective sheets of material. Some material from these sheets must be saved for calibration purposes; the calibration procedure is given in Appendix C. Any leftover material from these sheets should be saved so that the same calibration can also be used on a future project. The 7075-T6 and 6061-T6 inserts must not be mixed. One way of avoiding this is to identify each sheet with layout dye of a different color.

A.3.2 Diameter. 2.860 $\pm$0.005 inch. Edges must be deburred. On the 7075-T6 inserts, one edge must be broken 1/64 inch minimum. The diameter may be turned in a lathe with disks clamped between the headstock and a live center in the tailstock.

A.3.3 Surface Finish. The mill finish of the aluminum sheets is adequate, but scratching during handling and fabrication must be minimized.

A.3.4 Flatness. The flatness of the inserts should be such that the measured thickness of the assembled gage at the center minus the sum of the measured thicknesses of the parts does not exceed 0.0012 inch; the assembly procedure is given in Appendix B. Good results have been obtained with the as-milled flatness of the material, provided that care is taken not to bend it during fabrication of the inserts. For example, it has been found that material closer than 2 inches to a sheet edge, or to any shear-cut edge should be discarded. Rough-cutting with a band saw having a 10-pitch blade or finer has been found satisfactory provided that the sheet is supported underneath right next to the saw blade by a plate with a slot as narrow as the saw blade.

Half-inch-thick micarta has been found satisfactory for the support plate.

A.4 STEEL BALLS

Specifications for the steel balls used in the gage are as follows.

1. Material. Chrome alloy steel, minimum hardness 62 Rockwell C.
2. Diameter. 3/32 inch.
3. Diametral Tolerance. SAE grade 25. Never mix steel balls from different containers. Diametral tolerances are much looser for balls out of different lots than for balls out of the same container. Significant differences in the size of the balls within a given gage would result in the larger balls making significantly larger impressions than the rest.

A.5 O-RINGS

Specifications for the O-rings are as follows.

1. Parker Size Number. 2-039.
2. Parker Compound Number. N674-70.

A.6 SCREWS

Specifications for the screws are as follows.

1. Material. Stainless steel.
2. Head Type. Slotted pan head.
3. Size. No. 6-32, 1/4 inch long.

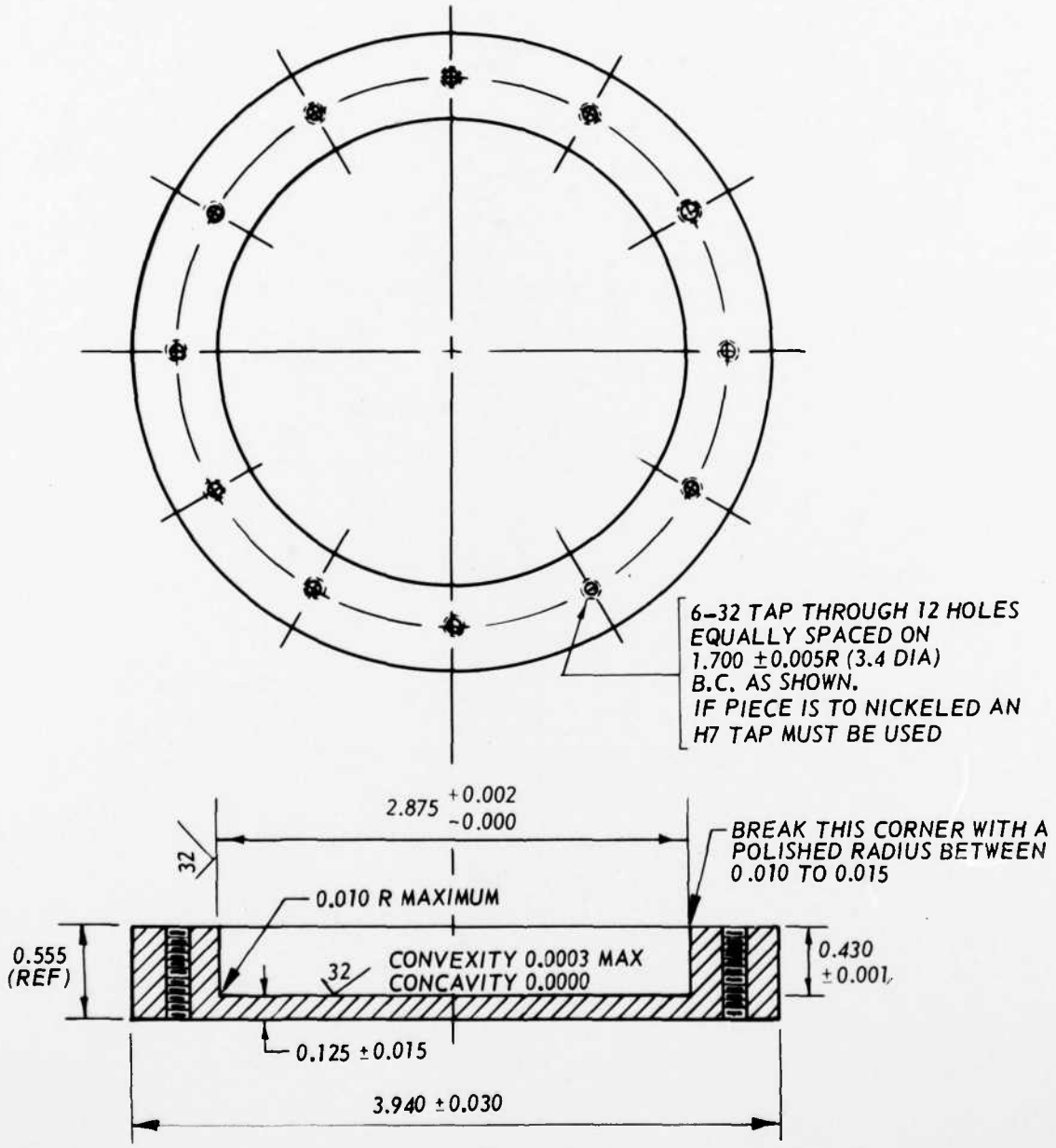

PASSIVE STRESS GAGE, GAGE BOWL
MATERIAL: 7075-T651 ALUMINUM
ALL DIMENSIONS ARE IN INCHES

ALLDIMENSIONS APPLY TO THE FINISHED PIECE

APPROPRIATE ALLOWANCE MUST BE MADE FOR THE NET BUILDUP IN ELECTROLESS NICKEL PLATING WHEN MACHINING

Figure A.1. Gage bowl.

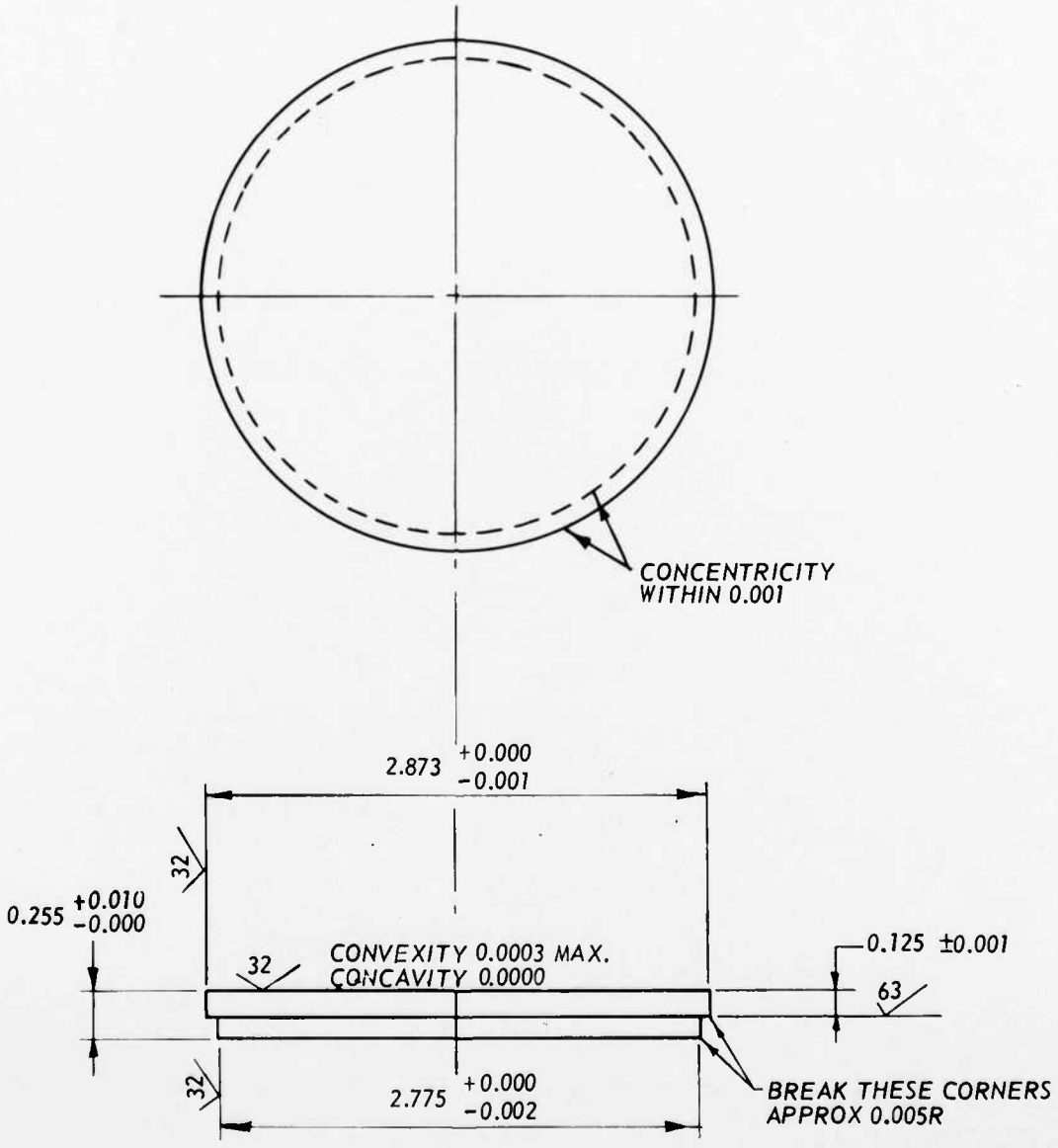

PASSIVE STRESS GAGE, PISTON PLATE
MATERIAL: 7075-T651 ALUMINUM
ALL DIMENSIONS ARE IN INCHES

ALL DIMENSIONS APPLY TO THE FINISHED PIECE
APPROPRIATE ALLOWANCE MUST BE MADE FOR
THE NET BUILDUP IN ELECTROLESS NICKEL
PLATING WHEN MACHINING

Figure A.2. Piston plate.

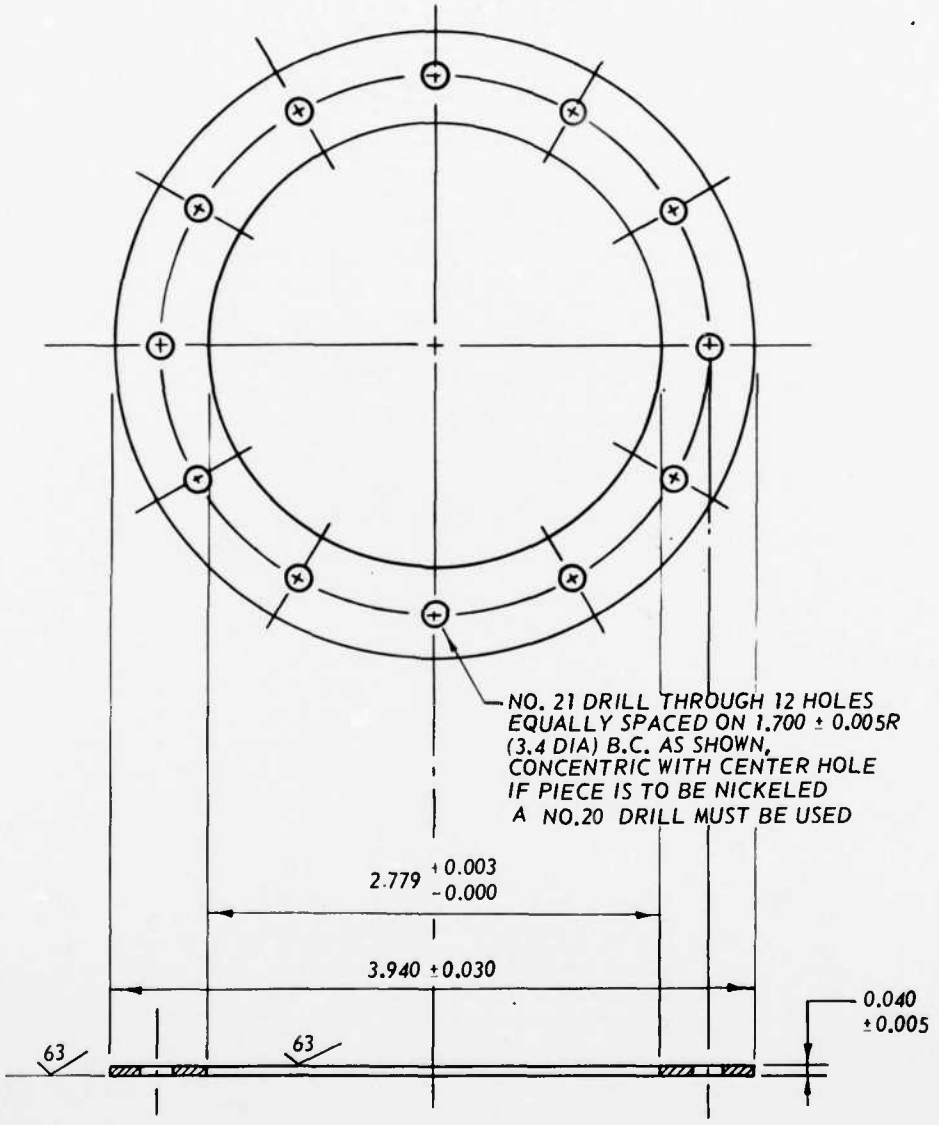

Figure A.3. Retainer ring.

FLATNESS INSPECTION METHOD:

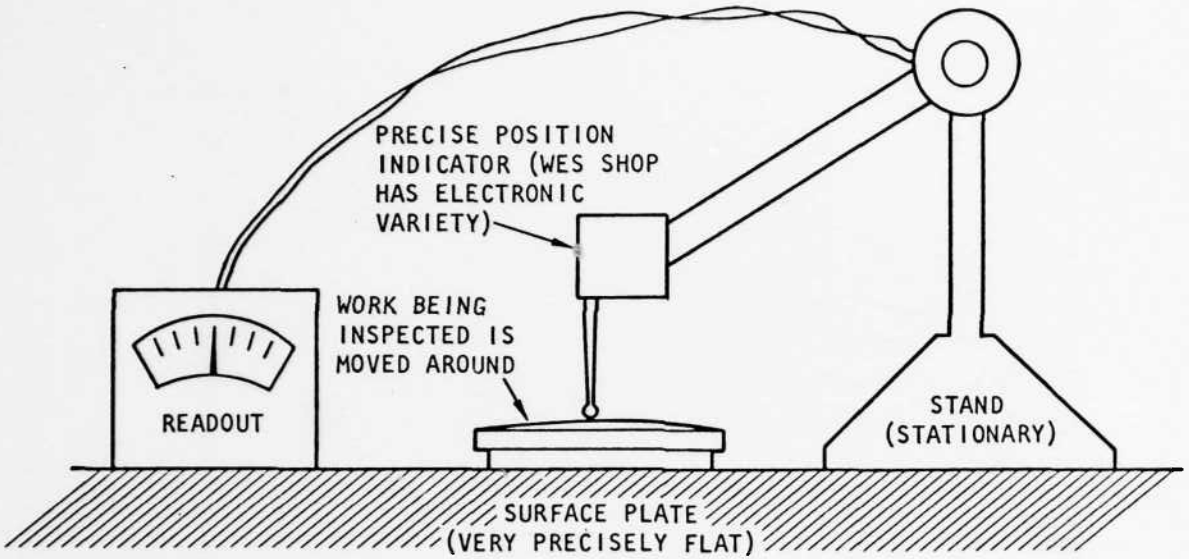

IF LOWER SURFACE OF WORK BEING INSPECTED IS CONVEX, THEN WORK IS SUPPORTED ON THE SURFACE PLATE BY A RING.

Figure A.4. Flatness inspection method.

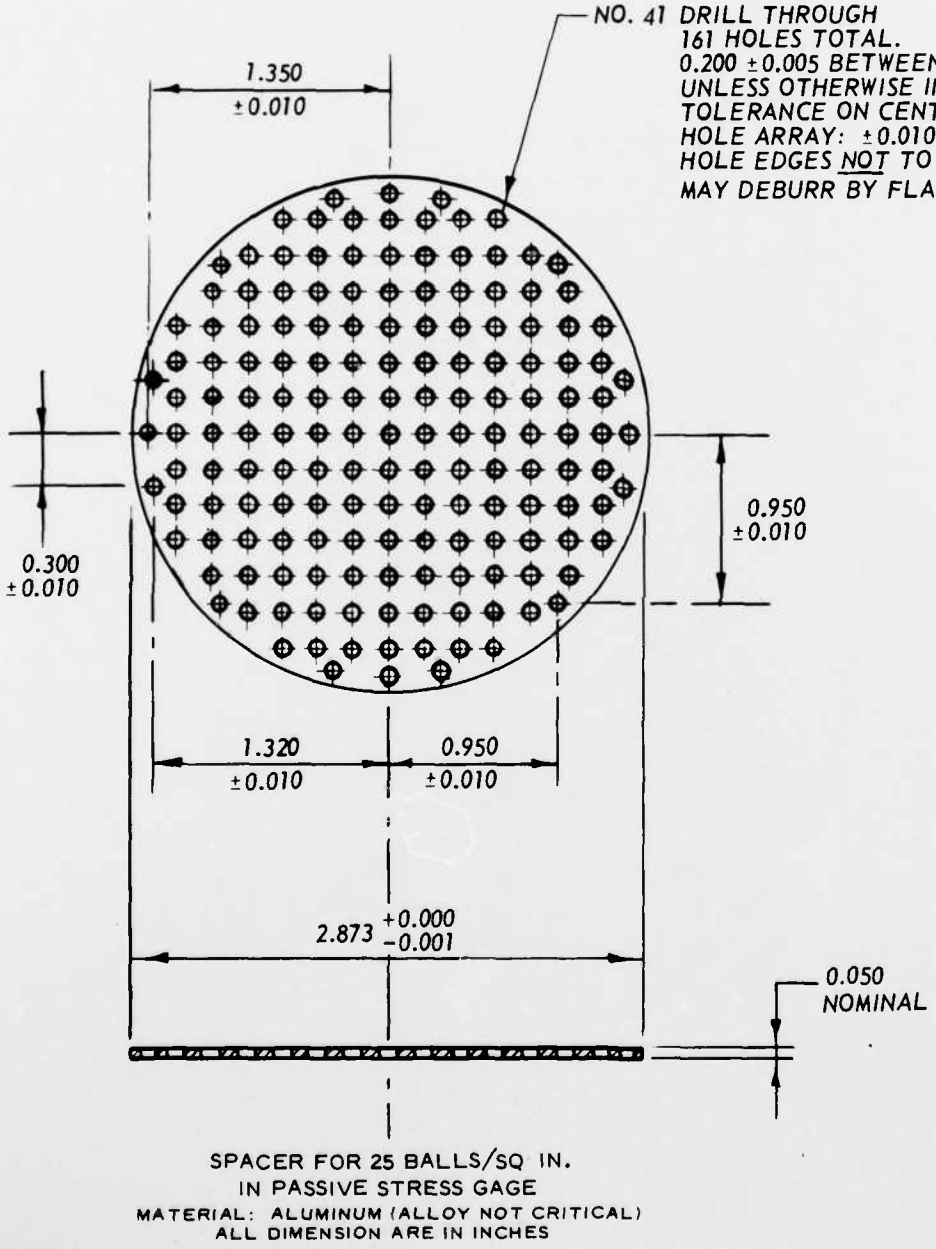

Figure A.5. Spacer for 3.875 balls per square centimeter (25 per square inch).

APPENDIX B

ASSEMBLY PROCEDURE

B.1 TOOLS AND EQUIPMENT

The tools and equipment necessary for gage assembly are as follows:

1. Numbering tool for gage parts:
   a. Electric pencil, or
   b. Scratch marker.
2. Abrasive cloth, No. 320 Grit.
3. Paper towels or tissues (lint free).
4. Cleaning Solvents:
   a. Freon 113.
   b. Acetone.
5. Micrometer, deep-throated, 1 inch capacity, measures to 0.0001 inch.
6. Micrometer holder (stand).
7. Screwdriver.
8. Tweezers (anti-magnetic).
9. Teaspoon (a long-handled small-bowled baby spoon is best).
10. Wooden dowels, 3 mm (1/8 inch) diameter.
11. Lubricant for O-ring: Dow Corning 103 Compound.
12. Good rigid straight-edge, minimum length 10 cm (4 inches).
13. Sharp pointed tool, such as a divider point (used for removal of O-ring).
14. Suction cup, 5 to 6 cm (2 to 2-1/2 inch) diameter.
15. Cloth adhesive tape.
16. Assembly ring (see Figure B.1).
17. Piece of hard wood, approximately 0.5 x 1.3 x 10 cm (3/16 x 1/2 x 4 inches).

B.2 PREPARING THE GAGE PARTS

The first step in assembly of the Brinell Sandwich soil stress gage is the preparation of the individual parts. The care taken in this step could make the difference as to whether the gage meets the tolerance for a tight assembly.

The inserts used in the gage may have layout dye on them which is used during the cutting process. Since the layout dye may encapsulate chips or pieces of dirt, it should be removed. This can be done easily by washing in acetone. Since the dye was used to color code the inserts, the 7075 and 6061 inserts should not be mixed.

After the dye has been removed, all parts (except the balls) should be washed in a degreaser. Freon 113 was found very effective for this. In most cases the parts will dry in a few seconds and will not have to be wiped.

After the parts have been cleaned, a gage bowl, piston plate, retainer ring, and two inserts should be selected for assembly. The inserts should now be numbered and marked for orientation. This is done by marking a small arrow and the gage number at the edge of the inserts (Figure B-2). If possible reuse of the gage body is anticipated, or if the gage body has been used previously, a dash number should be added to the gage number on the inserts, in order to later distinguish between different sets of inserts which have been in the same gage. The alloy number, 7075 or 6061, may also be marked on the respective inserts. On the 7075-T6 inserts, (which will be on the bottom), the arrow and number must be on the side with the beveled edge. An orientation marker, arrow or notch, and gage number are also required on the edge of the gage bowl. The orientation mark should have been made before plating with electroless nickel, but it may not always be practical to number the gage before nickeling. Scratch-marking an already nickeled gage is not recommended; rather, a small piece of cloth adhesive tape may be put on the edge of the gage bowl and the gage number written on it with a ball-point pen.

Any burrs left on the inserts by the numbering process should be removed with 320 grit abrasive cloth. Do not sand a larger area than needed.

Measure the thickness at the center of each part with a deep-throat micrometer, to 0.0001 inch accuracy. Record this on the data sheet for the gage. Total these four measurements and the diameter of the balls (0.0938 inch). The gage is now ready to be assembled.

B.3 ASSEMBLY

Place the gage bowl on a flat surface with the orientation mark toward you. Take the 7075-T6 insert and put a pencil mark on the edge to correspond with the arrow on the insert. Place the insert in the gage bowl with the arrow side down and the pencil mark lined up with the orientation mark on the gage bowl. The gage is now ready for the steel ball array.

Never mix steel balls from different containers. Dimensional tolerances are much looser for balls out of different lots than for balls out of the same container. Significant differences in the size of the balls within a given gage would result in the larger balls making significantly larger impressions than the rest.

In the event that the steel balls have not been oiled by the supplier, it is recommended that a small amount of light oil (such as 3-in-1) be introduced into the container as soon as the seal is broken. This helps prevent rust during storage, and also from possible sealed-in moisture inside an assembled gage.

If the gage is to be a lower-ranged version, place the 0.050-inch-thick spacer plate (Figure A.5) in the gage bowl such that the array is lined up with the orientation mark, and fill each hole with a steel ball.

If the gage is to be high-ranged, no spacer plate is used. The balls are placed in the gage bowl closely packed, forming a plane hexagonal array except at the edge (Figure B.3). Approximately 800 balls per gage are required. However, the precise number needed to make a tight array will not be the same from one gage to the next. It is best to start with fewer balls than are required, crowd them into a hexagonal array at the center, and add balls around the edge as needed. Wooden dowels, with tips cut into chisel-shaped points, are handy in moving the balls around within the gage bowl. Placing a finger on the array and feeling for lateral movement is a good test of compaction. If it feels too loose, see if one or two more balls can be added at the edge; experience will form a guide in this respect. A good experienced

assembler can complete an array in approximately 15 minutes. Many of the details in making a closely packed array are much easier to demonstrate than to describe, and instruction from an experienced assembler is highly recommended.

Once the ball array is satisfactory the 6061-T6 insert is placed in the gage bowl. The arrow side is up and matched to the arrow on the bowl. Before placing the piston plate in the bowl, the assembly ring shown in Figure B.1 should be centered and attached to the bowl with four screws.

The assembly ring can be centered easily by placing two spacers (Figure A.5) and the piston plate in the bowl on top of the 6061-T6 insert. This will hold the piston plate high enough that the ring will be centered around the piston plate. If spacer plates are not available, anything 0.1 inch thick that can be easily removed from the bowl may be used.

After the assembly ring is centered and attached, the spacers can be removed. Recheck the 6061-T6 insert orientation. Place the piston plate in the bowl. Do not allow the piston plate to rotate or the orientation will be affected.

The O-ring must be lightly lubricated. Dow Corning 103 Compound (a white silicone grease) has been found satisfactory in helping the O-ring to slide properly into its groove, and is more resistant to chemical attack by substances in the groundwater and/or grout than many other lubricants. The O-ring should be placed on the groove between the piston plate and the assembly ring.

The O-ring is forced into the groove by using a piece of hardwood approximately 1/2 x 3/16 inches and 4 inches or more long. One end should be trimmed to the shape of the O-ring groove and 1 cm (0.4 inch) width, with slightly rounded corners. The other end can be placed in a file handle to make it easier to hold.

In order to make sure that the O-ring goes down evenly, it should be forced into the groove using the following sequence. Always working at diametrically opposite points, divide the O-ring into halves, quarters, eights, sixteenths, etc. until the O-ring is in the groove

all the way around. The sequence is illustrated in Figure B.4. After this is accomplished, the assembly ring can be removed.

The parting operation in machining the retainer ring may result in a slightly bent cross section, exaggerated in Figure B.5. This may be checked with a straight-edge, as shown in Figure B.5. Such a retainer ring should be placed concave side downward. A screw is started in each of the 12 holes and tightened.

Measure the thickness at the center of the gage with a deep-throat micrometer, to 0.0001 inch accuracy. Record this on the data sheet for the particular gage. Take the difference between your reading and the sum of the thicknesses of the parts. This difference must not exceed 0.0012 inch.

B.4 DISASSEMBLY AND TROUBLESHOOTING

When removing the retainer ring, first loosen each screw by a quarter turn before backing them all the way out.

It is essential to avoid scratching or damaging the metal sealing surfaces in any way during O-ring removal. This is ensured by the procedure described here: Insert a sharp pointed tool (a divider point or compass point is excellent for this purpose) tangentially into the O-ring (see Figure B.6), but do not push the point all the way through the O-ring, and do not allow the divider point to touch any of the metal surfaces. Slowly pull the divider point directly upward. The O-ring will pull out slowly, especially at first. Yanking or excessive force may break the divider point; steady force works best. As soon as approximately one-half inch of the O-ring is out of its groove, it may be grabbed with the fingers of the other hand. Once this is done, take out the divider point, and with a finger at or near the center of the piston plate (to prevent it from slipping up or rotating) pull the O-ring entirely free from its groove. Discard the old O-ring.

A clean piston plate may usually be removed with a suction cup, without turning the gage upside down. In case of an especially close fit, or in case excess lubricant or oil from the steel balls has formed a seal in the radial clearance, a jet of compressed air aimed at

several points around the piston plate perimeter will suffiee. The topmost insert may also be removed with a suction cup, though a piece of adhesive tape is usually just as effeetive here. Occasionally excess oil from the steel balls may make the bottom insert stick to the gage bowl bottom; it ean be shaken loose by turning the gage upside down and hitting it against a wooden board. Never use a pointed metal tool or screwdriver to pry out gage parts.

Reeovered gages which have been severely deformed in the application event may have to be cut apart on a lathe; it is advisable to position a flat block on a live eenter gently in eontact with the open face during cutting.

Some reasons why a gage may have exceeded the assembly axial tightness tolerance of 0.0012 inch are the following: a chip or pieee of dirt between an insert and a gage body faee (eheek for this during disassembly after the attempt), excessively bent or dished inserts for which the force exerted by the O-ring is insufficient to squeeze them flat inside the gage, or too many balls in a elosely paeked array. In the latter event, the tightness tolerance is usually exceeded by several thousandths of an inch. If excessively bent inserts are suspeeted, check this by positioning the insert against a good rigid straight-edge in several directions, compare with other inserts, and try a flatter set. If all else fails, eheck if the gage body part dimensions meet specifications. For example, excessive bowl depth will diminish the force exerted by the O-ring, by inereasing the groove volume.

B.5 INCREASE IN ALTITUDE AND RESEALING

Gages which have been assembled at low altitude will eontain a positive internal "gage" pressure when brought to a higher altitude. For example, an altitude change from near sea level to 1900 m (6,200 feet) will result in an internal "gage" pressure of approximately 20 kPa (3 pounds per square inch). Tests have shown that this can be sufficient to expand the assembled gage thickness (measured with a deep-throat micrometer at the center) by as much as 0.0016 inch. In

the event that the altitude at the field test site is significantly higher than at the gage assembly location, the assembled gage thickness should be rechecked at the higher altitude. If the measured gage thickness now exceeds the sum of the measured thicknesses of the parts (recorded on the assembly data sheet) by more than 0.0012 inch, the internal pressure should be relieved by removing and replacing the O-ring according to the foregoing procedures. In order to preserve aximuthal orientation of internal parts, the piston plate must not be rotated with respect to the gage bowl. To check on this, make a pencil mark on the piston plate corresponding to the arrow on the gage bowl before removing the O-ring.

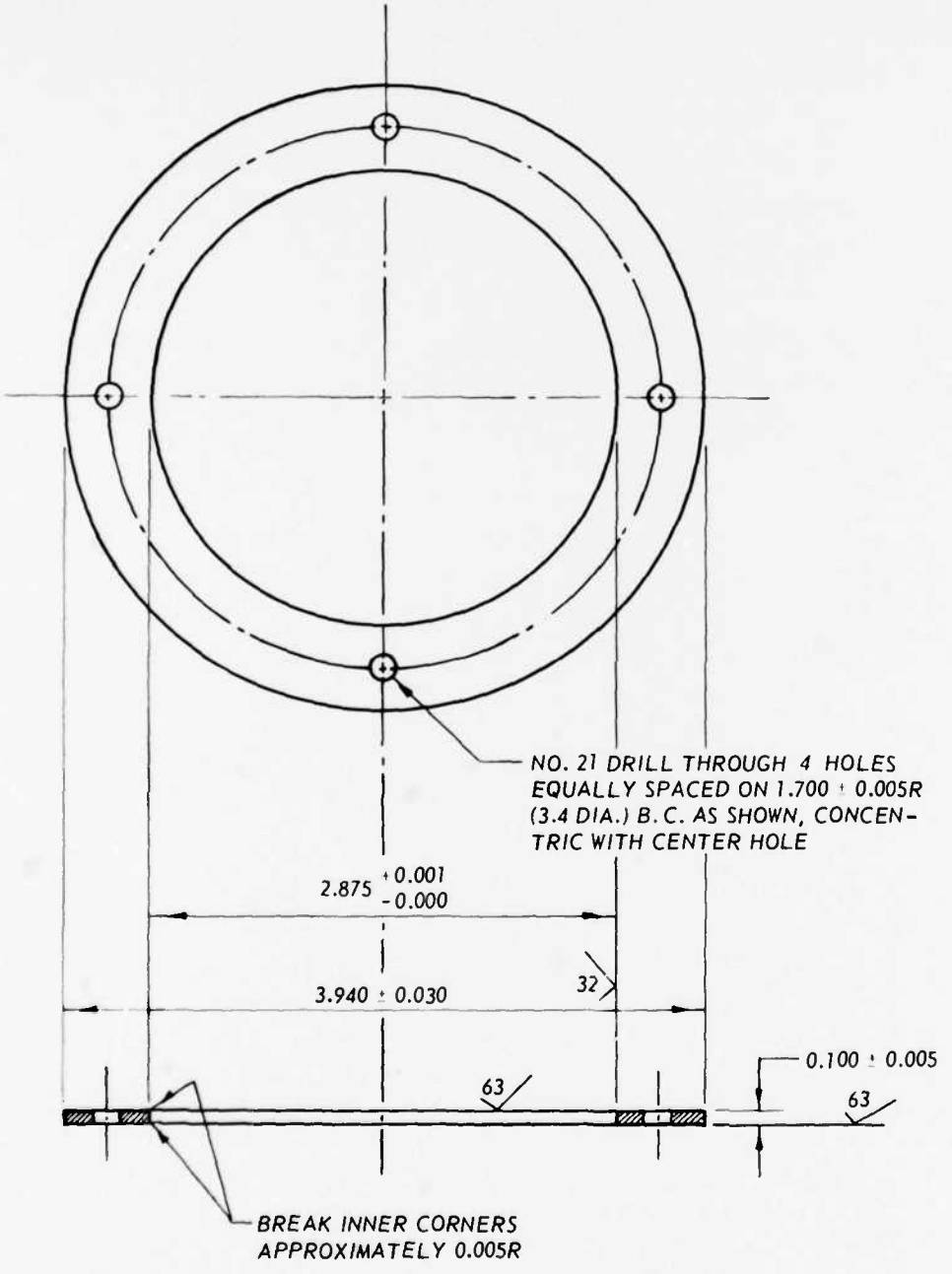

ASSEMBLY RING FOR PASSIVE STRESS GAGE
MATERIAL: STEEL OR STAINLESS
ALL DIMENSIONS ARE IN INCHES

Figure B.1. Assembly ring.

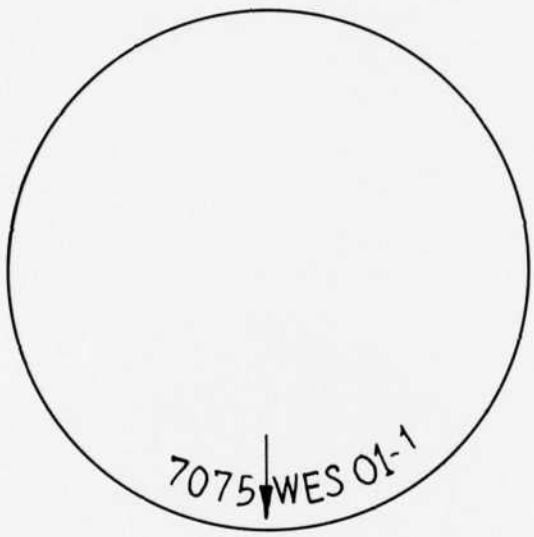

7075
AND 6061
INSERTS

GAGE
BOWL

Figure B.2. Numbering and marking of inserts and gage bowl.

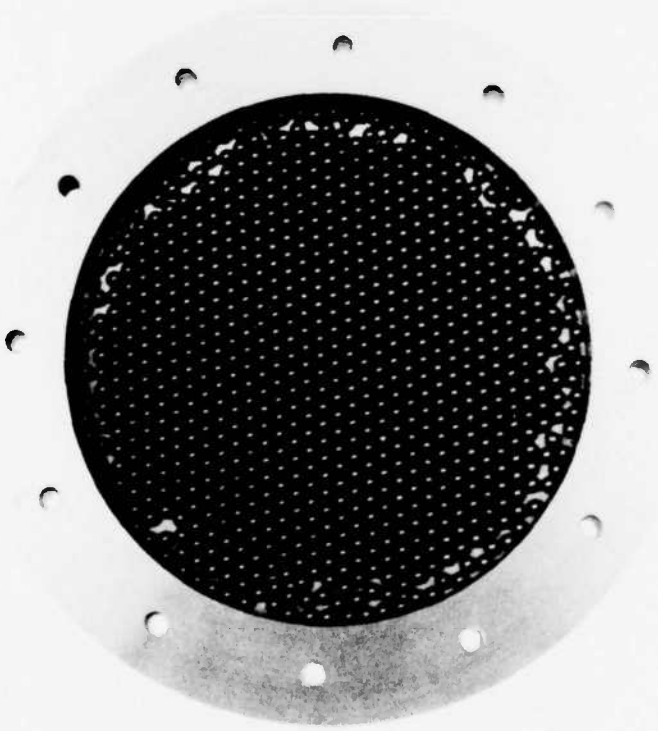

Figure B.3. Closely packed array of steel balls.

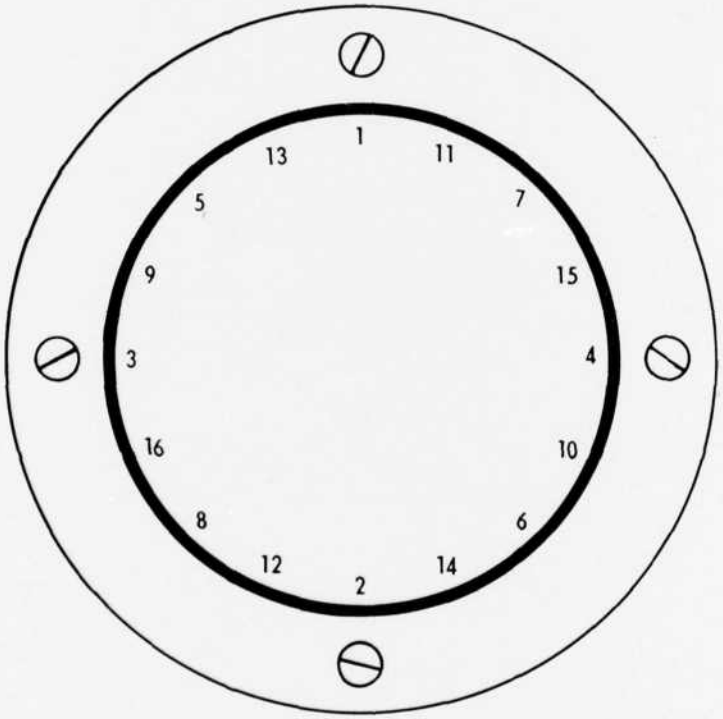

Figure B.4. O-ring insertion sequence.

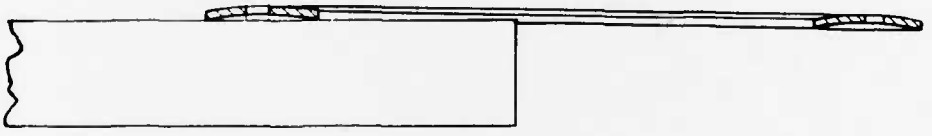

Figure B.5. Cross-sectional view of retainer ring; nonflatness greatly exaggerated.

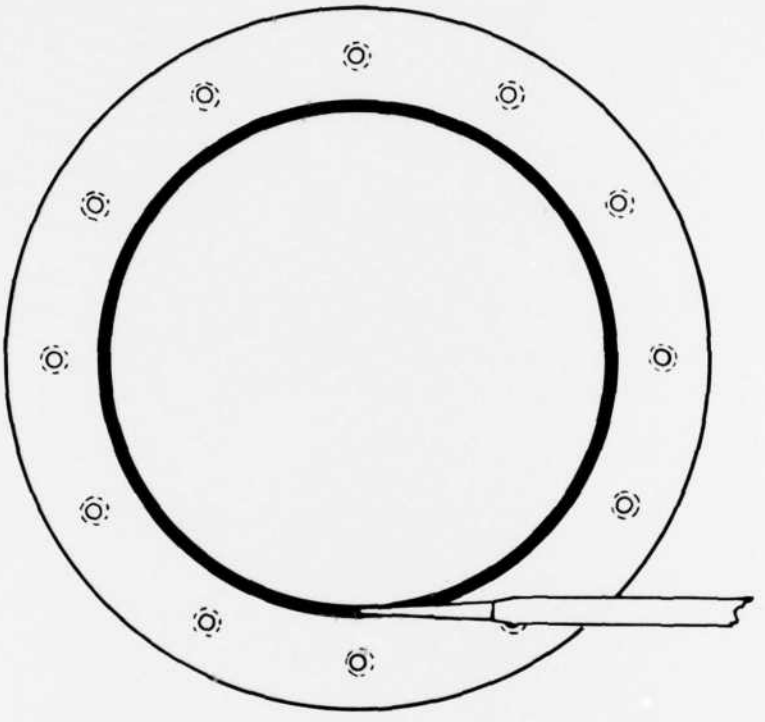

TOP VIEW

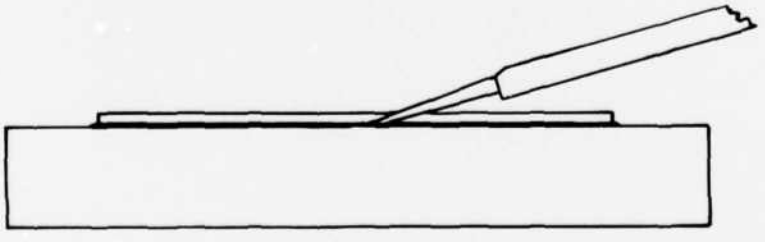

SIDE VIEW

Figure B.6. Inserting divider point into the O-ring.

APPENDIX C

CALIBRATION PROCEDURE

C.1 BALL HOLDER

The ball is most conveniently held in a ball holder designed for Rockwell or Brinell hardness testing. Such fixtures are available for 2.5-mm balls.

C.2 SPECIMENS

The 7075-T6 and 6061-T6 specimens to be calibrated should preferably be cut from their respective sheets on a band-saw having a 10-pitch blade, or finer. The work should be supported underneath by a plate with a slot as narrow as the saw blade. If shear cutting was used, then impressions should not be made closer than 5 cm (2 inches) to a shear cut edge; this is in order to avoid the effects of possible work hardening due to a slight bend at a sheared edge. The edges should be deburred so that the specimens may rest flat upon the anvil.

C.3 ANVIL

The anvil should be of a material at least as hard as the aluminum specimens and should have a flat machined surface with ASA 32 finish (32 microinch roughness) or better. Any protuberance (such as sometimes occurs at the center of a lathe-cut surface) or indent must be avoided, especially at the location under the ball. The ball should not be allowed to touch the anvil. If this should occur, the anvil should be carefully examined for damage, and the ball should be replaced.

C.4 LOAD CELLS

Loads ranging from 20 N (4.5 lbs) to 3000 N (675 lbs) on a 2.5-mm ball would cover the sensing range of the gage. In order to maintain adequate precision, the use of load cells of at least two different rated ranges is recommended; for example, 4448-N (1000-lb) and 445-N (100-lb) capacities would usually be sufficient.

C.5 METHOD OF LOAD APPLICATION

Since the size of the indentation is determined by the maximum (peak) load, the load application and recording method must be such that the actual maximum load on the ball can be accurately recorded. For example, when using a digital voltmeter to read the load cell output, any spurious highs in the applied load must be avoided. This can be accomplished by the careful use of a suitable hydraulic system for applying the load. By contrast, stacking weights by hand would probably result in impact loads that may go unrecorded, or be inaccurately recorded.

C.6 NUMBER AND SPACING OF LOADS

The total number and spacing of loads clearly depends on the precision desired as well as the range of primary interest. It must be kept in mind that a gage reading is based on an average of five impressions. For example, for most purposes the sensing range would be adequately covered by the equivalent of 40 gage readings (one every factor of 1.13); this would correspond to 200 individual impressions in each alloy. Because the 7075-T6 insert is the primary indicator in the actual use of the gage except near the low end of the sensing range, it is recommended that the number and spacing of loads be divided accordingly.

C.7 NUMBERING IMPRESSIONS AND RECORDING LOADS

Because the balls as used in the gage are coated with light oil (Appendix B), light oil (such as 3-in-1) should be applied to the specimen before making the impressions. The impressions should be spaced a minimum distance of 0.5 cm (0.2 inch) apart. Each individual impression must be numbered and the corresponding maximum load recorded.

C.8 MEASURING IMPRESSION DIAMETERS

Diameters of the impressions from these calibrations should be measured in mutually perpendicular directions with a binocular microscope calibrated with a stage micrometer; nominal magnifications of

160X, 80X, and 56X provide an adequate range. The average of the mutually perpendicular measurements is taken as the diameter of each individual impression.

C.9 SCALING AND CONVERTING TO EQUIVALENT PEAK PRESSURE

C.9.1 Loads. All loads must be scaled by multiplying by the square of the ratio of the ball diameter in the gage to the ball diameter in the calibration, i.e., by

$$\left(\frac{2.38125}{2.5}\right)^2$$

C.9.2 Impression Diameters. All impression diameters must be scaled by multiplying by the ratio of the ball diameter in the gage to the ball diameter in the calibration, i.e., by

$$\frac{2.38125}{2.5}$$

C.9.3 Equivalent Pressure. To get the equivalent peak pressure, multiply the result of (C.9.1) by the ball density in the gage. This is:

203050 per m^2 (131.00 per $in.^2$) in the high-ranged gage, with balls closely packed, and

38750 per m^2 (25 per $in.^2$) in the lower-ranged version.

If the loads are in newtons and the ball density in balls per square metre, the equivalent pressures will be in MPa. If the loads are in pounds and the ball density in balls per square inch, the equivalent pressures will be in psi.

C.9.4 Plotting the Results. Log-log paper is most convenient. The results of (C.9.3) are usually plotted on the vertical axis, and the results of (C.9.2) on the horizontal. Instead of connecting the points by straight-line segments, a smooth curve should be drawn through the middle of the point-scatter band for each alloy. Due to local variations in the hardness of the specimen material, there will always be some point scatter. These curves are used to convert measured impression diameters from recovered gages to indicated peak stress.

APPENDIX D

CIRCULAR PLATE OF CONSTANT THICKNESS
ON A LINEAR FOUNDATION

D.1 GENERAL EQUATIONS AND NOTATION

The notation used here is the same as in Reference 68. A linear foundation is one for which

$$p = Cw$$

where p is the pressure exerted on the foundation by the plate at a point, w is the deflection of the plate at that point, and C is a constant called the modulus of the foundation. Defining K as

$$K = \frac{Eh^3}{12(1 - \mu^2)}$$

where E and μ are the Young's modulus and Poisson's ratio of the plate material and h is the plate thickness, and ι as

$$\iota = \sqrt[4]{\frac{K}{C}}$$

the solutions are most conveniently expressed in terms of the quantities

$$x = \frac{r}{\iota} \qquad \alpha = \frac{a}{\iota}$$

where r is the radial distance and a is the radius of the plate.

With a uniform load q acting on the entire external area of the plate, and with axisymmetric edge conditions, the solutions are given in terms of the Kelvin functions ber x, bei x, ber' x, bei' x, and the constants C_1 and C_2 :

Deflection:

$$w = \frac{q}{C} + C_1 \text{ ber } x + C_2 \text{ bei } x \qquad \text{(D.1)}$$

Slope:

$$\theta = -\frac{1}{\iota}(C_1 \text{ ber' } x + C_2 \text{ bei' } x) \qquad \text{(D.2)}$$

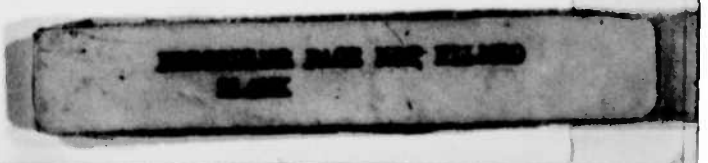

Moment per unit length along a circumferential section:

$$M_r = \frac{K}{\ell^2}\left[C_1\left(\text{bei } x + \frac{1-\mu}{x}\,\text{ber' } x\right) - C_2\left(\text{ber } x - \frac{1-\mu}{x}\,\text{bei' } x\right)\right] \quad (D.3)$$

Moment per unit length along a radial section:

$$M_\phi = \mu\frac{K}{\ell^2}\left[C_1\left(\text{bei } x - \frac{1-\mu}{\mu x}\,\text{ber' } x\right) - C_2\left(\text{ber } x + \frac{1-\mu}{\mu x}\,\text{bei' } x\right)\right] \quad (D.4)$$

Shear per unit length along a circumferential section:

$$Q_r = \frac{K}{\ell^3}\left(C_1\,\text{bei' } x - C_2\,\text{ber' } x\right) \quad (D.5)$$

The constants C_1 and C_2 depend on the conditions at the edge.

D.2 UNIFORM EXTERNAL LOAD; EDGE SIMPLY SUPPORTED

This configuration is shown in Figure D.1a. The constants C_1 and C_2 are given by:

$$C_1 = -\frac{q}{C}\,\frac{\text{ber } \alpha - \frac{1-\mu}{\alpha}\,\text{bei' } \alpha}{\left(\text{ber } \alpha - \frac{1-\mu}{\alpha}\,\text{bei' } \alpha\right)\text{ber } \alpha + \left(\text{bei } \alpha + \frac{1-\mu}{\alpha}\,\text{ber' } \alpha\right)\text{bei } \alpha}$$

$$C_2 = -\frac{q}{C}\,\frac{\text{bei } \alpha + \frac{1-\mu}{\alpha}\,\text{ber' } \alpha}{\left(\text{ber } \alpha - \frac{1-\mu}{\alpha}\,\text{bei' } \alpha\right)\text{ber } \alpha + \left(\text{bei } \alpha\,\frac{1-\mu}{\alpha}\,\text{ber' } \alpha\right)\text{bei } \alpha}$$

The deformations, moments, and shear may be found by using the above values of C_1 and C_2 in Equations D.1 through D.5.

D.3 LINEAL MOMENT APPLIED TO A SIMPLY SUPPORTED EDGE

This configuration is shown in Figure D.1b; M is the moment per unit length of the circumference. The constants C_1 and C_2 are given by:

$$C_1 = \frac{M\ell^2}{K}\,\frac{\text{bei}\alpha}{\left(\text{bei } \alpha + \frac{1-\mu}{\alpha}\,\text{ber' } \alpha\right)\text{bei } \alpha + \left(\text{ber } \alpha - \frac{1-\mu}{\alpha}\,\text{bei' } \alpha\right)\text{ber } \alpha}$$

$$C_2 = \frac{M_1^2}{K} \frac{-\text{ber}\alpha}{\left(\text{bei}\ \alpha + \frac{1-\mu}{\alpha}\ \text{ber}'\ \alpha\right)\text{bei}\ \alpha + \left(\text{ber}\ \alpha - \frac{1-\mu}{\alpha}\ \text{bei}'\ \alpha\right)\text{ber}\ \alpha}$$

The expression for C_1 as given in Reference 68 contains an error. The above version is correct; this may be verified by solving for C_1 from the more general equations in Reference 68.

The deformations, moments, and shear may be found by using these values of C_1 and C_2 in Equations D.1 through D.5.

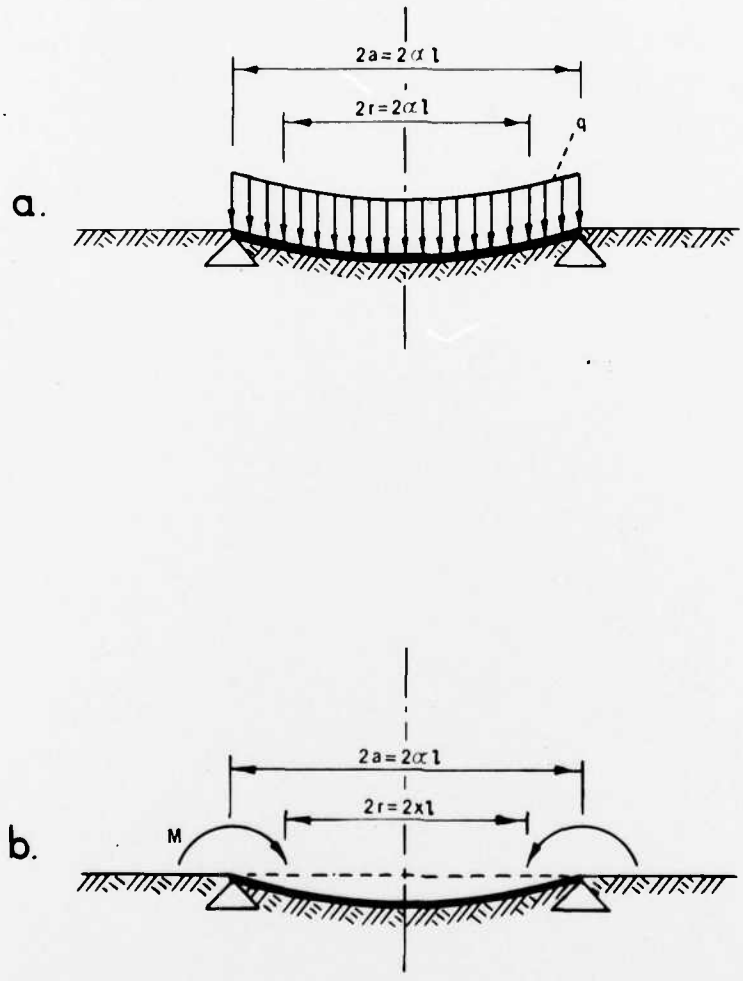

Figure D.1. Loads and edge conditions.

APPENDIX E

MODEL OF THE SINGLE-BALL DYNAMIC LOADING SYSTEM IN TERMS OF LUMPED MASSES

The actual system and the model are depicted in Figure E.1. The reaction mass is considered as fixed. The mass of the bob is divided into two lumped masses concentrated at the ends.

Analysis of vibratory systems consisting of several lumped masses may be found in several graduate level texts on mechanics, such as Reference 75. The model in Figure E.1 has two normal modes. Their natural frequencies f_1 and f_2 are given in terms of the parameters indicated in Figure E.1 as

$$(2\pi f_1)^2 = \omega_1^2 = \frac{1}{2}\left[\left(\frac{k_1 + k_2}{M_1} + \frac{k_2}{M_2}\right) - \sqrt{\left(\frac{k_1 + k_2}{M_1} + \frac{k_2}{M_2}\right)^2 - \frac{4k_1k_2}{M_1M_2}}\right] \qquad (E.1)$$

$$(2\pi f_2)^2 = \omega_2^2 = \frac{1}{2}\left[\left(\frac{k_1 + k_2}{M_1} + \frac{k_2}{M_2}\right) + \sqrt{\left(\frac{k_1 + k_2}{M_1} + \frac{k_2}{M_2}\right)^2 - \frac{4k_1k_2}{M_1M_2}}\right] \qquad (E.2)$$

The general expressions for the displacements from equilibrium y_1 and y_2 of the masses M_1 and M_2 as a function of time t may be written as

$$y_1 = c_1a_{11} \sin(\omega_1 t + \phi_1) + c_2a_{12} \sin(\omega_2 t + \phi_2)$$

$$y_2 = c_1a_{21} \sin(\omega_1 t + \phi_1) + c_2a_{22} \sin(\omega_2 t + \phi_2)$$

where the c-s, a-s, and ϕ-s are constants. For each normal mode j

$$\frac{a_{2j}}{a_{1j}} = 1 + \frac{k_1}{k_2} - \omega_j^2 \frac{M_1}{k_2} \qquad (E.3)$$

Letting $\dot{y}_1$ and $\dot{y}_2$ represent the velocities of the masses M_1 and M_2, the initial conditions are

$$y_1(0) = y_2(0) = 0$$

$$\dot{y}_1(0) = \dot{y}_2(0) = V_o$$

where V_o is the velocity before impact. These initial conditions arise from the fact that the load sensor and bob system is not vibrating and is moving with velocity V_o before making contact with the specimen. From these initial conditions, for any V_o

$$y_1 = c_1 a_{11} \sin \omega_1 t + c_2 a_{12} \sin \omega_2 t \tag{E.4}$$

$$y_2 = c_1 a_{21} \sin \omega_1 t + c_2 a_{22} \sin \omega_2 t \tag{E.5}$$

and

$$\frac{c_2 a_{12}}{c_1 a_{11}} = \frac{\omega_1 \left(\frac{a_{21}}{a_{11}} - 1 \right)}{\omega_2 \left(1 - \frac{a_{22}}{a_{12}} \right)} \tag{E.6}$$

The ratio $c_2 a_{12}/c_1 a_{11}$ is of interest because it expresses the ratio of mode 2 displacement amplitude to mode 1 displacement amplitude of the mass M_1 (Equation E.4), and this is the same as the corresponding ratio of <u>force</u> amplitudes in the spring k_1. Since this spring represents the indentation during loading, the quantity $c_2 a_{12}/c_1 a_{11}$ expresses the force amplitude ratio at the indentation of second to first normal mode.

Frequencies of the normal modes and the quantity $c_2 a_{12}/c_1 a_{11}$ are given in Table E.1 for two sets masses and spring constants. In both cases each lumped mass is half the mass of the 45-gram bob and k_1 is the indentation spring constant during loading. In one case, k_2 was taken as the spring constant of a 45-gram steel bob of 5-cm length; this is 490 MN/m. The other value of k_2, 140 MN/m, was chosen to produce $f_2 \approx 18000$ Hz. From the tabulated values of $c_2 a_{12}/c_1 a_{11}$ it is evident that, in this model, the predicted contributions of the

second normal mode to the total force amplitude at the indentation are very small.

The tabulated values of f_1 are very nearly the same as the 2424 Hz natural frequency of a single 45-gram mass at the end of a spring with force constant equal to k_1. For k_2 = 490 MN/m, the value of f_2 is very nearly the same as the 33402 Hz natural frequency predicted for a free 45-gram steel bar of 5-cm length when all its mass is assumed concentrated at the ends.

Table E.1. Frequencies of the normal modes and the force amplitude ratio in the spring k_1, second to first normal mode, for two values of k_2.

Quantity	$M_1 = M_2 = 22.5$ grams; $k_1 = 10.1$ MN/m	
	$k_2 = 490$ MN/m	$k_2 = 140$ MN/m
f_1	2417	2402
f_2	33490	17874
$\frac{c_2 a_{12}}{c_1 a_{11}}$	0.0004	0.0026

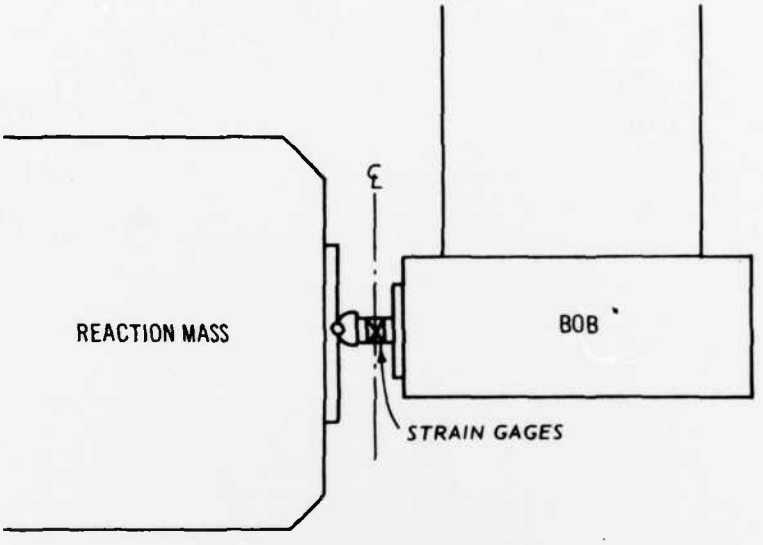

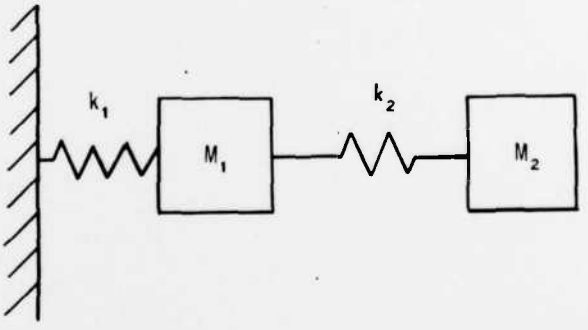

Figure E.1. Dynamic loading system of Chapter 7 and model with lumped masses at the ends of the bob.

DISTRIBUTION LIST

DEPARTMENT OF DEFENSE

Assistant to the Secretary of Defense
Atomic Energy
ATTN: Executive Assistant

Defense Advanced Rsch. Proj. Agency
ATTN: TIO
ATTN: NMRO
ATTN: PMO
ATTN: STO

Defense Documentation Center
Cameron Station
12 cy ATTN: TC

Defense Nuclear Agency
4 cy ATTN: TITL
ATTN: DDST
2 cy ATTN: SPSS

Field Command
Defense Nuclear Agency
ATTN: FCTMOF
ATTN: FCT
ATTN: FCPR

Livermore Division, Fld. Command, DNA
Department of Defense
Lawrence Livermore Laboratory
ATTN: FCPRL

Commandant
NATO School (SHAPE)
ATTN: U.S. Documents Officer

DEPARTMENT OF THE ARMY

Deputy Chief of Staff for Rsch., Dev. & Acq.
Department of the Army
ATTN: DAMA-AOA-M

Harry Diamond Laboratories
Department of the Army
ATTN: DELHD-TI
ATTN: DELHD-NP

U.S. Army Ballistic Research Labs.
ATTN: DRXBR-X, J. Meszaros
ATTN: Technical Library
ATTN: DRDAR-BLE, J. Keefer

U.S. Army Engr. Waterways Exper. Station
ATTN: W. Flathau
ATTN: Library
ATTN: L. Ingram
ATTN: F. Hanes
ATTN: J. Ingram
ATTN: A. Peekna

U.S. Army Materiel Dev. & Readiness Cmd.
ATTN: DRXAM-TL

DEPARTMENT OF THE NAVY

Chief of Naval Research
ATTN: Code 715

DEPARTMENT OF THE NAVY (Continued)

Civil Engineering Laboratory
Naval Construction Battalion Center
ATTN: R. Odello
ATTN: Code L08A

David W. Taylor Naval Ship R & D Ctr.
ATTN: Code L42-3

Naval Facilities Engineering Command
Headquarters
ATTN: Code 09M22C

Naval Ship Engineering Center
Department of the Navy
ATTN: Code 09G3

Naval Surface Weapons Center
ATTN: Code F31

DEPARTMENT OF THE AIR FORCE

AF Institute of Technology, AU
ATTN: Library

AF Weapons Laboratory, AFSC
ATTN: SUL
ATTN: DES-S, M. Plamondon
ATTN: DEX, J. Renick
ATTN: DEX

Assistant Chief of Staff
Intelligence
ATTN: INATA

DEPARTMENT OF ENERGY

Department of Energy
Albuquerque Operations Office
ATTN: Doc. Con. for Technical Library

Department of Energy
Library Room G-042
ATTN: Doc. Con. for Classified Technical Library

Department of Energy
Nevada Operations Office
ATTN: Doc. Con. for Technical Library

Lawrence Livermore Laboratory
ATTN: Doc. Con. for Technical Information Department Library

Oak Ridge National Laboratory
Union Carbide Corporation-Nuclear Division
X-10 Laboratory Records Department
ATTN: Civ. Def. Res. Proj., Mr. Kearny

Sandia Laboratories
Livermore Laboratory
ATTN: Doc. Con. for Library & Security Classification Division

DEPARTMENT OF ENERGY (Continued)

Sandia Laboratories
ATTN: Doc. Con. for A. Chaban
ATTN: Doc. Con. for L. Vortman
ATTN: Doc. Con. for 3141

OTHER GOVERNMENT AGENCY

National Bureau of Standards
ATTN: P. Lederer

DEPARTMENT OF DEFENSE CONTRACTORS

Aerospace Corp.
ATTN: Technical Information Services
ATTN: P. Mathur

Agbabian Associates
ATTN: M. Agbabian

Artec Associates, Inc.
ATTN: D. Baum

Civil/Nuclear Systems Corp.
ATTN: R. Crawford

EC&C Washington Analytical Services Center, Inc.
ATTN: Library

Electromechanical Sys. of New Mexico, Inc.
ATTN: R. Shunk

General Electric Company-TEMPO
Center for Advanced Studies
ATTN: DASIAC

H-Tech Laboratories, Inc.
ATTN: B. Hartenbaum

IIT Research Institute
ATTN: Documents Library

Kaman Sciences Corp.
ATTN: D. Sachs
ATTN: Library

Merritt CASES, Inc.
ATTN: Technical Library
ATTN: J. Merritt

DEPARTMENT OF DEFENSE CONTRACTORS (Continued)

Nathan M. Newmark Consulting Services
ATTN: N. Newmark
ATTN: W. Hall

Physics International Co.
ATTN: C. Vincent
ATTN: F. Sauer, C. Codfrey
ATTN: Technical Library

R & D Associates
ATTN: Technical Information Center
ATTN: C. Knowles, J. Lewis

Science Applications, Inc.
ATTN: Technical Library

Southwest Research Institute
ATTN: A. Wenzel
ATTN: W. Baker

SRI International
ATTN: B. Casten, P. De Carli
ATTN: G. Abrahamson

Systems, Science & Software, Inc.
ATTN: D. Grine
ATTN: Library

TRW Defense & Space Sys. Group
2 cy ATTN: P. Dai
ATTN: Technical Information Center

TRW Defense & Space Sys. Croup
San Bernardino Operations
ATTN: F. Wong

The Eric H. Wang Civil Engineering Rsch. Facility
University Station
ATTN: N. Baum

Weidlinger Assoc,. Consulting Engineers
ATTN: M. Baron

Weidlinger Assoc., Consulting Engineers
ATTN: J. Isenberg